UNIVERSITÄT BONN

Characterization of the Sulfite-Generating rDsrABL Complex of *Allochromatium vinosum*

Dissertation

zur

Erlangung des Doktorgrades (Dr. rer. nat.)

der

Mathematisch-Naturwissenschaftlichen Fakultät

der

Rheinischen Friedrich-Wilhelms-Universität Bonn

vorgelegt von

Julia Lofi, geb. Feldhues

aus Bergisch Gladbach

Bonn 2020

Angefertigt mit Genehmigung der Mathematisch-Naturwissenschaftlichen Fakultät der Rheinischen Friedrich-Wilhelms-Universität Bonn

1. Gutachterin: PD Dr. Christiane Dahl
2. Gutachter: Prof. Dr. Uwe Deppenmeier

Tag der Promotion: 23.10.2020
Erscheinungsjahr: 2020

Teile dieser Arbeit wurden bereits veröffentlicht.

Löffler, M., Feldhues, J., Venceslau, S.S., Kammler, L., Grein, F., Pereira, I.A.C., and Dahl, C. (2020) DsrL mediates electron transfer between NADH and rDsrAB in *Allochromatium vinosum*. *Environmental Microbiology* **22**: 783–795, doi: 10.1111/1462-2920.14899.

Table of Contents

List of Abbreviations

[4Fe4S] cluster	4 iron, 4 sulfur cluster
A. fulgidus	*Archaeoglobus fulgidus*
A. vinosum	*Allochromatium vinosum*
aa	amino acids
aNir	assimilatory nitrite reductase
approx.	approximately
APS	adenosine 5'-phosphosulfate
aSir	assimilatory sulfite reductase
Asr	anaerobic sulfite reductase
ATP	adenosine triphosphate
BCA	bicinchoninic acid assay
BSA	bovine serum albumin
C-terminal	carboxyl-terminal
C. tetanomorphum	*Clostridium tetanomorphum*
CV	column volume
Cys	cysteine
D. vulgaris	*Desulfovibrio vulgaris*
DNA	desoxyribonucleic acid
dSir	dissimilatory sulfite reductase
Dsr	dissimilatory sulfite reduction
DTT	dithiothreitol
E. coli	*Escherichia coli*
FAD	flavin adenine dinucleotide
FeS cluster	iron-sulfur cluster
FMN	flavin mononucleotide
Hdr	heterodisulfide reductase
HF	high-fidelity
His	histidine
HRP	horse radish peroxidase
HTH	helix-turn-helix
IPTG	isopropyl-β-D-thiogalactopyranoside
Isc	iron-sulfur cluster
LB	Luria-Bertani

MALDI-ToF	matrix-assisted laser desorption ionization time-of-flight
MalPEG	methoxy-polyethylene glycol maleimide
MOPS	3-(*N*-morpholino)propanesulfonic acid
MTT	thiazolyl blue tetrazolium bromide
MW	molecular weight
N-terminal	amino-terminal
NAD(P)	nicotinamide adenine dinucleotide (phosphate)
NAD(P)H	nicotinamide adenine dinucleotide (phosphate) hydrogen
NEB	New England Biolabs
OD_{600}	optical density at a wavelength of 600 nm
PCR	polymerase chain reaction
rDsr	reverse-acting dissimilatory sulfite reductase
redox	reduction and oxidation
Rhd	rhodanese
SAM	S-adenosyl-L-methionine
Sat	sulfate adenylyl transferase
SDS-PAGE	sodium dodecyl sulfate polyacrylamide gel electrophoresis
sHdr	sulfide-oxidizing heterodisulfide reductase-like
TEMED	tetramethyl ethylenediamine

List of Symbols

%	percentage
°C	degree celsius
ε	molar absorption coefficient
A	ampere
bp	basepairs
E_0	redox potential
g	gram
h	hour
kb	kilobases
kDa	kilodalton
K_M	concentration of substrate needed to get half-maximal velocity
mg	milligram
min	minute
ml	milliliter
mm	millimeter
mM	millimolar
mmol	millimol
mV	millivolt
ng	nanogram
nm	nanometer
nt	nucleotides
rpm	revolutions per minute
RT	room temperature
s	second
U	units [µmol min^{-1}]
V	volt
V_{max}	maximum enzyme velocity
W	watt
xg	multiple of gravity acceleration
µg	microgram
µl	microliter
µM	micromolar
µmol	micromol

1 Introduction

1.1 Sulfur Cycle

The tenth most abundant element in the universe is sulfur (Steudel and Chivers, 2019). Together with inter alia oxygen and selenium, sulfur belongs to the sixteenth group of the periodic system and consequently has six valence electrons. It occurs in oxidation states from -2 to +6 in various inorganic and organic molecules, of which sulfide is the most reduced and sulfate the fully oxidized form. These sulfur compounds play a significant role in both the bio- and the geosphere, between which they are dynamically cycled (Figure 1). Abiotic reactions, geological processes and various microbial pathways all contribute to the biogeochemical sulfur cycle through various reservoirs (Fike *et al.*, 2015).

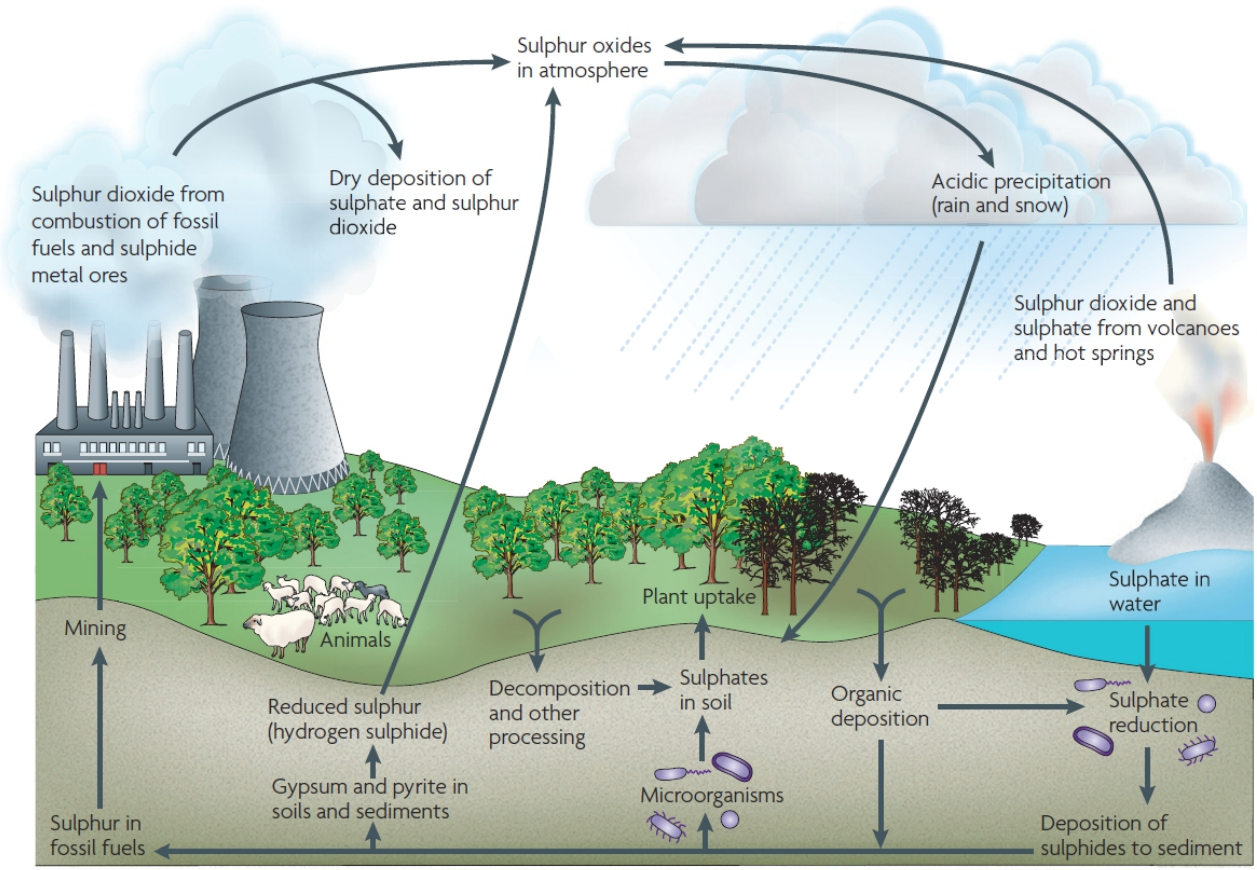

Figure 1: The biogeochemical sulfur cycle (Muyzer and Stams, 2008). Sulfur occurs in a broad range of oxidation states in several inorganic and organic molecules. These sulfur compounds are cycled between the bio- and the geosphere in various abiotic, geological, microbial and human-made processes.

On earth the major sulfur reservoirs are the ocean, as it holds great amounts of dissolved sulfate, and rocks and sediment, where sulfur is present in the minerals pyrite (FeS_2) and gypsum ($CaSO_4$) (Middelburg, 2000; Muyzer and Stams, 2008). In aerobic environments sulfate is the most stable sulfur compound, while reduced inorganic sulfur compounds are more prevalent in anoxic environments. In the atmosphere the toxic gas sulfur dioxide can be detected, which is emitted naturally due to volcanic activity, but also due to the burning of fossil fuels contaminated with sulfur compounds (Figure 1). Coal for example often contains high amounts of sulfur in form of the mineral pyrite (FeS_2). The emission of sulfur dioxide induced by the burning of pyrite-containing coal is one cause of acid precipitation (Chou, 1990; Muyzer and Stams, 2008). In this study the two inorganic sulfur compounds sulfite and sulfide will be of relevance. The fully reduced sulfur compound sulfide can be found in hydrothermal fluids emitted by hydrothermal vents, also called black smokers, at the seafloor of the oceans (Colín-García, 2016). Sulfite is nucleophilic and shows strong reducing capacity, which contributes to its toxicity and antimicrobial activity (Kappler and Dahl, 2001; Ough and Were, 2005).

Sulfur does not only occur in inorganic compounds, it is also abundant in all living organisms, for example, in the amino acids methionine and cysteine and it contributes to poly-peptide structure due to disulfide bridges between cysteine residues. Furthermore sulfur is present in sulfolipids such as sulfoquinovosyl diacylglycerol, which is abundant in many photosynthetic organisms (Benning, 1998). Sulfur also contributes to electron transfer in redox reactions, as it is part of redox-active enzyme cofactors such as iron-sulfur clusters. Many prokaryotes, plants, fungi and algae are capable of incorporating inorganic sulfur compounds into the above-mentioned organic compounds by sulfur assimilation (Figure 1, Figure 2). In the absence of external reduced sulfur compounds, sulfate is taken up by the organism, reduced to sulfide, which can thereafter be incorporated into biomolecules.

However, sulfur assimilation is not the only way living organisms take part in the biogeochemical sulfur cycle. Various microbial metabolic processes transform the oxidation state of sulfur and in doing so, play a major role in the regulation of Earth's surface conditions (Fike *et al.,* 2015). Inorganic sulfur compounds can be used as electron acceptors and donors by prokaryotes for energy conservation (Figure 2). This so-called dissimilation of sulfur compounds establishes an electrochemical membrane potential,

which can be used for energy-consuming processes such as ATP synthesis and NAD^+ reduction. In these dissimilatory processes sulfate and sulfite are reduced to sulfide, which is then re-oxidized to sulfate via zero-valent sulfur (Figure 2, Barton *et al.,* 2014). While dissimilatory sulfate, sulfite and sulfur reduction and the disproportionation of thiosulfate to sulfide and sulfate only occur under anaerobic conditions, dissimilatory sulfide and sulfur oxidation is preformed by aerobic and anaerobic bacteria (Figure 2). Although the capability for sulfate assimilation is widespread over the three domains of life and the prokaryotic group of dissimilatory sulfate reducers is also phylogenitically diverse, the pathways of sulfate reduction are quite similar. As the reduction of sulfate to sulfite has a very low redox potential ($E_{0'}$ = -516 mV) (Thauer *et al.,* 1977), sulfate has to be activated with ATP to adenosine 5'-phosphosulfate (APS) before reduction to sulfite in both assimilatory and dissimilatory sulfate reduction. The reduction of sulfite is thereafter catalyzed by an assimilatory or dissimilatory sulfite reductase. The group of prokaryotes capable of dissimilatory sulfide and sulfur oxidation is very heterogeneous and so are the pathways, as no universal mechanism for the oxidation of reduced sulfur compounds exists (Dahl, 2015). Interestingly, in one pathway the cytoplasmic oxidation of sulfane sulfur to sulfite is catalyzed by an enzyme homologous to the above-mentioned sulfite reductases, the so-called reverse-acting dissimilatory sulfite reductase.

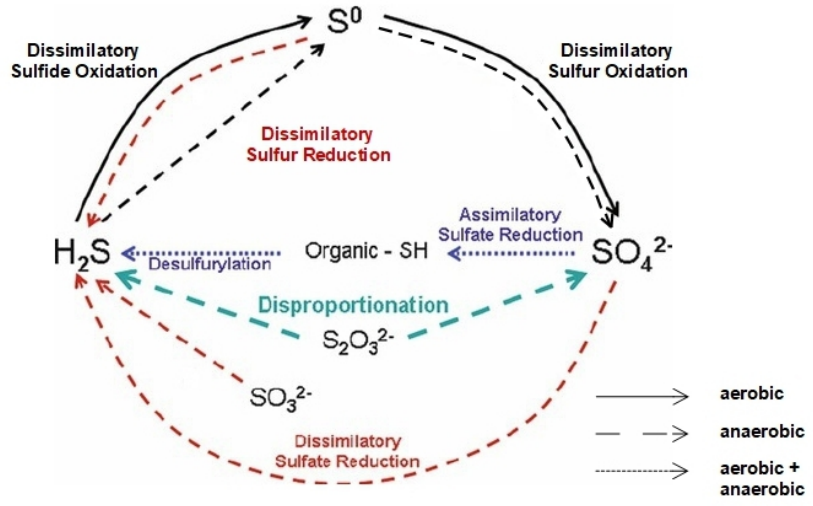

Figure 2: The biological sulfur cycle. Sulfate can be incorporated into organic sulfur compounds via assimilatory sulfate reduction by aerobic and anaerobic organisms. Disproportionation of thiosulfate and dissimilatory sulfate, sulfite and sulfur reduction only occur under anaerobic conditions, while dissimilatory sulfide and sulfur oxidation can take place under aerobic and anaerobic conditions. Modified after Barton *et al.* (2014).

1.2 Assimilatory and Dissimilatory Sulfite Reductases

Sulfite reductases are key enzymes in the biogeochemical sulfur cycle, as they catalyze the six electron reduction of sulfite to sulfide, which is a central step in both assimilatory and dissimilatory sulfate reduction (Figure 2). Assimilatory sulfite reductases can be found in bacteria, archaea, plants and fungi, where they generate sulfide for incorporation into sulfur-containing biomolecules. This is an essential and ancient pathway, which is widespread throughout the three domains of life. Dissimilatory sulfite reductases are restricted to the domain of prokaryotes, where they occur in both sulfate-reducing and sulfur-oxidizing organisms (Dhillon *et al.,* 2005). Many sulfate reducers belong to the class *Deltaproteobacteria*, there are also gram-positive sulfate reducers and representatives can be found in the bacterial classes *Nitrospira*, *Thermodesulfobacteria* and the archaeal genus *Archaeoglobus*. In the very diverse group of sulfur oxidizers, the reverse-acting dissimilatory sulfite reductase (rDsr) is mainly found in species, which are capable of sulfur storage and belong to the phyla *Proteobacteria* and *Chlorobi* (Loy *et al.,* 2009).

Sulfite reductases are both structurally and functionally related to nitrite reductases, which catalyze the six electron reduction of nitrite to ammonium (Crane and Getzoff, 1996). Nitrite and sulfite reductases share a common prosthetic group, which is termed siroheme (Murphy *et al.,* 1974). This heme-like prosthetic group consists of an iron-chelated sirohydrochlorin, which is a class of tetrahydroporphyrin with eight carboxyl side chains and was first isolated from the assimilatory NADPH-sulfite reductase from *Escherichia coli* (Murphy and Siegel, 1973; Murphy *et al.,* 1973). Further analysis of the aforementioned enzyme complex revealed, that the siroheme is covalently coupled to an [4Fe4S] cluster (Janick and Siegel, 1982; Crane *et al.,* 1995). In the dissimilatory sulfite reductases of the purple sulfur bacterium *Allochromatium vinosum* and of the sulfate reducers in the *Desulfovibrio* genus the prosthetic group was identified as siroamide, in which one of the siroheme carboxyl groups is replaced by an amide (Lübbe *et al.,* 2006; Matthews *et al.,* 1995). Uroporphyrinogen III, as a common tetrapyrrole precursor, is an intermediate in biosynthesis of vitamin B12 (cobalamin), of hemes (Scott, 1993; Jordan, 1994) and also of sirohemes. The enzyme, which catalyzes the four reactions transforming uroporphyrinogen III to siroheme is the homodimeric CysG (Spencer *et al.,* 1993; Stroupe *et al.,* 2003). In *A. vinosum* DsrN, a protein encoded in proximity to the reverse-acting

dissimilatory sulfite reductase, was proposed to function as siroamidase (Lübbe *et al.,* 2006).

The assimilatory sulfite reductase from *E. coli* has two subunits, which build an $\alpha_8\beta_4$ holoenzyme. The α subunit is a flavoprotein, which binds NADPH, FAD and FMN cofactors and the β subunit is an iron-containing hemoprotein and binds an [4Fe4S] cluster, which is covalently bound to siroheme (Siegel and Davis, 1974; Crane *et al.,* 1995; Askenasy *et al.,* 2015). Electrons deriving from NADPH are transferred via FAD and FMN of the flavoprotein onto the siroheme in the active site of the hemoprotein, where sulfite is reduced (Crane *et al.,* 1997).

The well characterized dissimilatory sulfite reductase DsrAB catalyzes the reduction of the intermediate sulfur compound sulfite in dissimilatory sulfate reducers. The two related subunits DsrA and DsrB are arranged in a $\alpha_2\beta_2$ conformation and both contain conserved binding motifs for a siroheme coupled to a [4Fe4S] cluster (Ostrowski *et al.,* 1989; Fauque *et al.,* 1990; Dahl *et al.,* 1993). While the siroheme-[4Fe4S] of DsrB is catalytically active, that of DsrA seems to have a structural role (Oliveira *et al.,* 2008; Schiffer *et al.,* 2008). Both subunits also contain a ferredoxin domain, which binds a second [4Fe4S] cluster. The high similarity between the two subunits DsrA and DsrB indicate that they may have arisen by duplication of an ancestral gene (Dahl *et al.,* 1993). In contrast to the assimilatory sulfite reductase from *E. coli*, a flavoprotein is not part of the DsrAB holoenzyme for sulfite reduction. However, the physiological electron donor for sulfite reduction catalyzed by DsrAB is so far unknown (Oliveira *et al.,* 2008) and could possibly be a flavoprotein or a ferredoxin as confirmed for the spinach assimilatory nitrite reductase (Swamy *et al.,* 2005). In several sulfur oxidizers, which accumulate sulfur as a storage intermediate, a reverse-acting dissimilatory sulfite reductase catalyzes the cytoplasmic oxidation of stored sulfur to sulfite (Schedel *et al.,* 1979; Pott and Dahl, 1998; Loy *et al.,* 2009). This enzyme is homologous to, but physiologically and phylogenetically clearly distinct from the above-described DsrAB (Hipp *et al.,* 1997; Wagner *et al.,* 1998; Loy *et al.,* 2009). The two subunits of sulfite-generating rDsrAB are also arranged in a $\alpha_2\beta_2$ conformation and contain siroheme coupled to a [4Fe4S] cluster and an additional ferredoxin domain, which presumably enables electron transfer to the as yet unknown electron acceptor of sulfur oxidation.

A further dissimilatory sulfite reductase has been identified in *Salmonella enterica* serovar Typhimurium, an organism capable of sulfite respiration. The trimeric holoenzyme consists of a flavoprotein (AsrB), a siroheme-binding hemoprotein (AsrC) and additionally includes a ferredoxin protein (AsrA) (Huang and Barrett, 1991; Dhillon *et al.,* 2005). Possibly the holoenzyme catalyzes the reduction of sulfite with NADH in the cytoplasm. In the methonarchaeon *Methanocaldococcus jannaschii* a coenzyme F_{420}-dependent sulfite reductase (Fsr) catalyzes sulfite reduction (Johnson and Mukhopadhyay, 2005). The N-terminal half of Fsr represents a H_2F_{420} dehydrogenase, which shows similarities to the H_2F_{420} dehydrogenase subunits of H_2F_{420}:quinone oxidoreductase (Fqo) complex of *A. fulgidus* and of H_2F_{420}:phenazine oxidoreductase (Fpo) complex of *Methanosarcina mazei*. The C-terminal half is homologous to *Salmonella* AsrC, the siroheme-binding hemoprotein of AsrABC, and to the two subunits of the most common dissimilatory sulfite reductase, DsrAB. This enzyme contains iron-sulfur clusters, siroheme and presumably FAD and it couples the oxidation of H_2F_{420} to the reduction of sulfite. In *M. mazei* sulfite reduction catalyzed by Fsr plays a detoxification role, as methanogens are inhibited by sulfite, and it additionally enables the anabolic use of sulfite as a sulfur source (Johnson and Mukhopadhyay, 2005).

1.3 The (r)Dsr Pathway

Dissimilatory sulfate reducers and sulfur oxidizers, encoding for the dissimilatory sulfite reductases DsrAB and rDsrAB respectively, also encode for a whole set of further Dsr proteins, which enable a fully functional sulfur metabolism. The genes *dsrC* and minimally *dsrMK* are included in the genomes of all organisms encoding for (r)DsrAB (Grein *et al.,* 2013; Venceslau *et al.,* 2014). However other *dsr* genes are only found in sulfate reducers or in sulfur oxidizers respectively, indicating that the Dsr pathways in reductive and oxidative direction, while bearing several similarities, are distinct from one another.

1.3.1 The Dsr Pathway of Sulfate Reducers

The Dsr pathway of sulfite reduction occurs in all so far described dissimilatory sulfate reducers. After the sulfate adenylyl transferase (Sat) has activated sulfate to form adenosine 5'-phosphosulfate (APS) and the APS reductase has generated sulfite due to

the reduction of APS, sulfite is further reduced in the Dsr pathway (Figure 3). The reduction is catalyzed by the dissimilatory sulfite reductase DsrAB with its physiological partner DsrC (Venceslau *et al.,* 2014; Santos *et al.,* 2015). DsrC, a small protein (12-14 kDa) binding no prosthetic groups, has a highly conserved C-terminal arm with two strictly conserved cysteine residues (Cort *et al.,* 2001; Cort *et al.,* 2008; Oliveira *et al.,* 2008). One cysteine is the penultimate residue at the C-terminus (Cys_A) and the other lays eleven residues upstream (Cys_B). The flexible arm of DsrC from the sulfate reducer *Desulfovibrio vulgaris* is able to extend into the interface between DsrA and DsrB, bringing Cys_A in proximity of the substrate binding site of DsrAB (Oliveira *et al.,* 2008). In sulfite reduction catalyzed by DsrAB, DsrC functions as a co-substrate and the released product is a DsrC trisulfide, in which a sulfur atom is bridging Cys_A and Cys_B of the C-terminal arm (Figure 3) (Santos *et al.,* 2015). DsrAB requires two electrons for the reduction of sulfite to DsrC trisulfide, as two further electrons stem from reduced DsrC. However, the physiological electron donor for DsrAB-catalyzed sulfite reduction is still unknown.

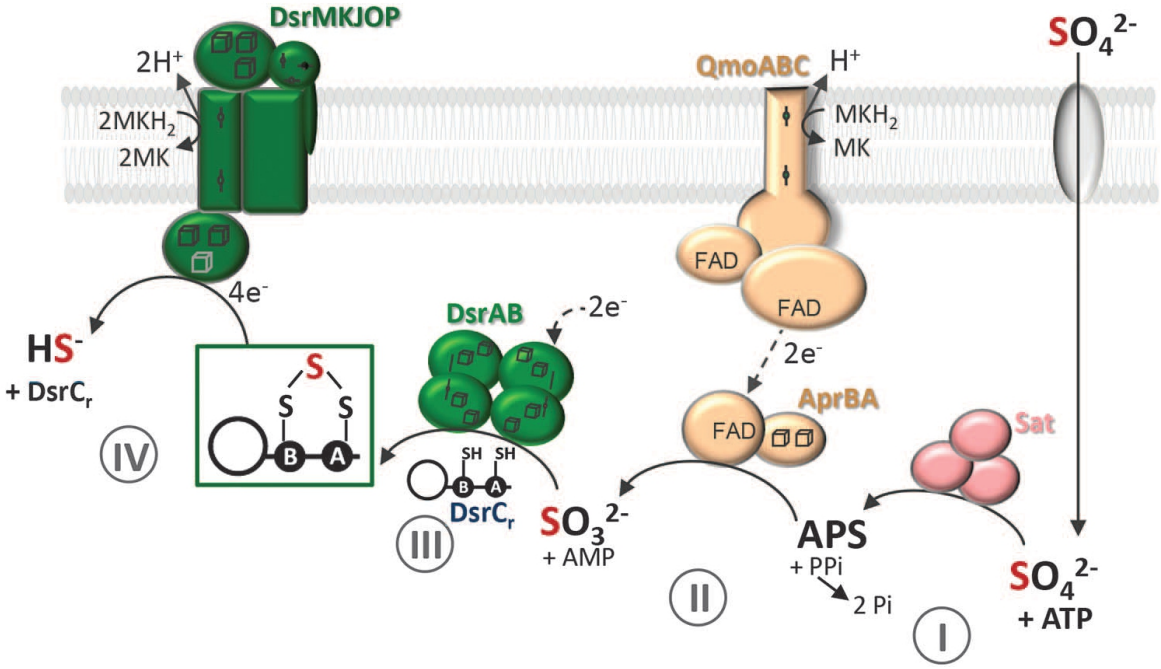

Figure 3: Model of the dissimilatory reduction of sulfate. Sulfate is imported into the cytoplasm, activated by sulfate adenylyl transferase (Sat) to adenosine 5'-phosphosulfate (APS) (I), APS is reduced to sulfite by the APS reductase (II), sulfite is reduced to DsrC trisulfide by DsrAB/DsrC (III) and the trisulfide is reduced to sulfide and reduced DsrC by the DsrMKJOP complex (IV) (Santos *et al.,* 2015).

The DsrC trisulfide is presumably reduced to sulfide and reduced DsrC at the transmembrane complex DsrMK(JOP) with electrons originated from the menaquione pool (Grein *et al.,* 2013; Santos *et al.,* 2015). The transmembrane complex DsrMKJOP seems to be a combination of two sub-complexes with DsrMK extending into the cytoplasm and DsrJOP ranging into the periplasm (Grein *et al.,* 2013). DsrJ is a periplasmic tri-heme cytochrome *c* and shows no sequence similarities to other known proteins. The DsrOP subunits resemble two of the Complex-Iron-Sulfur-Molybdoenyzme (CISM) units and probably enable, together with DsrJ an electron exchange between the periplasm and the quinone pool (Grein *et al.,* 2013). DsrMK is homologous to the membrane-bound HdrDE complex of methanogens, which catalyzes heterodisulfide reduction (Heiden *et al.,* 1994). Thereby DsrM binding two hemes *b* is homologous to HdrE and the cytoplasmic iron-sulfur protein DsrK resembles the catalytic subunit HdrD (Grein *et al.,* 2013). The potential substrate for DsrK is a DsrC trisulfide in analogy to the heterodisulfide substrate for HdrD (Venceslau *et al.,* 2014; Santos *et al.,* 2015). Sulfate reducers also encode for the small protein DsrD, which is not present in sulfur oxidizers and possibly plays a regulatory role in sulfite reduction (Mizuno *et al.,* 2003). Some sulfate and sulfite reducers encode for the iron-sulfur flavoprotein DsrL (Anantharaman *et al.,* 2018), which can be found in all sulfur oxidizers using the rDsr pathway, as it is essential for the oxidation of stored sulfur (Lübbe *et al.,* 2006). The function of DsrL in these sulfate reducers is unclear, however its redox-active prosthetic groups make it a possible candidate for the electron donor of DsrAB.

1.3.2 The rDsr Pathway of Sulfur Oxidizers at the Example of *A. vinosum*

The rDsr pathway mainly occurs in sulfur oxidizers, which are capable of sulfur storage and belong to the phyla *Proteobacteria* and *Chlorobi* (Loy *et al.,* 2009). Among these are many photolithotrophic organisms, which use inorganic sulfur compounds as electron donors for reductive carbon dioxide fixation in anoxygenic photosynthesis, but also some chemolithotrophic sulfur oxidizers (Dahl, 2017). The genetically accessible purple sulfur bacterium *A. vinosum* is the best studied sulfur oxidizer with respect to the rDsr pathway (Pott and Dahl, 1998; Dahl *et al.,* 2005; Lübbe *et al.,* 2006; Sander *et al.,* 2006; Grein *et al.,* 2010; Stockdreher *et al.,* 2012). Thus it was used as a model organism in this study and the rDsr pathway will be described at the example of *A. vinosum*.

During the oxidation of reduced sulfur compounds such as sulfide or thiosulfate *A. vinosum*, like many other sulfur oxidizers, forms sulfur globules. These intermediates are stored in the periplasm, where many oxidative pathways of dissimilatory sulfur metabolism take place (Pattaragulwanit *et al.,* 1998). However, further oxidation of the sulfur intermediates is executed in the cytoplasm by soluble and membrane-bound proteins of the rDsr system (Pott and Dahl, 1998; Dahl *et al.,* 2005; Grein *et al.,* 2010; Lübbe *et al.,* 2006). Although the exact mechanism is still unknown, it has been proposed that sulfur is transferred from its periplasmic deposits into the cytoplasm via low molecular weight organic persulfides such as glutathione persulfide (Frigaard and Dahl, 2008). In the cytoplasm sulfur is shuttled through a cascade of protein persulfides, including a rhodanese (Rhd), TusA, possibly DsrE2A and DsrEFH, onto the substrate-binding protein DsrC (Figure 4) (Stockdreher *et al.,* 2012; Stockdreher *et al.,* 2014). Sulfur can be mobilized from the low molecular persulfide glutathione persulfide onto Rhd, indicating that cytoplasmic sulfur trafficking starts with a Rhd persulfide (Stockdreher *et al.,* 2014). The exact function of DsrE2A, which is encoded in a *rhd-tusA-dsrE2* gene arrangement in a large number of chemotrophic and phototrophic sulfur-oxidizing prokaryotes is as yet unknown (Stockdreher *et al.,* 2014; Venceslau *et al.,* 2014). TusA can receive sulfur from the rhodanese and serves as a sulfur donor for the DsrEFH complex, while DsrEFH transfers sulfur onto DsrC (Figure 4) (Stockdreher *et al.,* 2014; Stockdreher *et al.,* 2012).

DsrC of sulfur oxidizers is homologous to DsrC of sulfate reducers and insofar also has a highly conserved C-terminal arm containing the two cysteine residues Cys_A and Cys_B. Sulfur is transferred from DsrE-Cys78 of DsrEFH onto Cys_A of DsrC (Stockdreher *et al.,* 2012). Sulfur-binding DsrC is the proposed substrate for the sulfite-generating complex rDsrAB (Stockdreher *et al.,* 2012). It is however unclear if a DsrC Cys_A persulfide or a DsrC trisulfide with a sulfur atom bridging Cys_A and Cys_B is metabolized. In the current model (Figure 4) persulfurated DsrC is oxidized to a DsrC trisulfide at the membrane-bound DsrMKJOP complex and is then further oxidized by rDsrAB to sulfite and reduced DsrC. This was proposed as the exact reversal of the reaction mechanism found in sulfate reducers, in which DsrC and sulfite are reduced to DsrC trisulfide by DsrAB (Figure 3) (Santos *et al.,* 2015).

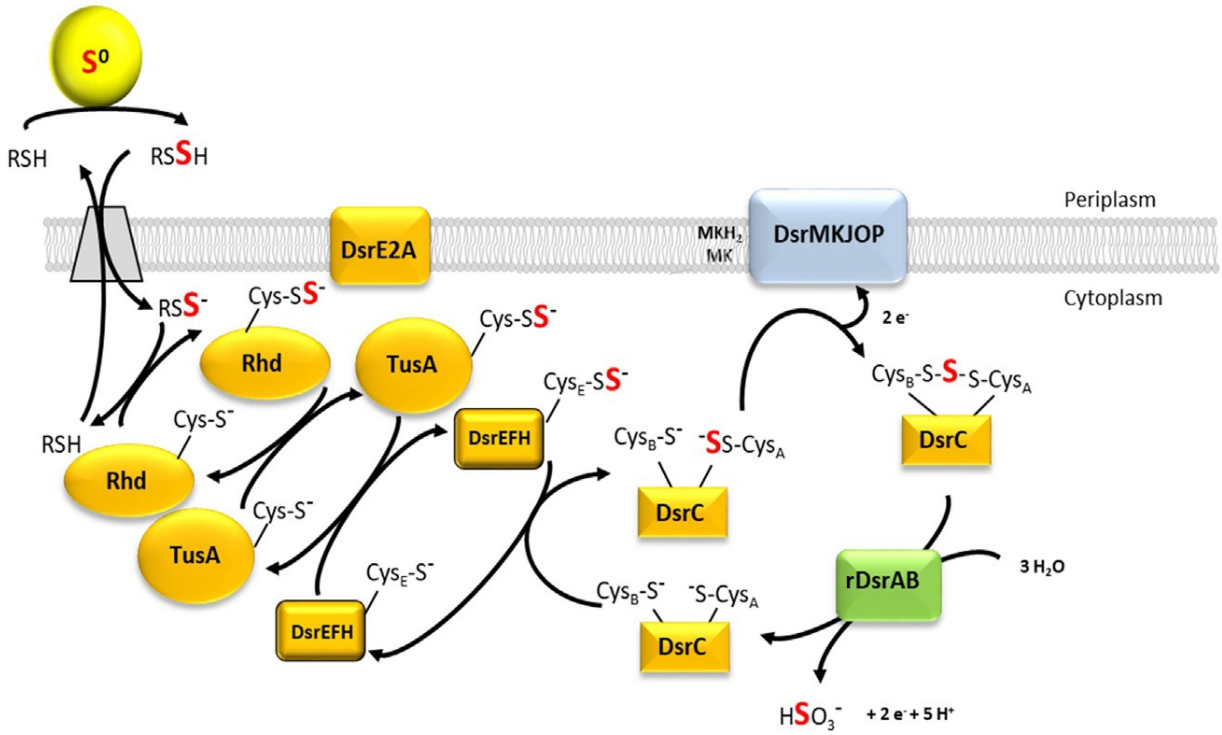

Figure 4: Model of rDsr mediated sulfane sulfur oxidation in *Allochromatium vinosum*. Sulfur is transferred from the periplasmic sulfur deposits into the cytoplasm onto a Rhodanese (Rhd). A cascade of protein persulfids, including TusA and DsrEFH, shuttles sulfur onto DsrC. The DsrC persulfide serves as a substrate for the membrane-bound DsrMKJOP complex. Its product, a DsrC trisulfide, is the substrate for rDsrAB and is oxidized to sulfite and reduced DsrC, which can once more be persulfurated by DsrEFH. Modified after Tanabe *et al.* (2019).

Another model (Stockdreher *et al.,* 2014; Venceslau *et al.,* 2014) suggests a persulfurated DsrC as the direct substrate for rDsrAB-catalyzed sulfur oxidation, whereafter Cys_A carries a sulfonate group. Through the formation of an intramolecular disulfide bound between Cys_A and Cys_B, sulfite is released. The DsrC disulfide is then reduced by the DsrMKJOP complex and can once more be persulfurated by DsrEFH.

In the first model the DsrMKJOP complex would receive electrons, while it would serve as electron donor for DsrC reduction in the second model. Biochemical evidence for the exact function of the electron-transferring transmembrane complex DsrMKJOP is currently not available, however in *A. vinosum* each individual component of the DsrMKJOP complex was shown to be essential for the oxidation of stored sulfur (Sander *et al.,* 2006). Furthermore DsrKJO proteins were co-purified with rDsrAB and DsrC and interaction between the catalytic subunit DsrK and its putative substrate DsrC could be demonstrated by coelution assays (Dahl *et al.,* 2005; Grein *et al.,* 2010).

Just as the origin of the electrons for DsrAB-catalyzed sulfite reduction in sulfate reducers is unknown, it is unclear where the electrons deriving from the oxidation of sulfur-binding DsrC catalyzed by rDsrAB are transferred to. A potential candidate for the electron acceptor for the rDsrAB-catalyzed oxidation of sulfane sulfur is the complex iron-sulfur flavoprotein DsrL. The 72 kDa protein carries an FAD and several FeS-clusters as redox-active groups and was shown to be absolutely essential for the oxidation of stored sulfur in *A. vinosum* (Lübbe *et al.,* 2006). On the basis of its sequence DsrL was proposed to function as NAD(P)H:oxidoreductase and could insofar couple the oxidation of stored sulfur to the generation of NAD(P)H (Dahl *et al.,* 2005).

1.4 Objective

Although the reverse-acting dissimilatory sulfite reductase rDsrAB from sulfur oxidizer *Allochromatium vinosum* has been of scientific interest for over forty years (Schedel *et al.,* 1979), there are still many unsolved aspects in the rDsr pathway of sulfane sulfur oxidation. In this study rDsrAB was investigated biochemically in both reductive and oxidative direction. As rDsrAB is predicted to oxidize DsrC-bound sulfur to sulfite (Stockdreher *et al.,* 2012), the interaction of rDsrAB and DsrC was examined especially. Thereby the influence of DsrC on the activity of rDsrAB and the conformation of the substrate-binding DsrC was of particular interest. A further very interesting potential interaction partner of rDsrAB is the iron-sulfur flavoprotein DsrL, as it could be the unknown electron acceptor of rDsrAB-catalyzed oxidation of stored sulfur. Moreover it could also be the electron donor for DsrAB in those sulfate and sulfite reducers, which encode for DsrL (Anantharaman *et al.,* 2018). The interaction of rDsrAB and DsrL was investigated structurally and kinetically, to elucidate whether an electron transfer between these proteins is possible.

2 Material

2.1 Chemicals, Enzymes, Kits

If not mentioned otherwise, all chemicals were purchased from the companies Bio-Rad, Eppendorf, ThermoScientific, Fluka, Invitrogen, Macherey & Nagel, Merck, Sigma-Aldrich, Roche and Roth.

2.1.1 Enzymes

All enzymes were used with the recommended and provided buffer.

Table 1: Used Enzymes and their Manufacturers

Enzyme	Manufacturer
Antarctic Phosphatase	NEB (Ipswich, USA)
Deoxyribonuclease I	Sigma-Aldrich (St. Louis, USA)
Lysozym	Roth (Karlsruhe, Germany)
Q5 High-Fidelity DNA-Polymerase	NEB (Ipswich, USA)
Restriction enzymes	NEB (Ipswich, USA)
T4-DNA-Ligase	NEB (Ipswich, USA)

2.1.2 Kits

Table 2: Used Kits and their Manufacturers

Kit	Manufacturer
Gene-JET Gelextraction Kit	Thermo Scientific
Gene-JET Plasmid Miniprep Kit	Thermo Scientific
BCA-Assay Kit	Thermo Scientific

2.1.3 Further Material and Chemicals

Table 3: Further Material and Chemicals

Material	Manufacturer
Vivaspin 500 Centrifugal Concentrators (5.000 kDa)	Sartorius (Göttingen, Germany)
Amicon Ultra Centrifugal Filters	Merck (Darmstadt, Germany)
HisTrap HP 5 ml	GE Healthcare Life Sciences
StrepTrap HP 5 ml	GE Healthcare Life Sciences
Complete^{TM} Protease Inhibitor Cocktail	Merck (Darmstadt, Germany)

2.2 Bacteria

Table 4: Used Bacteria

Strain	Genotype	Reference
***Escherichia coli* strains**		
E. coli NEB 10β	Δ*(ara-leu) 7697 araD139 fhuA* Δ*lacX74 galK16 galE15 e14-* ϕ*80*d*lacZ*Δ*M15 recA1 relA1 endA1 nupG rpsL* (Sm_R) *rph spoT1* Δ*(mrr-hsdRMS-mcrBC)*	New England Biolabs (Ipswich, USA)
E. coli BL21 (DE3)	F- *ompT hsdS*$_B$(r_B-m_B-) *gal dcm* (DE3)	Novagen (Darmstadt, Deutschland)
E. coli BL21 (DE3) Δ*iscR*	F- *ompT hsdS*$_B$(r_B-m_B-) *gal dcm* Δ*iscR*::Kan (DE3)	(Akhtar and Jones, 2008)
***Allochromatium vinosum* strains**		
A. vinosum Rif50	Rif^r, spontaneous rifampicin-resistant mutant of *A. vinosum* DSMZ 180	(Lübbe *et al.,* 2006)
A. vinosum Δ*tsdA*	Rif$_r$, *in frame* deletion in *tsdA*	(Denkmann *et al.,* 2012)

2.3 Plasmids

Table 5: Used Plasmids

Plasmid	Genotype	Reference
pETCEX	Ap_r, *Nde*I/*Bam*HI fragment of amplified *dsrC* in pET-15b	(Cort *et al.,* 2008)
pETCEXSer100	Ap_r, *Nde*I/*Bam*HI fragment of amplified *dsrC-Cys100Ser* in pET-15b	(Cort *et al.,* 2008)
pETCEXSer111	Ap_r, *Nde*I/*Bam*HI fragment of amplified *dsrC-Cys111Ser* in pET-15b	(Cort *et al.,* 2008)
pETCEXSer100/111	Ap_r, *Nde*I/*Bam*HI fragment of amplified *dsrC-Cys100SEr-Cys111Ser* in pET-15b	(Cort *et al.,* 2008)
pET22bDsrL-CSt	Ap_r, *Nde*I/*Bam*HI fragment of amplified *dsrL* with C-terminal streptag in pET22b	(Löffler *et al.,* 2020)

2.4 Primers

All primers were designed in this study and ordered at Eurofins MWG Synthesis GmbH (Ebersberg, Germany). The restriction sites are marked with bold letters and the cutting restriction enzyme is written in brackets.

Table 6: Used Primers

Primers	Sequence (5' → 3')
DsrABstrepN'fw	TAGGAGAGA**TCATGA**GCGCTTGGAGCCACCCGCAGTTCGAAAAAGCTATCGACAAGCACGCGACC (BspHI)
DsrABstrepN'rev	CCTGTCC**TCTAGA**GATCAGAAGCGGATATA (XbaI)
DsrABstrepC'fw	AGACCGC**CATATG**GCTATCGACAAGCA (NdeI)
DsrABstrepC'rev	TCCGCT**AAGCTT**CATTTTTCGAACTGCGGGTGGCTCCAAGCGCTGAAGCGGATATAGGA (HindIII)
CysG_SacI_for	CA**GAGCTC**CAGCATCATGGATCTAC (SacI)
CysG_NotI_rev	GTATGATTTTT**GCGGCCGC**TACTCG (NotI)
DsrN_NdeI_for	GGCCT**CATATG** GCGTCGCTCTAC (NdeI)
DsrN_XhoI_rev	CTGAAAG**CTCGAG**GCCCGCTGTT (XhoI)

3 Methods

3.1 Microbiological Methods

3.1.1 Cultivation of *Escherichia coli*

The organism *Escherichia coli* was used for cloning, amplification of plasmids (*E. coli* NEB 10β, Table 4) and for heterologous production of recombinant proteins (*E. coli* BL21 (DE3) Δ*iscR* and *E. coli* BL21 (DE3), Table 4).

3.1.2 Production of Chemically Competent *E. coli*

The method of Dagert and Ehrlich was used to make *E. coli* chemically competent (Dagert and Ehrlich 1979). 70 ml of main culture (2YT-medium, 10 g/l pepton, 10 g/l yeast extract, 5 g/l NaCl, pH 7) was inoculated with 700 µl of an overnight preculture at 37 °C at 180 rpm to an OD_{600nm} of 0.3 – 0.5. The cells were then pelleted at 4 °C and 4000 xg for 10 min, resuspended in 10.5 ml of icecold buffer (sterile 70 mM $CaCl_2$, 20 mM $MgSO_4$) and incubated on ice for 40 min. The above-mentioned centrifugal step was repeated and the pellet was resuspended in 3.5 ml of icecold buffer. After a following incubation step on ice (40 min) 876 µl glycerin was added to the cell suspension and it was stored in aliquots at -70 °C.

3.1.3 Transformation

Plasmids were transformed into chemocompetent *E. coli* NEB 10β, BL21 (DE3) or BL21 (DE3) *ΔiscR* cells by means of the heatshock method (Hanahan, 1983). Chemocompetent cells were stored at -70 °C and thawed on ice. 20 µl ligation solution or 1 µl plasmid DNA were given to 100 µl of competent cells and incubated on ice for 30 min. Then a 60 s heat shock at 42 °C was preformed, after which the mixture was directly placed back on ice for 5 min. Following 800 µl LB-0 medium was added and the mixture was incubated at 37 °C for a minimum of 45 min, while the mixture was regularly inverted. At least two different volumes of the incubated sample were given onto LB plates containing the appropriate antibiotic and the plates were incubated overnight at 37 °C.

3.1.4 Cultivation of *Allochromatium vinosum*

A. vinosum was cultivated photoorganoheterophically on RCV-medium (Weaver *et al.,* 1975) or photolithoautotrophically on 0 medium (Hensen *et al.,* 2006) to which sulfite and thiosulfate were added at the start of fermentation.

RCV medium (Weaver *et al.,* 1975)

RÄH medium	50 ml
yeast extract	0.5 g
NaOH	~1.8 g
dH_2O	ad 1000 ml

RÄH medium

malate	60 g
NH_4Cl	24 g
$MgSO_4$ x 7 H_2O	4 g
$CaCl_2$ x 2 H_2O	1.4 g
SL12 (10x)	20 ml
dH_2O	ad 1000 ml

Trace element solution SL12 (Pfennig and Trüper, 1992)

EDTA	30 g
$FeSO_4$ x 7 H_2O	11 g
H_3BO_3	3 g
$CoCl_2$ x 6 H_2O	1.9 g
$MnCl_2$ x 4 H_2O	0.5 g
$ZnCl_2$	0.42 g
$NiCl_2$ x 6 H_2O	0.24 g
Na_2MoO_4	0.18 g
$CuCl_2$ x 2 H_2O	0.02 g
dH_2O	ad 1000 ml

RÄH medium and the trace element solution were stored without sterilization. Before use of RCV medium, 5 % (v/v) of 180 mM K_2HPO_4 (pH 7.0) was added.

0 medium (Hensen *et al.,* 2006)

For photolilithoautotrophic growth *A. vinosum* was grown on 0 medium in a 10 l fermenter with thiosulfate and sulfite added. The following solutions were sterilized separately and combined afterwards:

Solution 1: salt solution prepared in a 10 l carboy

KCl	3.3 g
$MgCl_2$ x 6 H_2O	3.3g
$CaCl_2$ x 2 H_2O	4.3 g
NH_4Cl	3.3 g
SL12 (10x)	10 ml
dH_2O	ad 8000 ml

Solution 2: phophate solution

KH_2PO_4	3.3 g
dH_2O	ad 1000 ml

Solution 3: carbonate solution

$NaHCO_3$	15 g
dH_2O	ad 1000 ml

After autoclaving, the three solutions were combined under a nitrogen atmosphere. The cloudy medium was bubbled with CO2 until it was clear. At this point the pH of the medium was at about 6.8. Rifampicin (50 mg/l), NaHS (1.5 mM) and $Na_2S_2O_3$ (12.5 mM) were added to the medium through a steril filter.

The medium was inoculated with 2 l of *A. vinosum* grown on RCV. The cells were pelleted by centrifugation (8000 rpm, 12 min, RT) and washed with 0 medium before addition to the fermenter.

A. vinosum was grown at 30 °C under anoxic conditions. The fermenter was placed on a magnetic stirrer and the culture was illuminated by two 60 W lamps. During the experiment samples were taken in regular intervals to monitor pH, opitical density at 690 nm, and thiosulfate concentration. The pH was adjusted to 7.0 ± 1.0 by addition of 1 M HCl or 1 M NaOH.

The cells were harvested in the late exponential phase while the medium still contained a sufficient amount of thiosulfate (3.3.3 Harvesting and Breaking of Cells).

3.2 Molecular Biological Methods

3.2.1 Primer Design

Primers were designed to have GC-content of 40-60 % and if possible not more than four of the same nucleotides consecutively. The melting temperature should be in a range of 55-80 °C and two primers used in one PCR should have a similar melting temperature. The primers should not build primer dimers or form hairpin strutures. The hairpin and self dimerization calculations and melting temperature calculations were performed with Oligo Calc (http://biotools.nubic.northwestern.edu/OligoCalc.html). If possible the 3' end should contain 1 - 2 G or C. Normally primers should have a length of 18–30 nt. The primers designed in this study were extension primers, which contained a restriction site and in some cases a sequence encoding a strep-tag in addition to the sequence complementary to the gene to be amplified. For this reason some primers had a length of over 60 nt. The primers were ordered at Eurofins MWG Synthesis GmbH (Ebersberg, Germany). The primers are listed in Table 6.

3.2.2 Polymerase Chain Reaction (PCR)

For DNA amplification the polymerase chain reaction (PCR) was performed using the following protocol.

Q5 High-Fidelity DNA-Polymerase protocol:

Component	25 µl reaction	Final concentration
H_2O	Add to 25 µl	
5x Q5 reaction buffer	5 µl	1x
10 mM dNTPs	0.5 µl	200 µM each
10 µM forward primer	1.25 µl	0.5 µM
10 µM reverse primer	1.25 µl	0.5 µM
Template DNA	X µl	< 1000 ng
5x GC Enhancer (optional)	(5 µl)	(1x)
Q5 HF DNA-Polymerase	0.25 µl	0.02 U/µl

Cycling protocol:

Cycle step	Temperature	Time	Cycles
Initial denaturation	98 °C	30 s	1
Denaturation	98 °C	10 s	
Annealing	Primer specific	30 s	35
Extention	72 °C	30 s/kb	
Final extention	72 °C	2 min	1
	4 °C	hold	

3.2.3 Extension PCR

In an extension PCR nucleotides which are not complementary to the template are added to the 5' ends of the otherwise sequence specific primers. This renders the possibility to modify the ends of the DNA of interest.

In this case specific restriction sites and a sequence encoding for an affinity tag were added. This ensured that the amplified DNA could be inserted into the multiple cloning site of a vector after restriction digest and that the heterologously expressed gene product could be purified via affinity chromatography. The primers are listed in 2.3 Plasmids.

3.2.4 Agarose Gel Electrophoresis

The method of agarose gel electrophoresis visualizes DNA fragments and separates them according to their size.

The agarose gel electrophoresis was performed with 1% agarose gels and with 1x TAE buffer. The mix was heated in a microwave until there were no chunks of agarose left. After it was cooled down to about 60 °C the agarose was poured into a gel chamber and a comb was inserted. When the gel was polymerized the comb was removed and the gel was placed in a electrophoresis system with 1x TAE buffer. The samples and a size standard (1 kb ladder from NEB) were mixed with 10x loading dye and given into the gel pockets. 90 V were applied and the DNA fragments were separated according to their size. Afterwards they were stained with GelRed for 1 h and visualized under UV light.

3.2.5 DNA Purification

After an agarose gel electrophoresis or an enzymatic reaction like a restriction digest the DNA was purified with the GeneJet Gel Extraction Kit from ThermoScientific. The purification was performed according to the user manual.

3.2.6 Restriction Digest

In this study DNA fragments and plasmids were prepared for ligation with restriction enzymes and after cloning the potential recombinant constructs were analyzed via restriction digest.

Component	**Restriction analysis - Concentration**	**Preparative restriction - Concentration**
H_2O	Add to 30 µl	Add to 50 µl
DNA	1 µg	5 µg
10x buffer	3 µl	5 µl
Enzyme	2 U	10 U

The reaction was incubated at 37 °C for at least 1.5 hours and was heat inactivated afterwards at 65 °C for 20 min.

3.2.7 Ligation

The T4 DNA Ligase was used to ligate the cut insert and vector. The 10x ligation buffer contains ATP and is dispensed in aliquots to prevent frequent thawing of the ligation buffer and the breakdown of ATP. The molar ratio of insert DNA to vector DNA was 1:1, 3:1 or 5:1, furthermore the reaction mixture contained 1x ligation buffer and 0.5 µl of T4 DNA Ligase. Incubation occurred over night at 16 °C with a heat inactivation at 65 °C for 10 min afterwards.

3.2.8 Mini-Preparation of Plasmid DNA

A mini-preparation was used to quantify plasmid DNA on a minimum scale. Column and non-column mini-preparations were performed. The column mini-preparations were used when the product should be very pure, e.g. when it was to be used for sequencing. It was performed with the GeneJet Plasmid Miniprep Kit from ThermoScientific according to the users manual.

The non-column mini-preparation was used when many potentially positive colonies were to be screened. The following buffers were needed.

P1	50 mM Tris/HCl, pH 8, 10 mM EDTA + 10 µg/ml Rnase (freshly added)
P2	200 mM NaOH, 1% SDS
P3	3 M potassium acetate, pH 5.5)

An overnight culture of a single colony of transformed bacteria was set up with 4 ml of LB-medium (+ selecting antibiotic). The incubated culture was centrifuged at 13,000 rpm for 2 min. The supernatant was removed and the cell pellet was resuspended in 200 µl P1. Then 200 µl P2 were added, the mixture was inverted and 200 µl P3 were added directly afterwards, whereafter the mixture was inverted once more. Then it was centrifuged at 13,000 rpm for 10 min. In the meantime tubes with 500 µl of ice cold isopropyl alcohol were prepared, in which the supernatant was filled after centrifugation. A further centrifugal step followed at 13,000 rpm for 15 min at 4 °C. After this step a small white DNA pellet should be observable. The supernatant was discarded and 500 µl of ice cold 70% ethanol

were added to the pellet and the tubes were centrifuged at 13,000 rpm for 2 min at 4 °C. The supernatant was discarded and the pellets dried at 60 °C for 20 min. Then 30 – 50 µl of ultrapure H_2O were added to the pellet.

3.2.9 Sequencing

To sequence vector DNA plasmids were purified via column mini-preparation at least 500 ng in a volume of 20 µl were sent to GATC Biotech. The sequencing primer was selected online out of a list of primers.

3.3 Protein Biochemical Methods

3.3.1 Heterologous Protein Expression in *Escherichia coli* BL21 (DE3) Δ*iscR*

Medium pre-culture:	LB-medium (5 g yeast extract, 10 g Trypton, 5 g NaCl /1 L), 100 µg/ml ampicillin, 50 µg/ml kanamycin
Medium main culture:	LB-medium, 100 µg/ml ampicillin, 50 µg/ml kanamycin, 100 mM MOPS/NaOH-buffer pH 7.4, 25 mM glucose, 2 mM NH_4-Fe(III)-citrate
Supplements to main culture for induction:	0.1 mM IPTG, 2 mM L-cystein, 25 mM Na-fumarat

Heterologous production of DsrL was preformed in *E. coli* BL21 (DE3) Δ*isc*R, which had been transformed with the DsrL encoding vector pET22bDsrL-CSt. *E. coli* BL21 (DE3) Δ*iscR* has a resistance against kanamycin and the pET22bDsrL-CSt plasmid contains an ampicillin resistance gene. Heterologous production of rDsrAB together with CysG and DsrN was also attempted in *E. coli* BL21 (DE3) Δ*isc*R, which had been transformed with pET22b_DsrABstrepC and pACYCDuet_cysG+dsrN or with pBAD_dsrABstrepN and pACYCDuet_cysG+dsrN. Both pET22b and pBAD contain an ampicillin resistance gene, while pACYCDuet encodes for a chloramphenicol resistance.

The preparatory culture containing 50 ml LB-medium with 50 µg/ml kanamycin and 100 µg/ml ampicillin (and 50 µg/ml chloramphenicol) was cultivated over night under aerobic conditions at 37 °C and 180 rpm. On the next day 950 ml of medium for the main

culture was inoculated with the pre-culture (5%). In addition to ampicillin and kanamycin (and chloramphenicol) the LB medium of the main culture contained 100 mM MOPS buffer pH 7.4, 25 mM glucose and 2 mM NH_4-Fe(III)-citrate as iron source for the formation of FeS clusters. The main culture was then cultivated at 37 °C and 180 rpm until it reached an OD_{600} of 0.3-0.5. Then the induction of DsrL expression was preformed due to the addition of 0.1 mM IPTG. Furthermore 2 mM L-cystein was added as sulfur source for the formation of FeS-clusters and 25 mM sodium fumarate were added for fumarate respiration. The cultures were divided into two 500 ml flasks and put under anoxic conditions in the anaerobic chamber. The flasks were swiveled in the anaerobic chamber for at least 5 min before they were closed with plungers. The anaerobic cultivation followed at 16 °C at 180 rpm for at least 65 h for DsrL and for rDsrAB various conditions were tested.

3.3.2 Heterologous Protein Expression in *Escherichia coli* BL21 (DE3)

Medium pre-culture:	LB-medium (5 g yeast extract, 10 g Trypton, 5 g NaCl /1 L), 100 µg/ml ampicillin
Medium main culture:	LB-medium (5 g yeast extract, 10 g Trypton, 5 g NaCl /1 L), 100 µg/ml ampicillin
Supplements to main culture for induction:	1 mM IPTG

The overexpression of DsrC and DsrC variants was performed in *E. coli* BL21 (DE3). pET-15b served as expression vector and provided the host cells with the vector-encoded ampicillin resistance needed for selection.

The preparatory culture containing 50 ml LB-medium with 100 µg/ml ampicillin was cultivated over night under aerobic conditions at 37 °C and 180 rpm. On the next day 1000 ml of LB-medium with 100 µg/ml ampicillin was inoculated with the pre-culture (5%) for the main culture. The main culture was also cultivated at 37 °C and 180 rpm until it reached an OD_{600} of 0.3-0.5. Then the heterologous protein expression was induced by the addition of 0.5 mM IPTG. After induction the cultures were cultivated for another 2 h under the same conditions.

3.3.3 Harvesting and Breaking of Cells

Bacterial cultures were harvested through centrifugation in a Beckmann Coulter Avanti J-20XP centrifuge (8,000 rpm for 15 min at 4 °C). The pellet was either stored at -20 °C or used directly in the next step of disruption.

In order to break the cells the pellet was thawed and resuspended in disruption buffer. Per 1 g pellet 5 ml of disruption buffer were used and spatula tip of DNase and dissolved cOmplete protease inhibitor cocktail tablets (Sigma Aldrich) was added. The cells were then broken with ultrasound for 20 min at 50% on step 7 per 20 ml of resuspended pellet. To remove the cell debris a centrifugation at 15,000 xg at 4°C for 30 min was performed. The supernatant then contained the soluble fraction of the harvested and the broken cells. For *E. coli* cells expressing DsrC and DsrC variants this was always performed under aerobic conditions. *A. vinosum* cell material containing DsrABL was harvested and broken under aerobic as well as anaerobic conditions.

Production organism	Protein	Disruption buffer
E. coli BL21 (DE3)	DsrC, DsrC variants	50 mM NaH_2PO_4/Na_2HPO_4, pH 7.5
E. coli BL21 (DE3) Δ*iscR*	DsrL	Buffer W (100 mM Tris/HCl, pH 8, 150 mM NaCl, 0.1% Triton- X100)
A. vinosum Δ*tsdA*	DsrABL	50 mM Tris/HCl pH 7.5

Harvesting and breaking of *E. coli* cells expressing DsrL was performed under anoxic conditions in the anaerobic chamber. The main culture, which had been cultivated under anoxic conditions was placed in the anaerobic chamber via air lock and filled into centrifugal units, which were closed with a sealing ring. The cells were harvested outside of the chamber through centrifugation at 8,000 rpm for 15 min at 4 °C. The centrifugal units were then again placed in the anaerobic chamber, the supernatant was discarded and the pellet was resuspended in disruption buffer DsrL. The breaking of cells was also performed under anoxic conditions with an ultrasound (Bandelin Sonopuls) inside of the anaerobic chamber for 2x 15 min at 50% per 20 ml of resuspended pellet. For ultrasonication the resuspended pellet was given into a small glass beaker, which was placed in a larger glass beaker filled with small ice pads to insure cooling of the sample. The broken cells were then filled into centrifugal units and centrifuged at 15,000 xg at 4 °C for 30 min to remove the cell debris. After centrifugation the centrifugal units were placed inside the anaerobic

chamber once more and the supernatant containing the soluble fraction was used in further purification steps.

For the anoxic harvesting and breaking of *A. vinosum* cells, the culture was filled from the 10 l fermenter into centrifugal units (2 l per centrifugal run, 8,000 rpm, 15 min, 4 °C). After the last 2 l were centrifuged, the centrifugal units were placed in the anaerobic chamber, the pellets were washed in anaerobic disruption buffer and centrifuged once more. Afterwards the pellet was capped anaerobically and frozen at -20 °C.

For the purification of DsrABL from *A. vinosum* cell material from several fermentations was combined, thawed and resuspended in disruption buffer. The further procedure was analogous to the breaking of cells expressing DsrL.

3.3.4 Purification of Recombinant DsrC via HisTrap™ HP 5 ml

Buffer	50 mM NaH_2PO_4/Na_2HPO_4, pH 8
Sample & binding buffer	Buffer + 10 mM imidazole
Washing buffer	Buffer + 60 mM imidazole
Elution buffer	Buffer + 250 mM imidazole

The HisTrap™ HP 5 ml was used according to the user's manual. H_2O_{dest}, buffers and samples were applied to the column interconnected to a 0.22 µm filter. The flow rate was 5 ml/min.

Column volumes (CVs)	Applied buffer or sample	Collect
5	H_2O_{dest}	Waste
5	Buffer + 300 mM imidazole	Waste
10	Binding buffer	Waste
	Sample	Flowthrough
10	Washing buffer	Wash
4	Elution buffer	Elution

After the elution of the protein, the columns were washed and stored at 4 °C.

Column volumes (CVs)	Applied buffer or sample
5	Washing buffer
5	H_2O_{dest}
2	20 % Ethanol

The flowthrough, wash fraction and elution fractions were stored on ice until further analysis.

3.3.5 Purification of Recombinant DsrL and rDsrAB via Strep-Tactin Affinity Chromatography

Binding, sample and washing buffer	Buffer W (100 mM Tris/HCl, pH 8, 150 mM NaCl, 0.1% Triton-X100)
Elution buffer	Buffer E (Buffer W + 2.5 mM desthiobiotin)
Regeneration buffer	Buffer R (Buffer W + 1 mM HABA (2-[4'-hydroxy-benzeneazo]benzoic acid)

The purification was performed under anoxic conditions in the anaerobic chamber. A 5 ml column was filled with 5 ml of Strep-Tactin (IBA-Lifesciences) after resuspending and inverting the flask. The remaining fluid was released via gravity flow and the column was equilibrated with 6 CVs of binding buffer.

Column volumes (CVs)	Applied buffer or sample	Collect
5	Binding buffer	Waste
	Sample	Flowthrough (FT)
2 x 5	Washing buffer	Wash (W)
6 x 0.5	Elution buffer	E1 - E6

After the elution of the protein, the columns were regenerated and stored at 4 °C overlaid with 2 ml buffer W.

Column volumes (CVs)	Applied buffer or sample
3 x 5	Buffer R
2 x 4	Buffer W

The flowthrough, wash fraction and elution fractions were stored on ice until further analysis. The elution fractions were sealed with plugs in order to stay under anoxic conditions.

3.3.6 Purification of rDsrABL from *A. vinosum*

Purification of the rDsrABL complex was followed by the characteristic absorbance of the sulfite reductase at 392 and 595 nm. Per purification 50 – 60 g of thawed cells (*A. vinosum* Δ*tsdA* grown on thiosulfate) were disrupted and purified via hydrophobic interaction chromatography and a following anion exchange chromatography. The purification steps were performed under aerobic and anaerobic conditions with an Äkta Purifier and an Äkta Start respectively.

Aerobic Purification

After disruption and centrifugation of the thawed cells, an ammonium sulfate precipitation at 4 °C was performed. The protein solution was brought to 40 % ammonium sulfate saturation (226 g/l) and was incubated under permanent stirring on ice for 10-16 h. Afterwards precipitated protein was removed by centrifugation (18 000 rpm, 20 min, 4 °C) and the supernatant was subjected to a low-substitution phenyl sepharose matrix (40 ml packed in a XK-50 column) equilibrated with 50 mM Tris/HCl, pH 7.5, 40 % $(NH_4)_2SO_4$ buffer. Unbound protein was removed by a wash step with at least two column volumes of 40 % ammonium sulfate buffer (50 mM Tris/HCl, pH 7.5, 226 g/l $(NH_4)_2SO_4$). Bound protein was eluted by decreasing the $(NH_4)_2SO_4$ concentration in a linear gradient from 40-0 % in ten column volumes. Fractions containing rDsrABL were combined, dialysed against 50 mM Tris/HCl, pH 7.5 over night and further purified via an anion exchange chromatography. The dialysed fractions were loaded onto a 12 ml Source 15Q column, which had been equilibrated with 50 mM Tris/HCl pH 7.5. The column was washed with

50 mM Tris/HCl, pH 7.5 containing 300 mM NaCl and proteins were eluted by an increase of NaCl in 50 mM steps. The fractions containing rDsrABL were combined, concentrated and stored under anaerobic conditions at -20 °C for longer storage or on ice for direct use.

Anaerobic Purification

After anaerobic disruption of the thawed cells and centrifugation of the anaerobically sealed centrifugal units, the ammonium sulfate precipitation was carried out under anaerobic conditions. Inside the anaerobic chamber 40 % ammonium sulfate (226 g/l) was added to the supernatant in a 250 ml Schott flask, which was closed with a sealing ring and contained a magnetic stirrer. The protein solution was stirred for 10-16 h on ice, thereafter precipitated protein was removed by centrifugation. The following purification step through hydrophobic interaction chromatography proceeded in a similar manner to the procedure described for the aerobic purification with the difference that the Äkta Start and the phenyl sepharose column were located in the anaerobic chamber and the wash step was performed with 50 mM Tris/HCl, pH 7.5, 28 % $(NH_4)_2SO_4$. Accordingly the following elution gradient went from 28-0 % ammonium sulfate. The following dialysis of the fractions containing rDsrABL was also carried out against anaerobic 50 mM Tris/HCl, pH 7.5 buffer. For the anion exchange chromatography a 4.7 ml HiScreen Q HP column was used with the same procedure described for the Source 15Q column above. The fractions containing rDsrABL were combined, concentrated and stored under anaerobic conditions at -20 °C for longer storage or on ice for direct use.

3.3.7 Concentration and Dialysis of Protein Solutions

After purification proteins were concentrated through repeated centrifugation in Millipore Amicon centrifugal filter concentrators at 4000 rpm for 10 min at 4 °C or in VivaSpin 500 centrifugal concentrators at 13,000 xg for 15 min at 4 °C. For dialysis the needed buffer was given to the concentrated protein solution and the solution was again concentrated. This was repeated until the protein solution was desalted.

3.3.8 Protein Quantification

The protein concentration was determined via BCA (Bicinchoninic-acid) assay with the BCA™ Protein Assay Kit (ThermoScientific) in a 96-well microtiter plate according to the users manual. Samples were diluted to three different concentrations and the calibrating

curve was generated through dilution of a 2 mg/ml BSA solution. The absorption at 562 nm was measured with Tecan Infinite®.

3.3.9 UV/Vis Spectroscopy

UV/Vis spectra were measured with an Analytic Jena Specord 210 spectrophotometer in a wavelength range from 250 to 750 nm. The samples were measured in 500 µl quartz cuvettes.

3.3.10 Polyacrylamide Gelelectrophoresis

Tricine SDS-PAGE:

Acrylamide solution	30 % Acrylamide-Bisacrylamidesolution (37.5:1) (Roth, Karlsruhe)
3x gel buffer	3 M Tris, 1 M HCl, 0.3% SDS, pH 8.45
10x anode buffer	1 M Tris, 0,225 M HCl, pH 8.9
10x cathode buffer	Tris 1 M, Tricin 1 M, SDS 2%, pH 8,25 (do not adjust)

For the electrophoretic separation of denatured proteins a Tricine SDS-PAGE (Sodiumdodecylsulfat-Polyacrylamide-Gelelektrophoresis) was performed. Due to the binding of SDS the intrinsic charge of the proteins is masked and they are separated only according to their molecular weight.

Tricine SDS-PAGE:

		resolving gel		**stacking gel**
	10 %	**12.5 %**	**15 %**	**4 %**
Acrylamide	4 ml	5 ml	6 ml	0.4 ml
H_2O_{dest}	4 ml	3 ml	2 ml	1.65 ml
3x gel buffer	4 ml	4 ml	4 ml	1.25 ml
10% APS	100 µl	100 µl	100 µl	100 µl
TEMED	5 µl	5 µl	5 µl	5 µl

First acrylamide solution, H_2O_{dest} and 3x gel buffer were mixed. To start the polymerization APS and TEMED were added to the solution for the resolving gel, which was then given into the gel chamber and a layer of 70% ethanol was added. After the complete polymerization the ethanol was put to waste. The solution for the stacking gel was given unto the polymerized resolving gel after addition of APS and TEMED and a gel comb was added in order to form gel pockets for the application of samples.

For reducing gels 4x Roti Load (reducing) was added to the samples, which were then heated for 5 min at 95 °C. For non-reducing gels used to analyze MalPEG gel shift assays 4x Roti Load (non-reducing) was added to the samples, which were not heated before loading them onto the gel.

The gel ran at 60 – 100 V with 1x anode and 1x cathode buffer as running buffers.

Blue Native PAGE

Acrylamide solution	48 % Acrylamide, 1.5 % Bisacrylamide
3x gel buffer	150 mM BisTris pH 7
3x anode buffer	50 mM BisTris pH 7
3x cathode buffer	15 mM BisTris pH 7, 50 mM Tricin, 0.02 % Coomassie G

For the electrophoretic separation of native proteins a Blue Native PAGE was performed. Coomassie binds to the protein complexes providing the charges needed for electrophoretic separation and visualizing the protein bands for later analysis.

Blue Native PAGE:

	gradient resolving gel		**stacking gel**
	5 %	**15 %**	**4 %**
Acrylamide	280 µl	853 µl	125 µl
H_2O_{dest}	1.6 ml	568 µl	875 µl
3x gel buffer	940 µl	940 µl	500 µl
87 % glycerol	-	464 µl	-
10% APS	11 µl	11 µl	14 µl
TEMED	1.5 µl	1.5 µl	1.5 µl

The 5 % and 15 % solutions for the gradient resolving gel were prepared with all components apart from APS and TEMED. Both resolving solutions were added to the gradient mixer with the higher concentrated solution in front. Then APS and TEMED were added to start the polymerization and the resolving gel was poured and a layer of 70 % ethanol was added. After the complete polymerization the ethanol was put to waste. The solution for the stacking gel was given unto the polymerized resolving gel after addition of APS and TEMED and a gel comb was added in order to form gel pockets for the application of samples.

The samples were prepared according to the following volume ratios:

25 Protein : **6** Coomassie Blue 0.1 % : **3** Glycerol 87 %

The gel ran at 6 mA (constant), 500 V, 15 W for approx. 1 h with 1x anode and 1x cathode buffer as running buffers.

3.3.11 Coomassie Staining of SDS-Gels

Coomassie staining solution	0.25% Coomassie Blue R250, 50% methanol, 10% glacial acetic acid, 40% $Aqua_{demin}$
Destaining solution	20% methanol, 10% glacial acetic acid, 70% H_2O

To stain the proteins in the SDS gels, these were incubated for at least 1 h in coomassie staining solution at RT. Afterwards the gels were washed with destaining solution several times until one could make out distinct protein bands. To wash away the solvents the gels were washed with H_2O_{dest}.

3.3.12 Western Blot Analysis

Towbin-buffer	3.04 g/l Tris, 14.58 g/l glycin, 20 % (v/v) methanol in rH_2O
1x PBS	4 mM KH_2PO_4, 10 mM Na_2HPO_4, 115 mM NaCl
Chloronaphtol solution	30 mg 4-chloro-1-naphtol solved 7 ml ice cold ethanol, filled up to 50 ml with rH_2O
H_2O_2 solution	30 % v/v H_2O_2

To specifically identify a protein of interest in the separated bands of a polyacrylamide gel an analysis via Western Blot was performed. The proteins were transferred from the polyacrylamide gel onto a nitrocellulose membrane (0.45 µm pore-size, Roth) by a semi-dry transfer. The transfer was performed with a Trans-Blot SD Semi-Dry Transfer Cell (Bio-Rad). The membrane and the gel were incubated in Towbin-buffer for 20 min. For the transfer two layers of 3MM Gel-Blotting-Paper Whatman (Roth) were soaked with Towbin-buffer and placed on the anode. Then the membrane was placed on top without trapping any air bubbles in the interface. The procedure was repeated with the gel and two further layers of 3MM Gel-Blotting-Paper soaked in Towbin-buffer. The protein transfer was performed at 15 V for 20-45 min depending on the size of the protein of interest.

After the transfer the membrane was incubated over night at 4 °C in PBS with 5 % milk powder. Afterwards the membrane was washed thrice for 5 min with 50 ml PBS at RT under gentle shaking. For the detection of rDsrAB expressed with an N-terminal Strep-tag attached to rDsrA or with a C-terminal Strep-tag attached to rDsrB the primary antibody StrepMAB Classic (IBA-Lifesciences), a monoclonal mouse antibody against Strep-tag, and the secondary antibody Goat Anti-Mouse IgG, HRP-conjugate (Merck) were used. After the last washing step 10 ml PBS buffer with 0.5 % BSA and 1:1000 diluted primary antibody were added to the membrane. An incubation of 3.5 h at RT under gentle shaking followed. Thereafter the membrane was washed thrice for 5 min in PBS buffer and the membrane was transferred into 20 ml PBS with 0.5 % BSA and 1:500 diluted secondary antibody. An incubation of 1.5 h at RT under gentle shaking followed. Then the the membrane was washed twice for 5 min in PBT (PBS with 0.1 % Tween-20) and thrice for

1 min in PBS. Then the membrane was transferred into 50 ml chloronaphtol solution and 20 µl H_2O_2 solution were added for the chromogenic reaction. The membrane was incubated under gentle shaking until a optimal signal:background ratio was achieved, then the reaction was stopped by washing several times with distilled H_2O.

3.3.13 Reduction and Persulfuration of DsrC

DsrC was reduced with the strong reducing agent Dithiothreitol (DTT). 4 mM DTT were added to DsrC and the mixture was incubated for 30 min at 30 °C. VivaSpin 500 centrifugal concentrators 5,000 MWCO PES (VivaProducts) were used to remove DTT from the DsrC solution.

3.4 Analytical Methods

3.4.1 MalPEG-Gel Shift assay

To analyze the redox state of DsrC and DsrC variants a gel-shift assay using the labeling reagent MalPEG (methoxy-polyethylene glycol maleimide MW 5000 g/mol, Fluka) (Venceslau *et al.,* 2013) was performed. MalPEG selectively binds to free thiol groups covalently (Lu and Deutsch, 2001). The molecular mass of the labeled protein is increased by approx. 10 kDa per SH group and this rise of molecular mass can by detected by SDS-PAGE.

In the assay the analyzed proteins were treated with 1 mM MalPEG at 30° for 15 min, the reaction was stopped by addition of 4x Roti Load (non-reducing) and loaded onto a 12.5% Tricine-SDS-PAGE without boiling the sample.

3.4.2 Detection of Sulfur Binding via MalPEG Gel Shift Assay

For the sulfur binding experiments 50 µM of DsrC or of a DsrC variant was first reduced with 5 mM DTT at 30 °C for 30 min in a 50 mM Na_2HPO_4 pH 7.5 buffer. VivaSpin 500 centrifugal concentrators 5,000 MWCO PES (VivaProducts) were used to remove DTT from the DsrC solution. The DTT concentration was diluted 1:100 via two centrifugation steps at 13,000xg for 15 min with the addition of a tenfold volume of buffer per centrifugation step. Then the reduced protein was incubated with 2 – 4 mM NaSH at 30 °C

for 1 – 2 h. Two further centrifugation steps followed to remove NaSH from the sample. The protein was then treated with 1 mM MalPEG at 30 °C for 15 min. Afterwards the unbound MalPEG was removed via two centrifugation steps and the sample was once more treated with the reducing agent DTT (5 mM, 30 °C, 30 min). Samples were taken after the first treatment with DTT, to determine whether DsrC was fully reduced, after the treatment with MalPEG, to discover if there were free thiol groups to which MalPEG could bind causing a gel shift or if an intramolecular trisulfide bond had formed leaving no free thiol groups, and after the second treatment with DTT, to analyze if MalPEG was bound to a thiol or a perthiol group. A perthiol group can be formed through the incubation with NaSH, then marked through the binding of MalPEG and reduced again with DTT to a thiol group, whereby MalPEG would no longer be bound to the protein. If however MalPEG was bound to a thiol group, it would stay bound to the protein after treatment with DTT. Thus sulfur binding was detected.

3.4.3 Mass Spectrometry

Mass spectral analysis was done via matrix-assisted laser desorption ionization time-of-flight mass spectrometry (MALDI-ToF) (Karas and Hillenkamp, 1988). Bands resolved after SDS-PAGE and Blue Native PAGE of rDsrABL-containing preparations were subjected to in-gel tryptic digestion followed by peptide identification in a MALDI-TOF/TOF analyser (Applied Biosystems 4800). The data were analyzed in a combined mode using Mascot search engine and NCBI database. Measurements and data processing were performed at the UniMS Mass Spectrometry Core Facility of ITQB NOVA, Oeiras, Portugal.

Recombinant DsrC was analyzed via MALDI-ToF after reduction with DTT and the reaction with rDsrABL and sulfite or after a control reaction without rDsrABL. The protein samples were concentrated and desalted using ZipTip C4 pipette tips (Merck Millipore) according to the users manual. The matrix solution was prepared by dissolving 7.6 mg 2,5-Dihydroxyacetophenon (2,5-DHAP) in 375 µl ethanol and adding 125 µl of an 18 mg/ml aqueous solution of diammoniumhydrogencitrate. 2 µl sample were mixed with 2 µl 2% trifluoroacetic acid, then 2 µl matrix solution were added and the solution was mixed until crystallization started. 2 µl of the crystal solution were pipetted onto the MALDI target plate and allowed to dry. MALDI mass spectra were produced on an UltrafleXtreme instrument (Bruker Daltonics, Bremen, Germany).

3.4.4 Size Exclusion Chromatography

To determine the oligomerization status of DsrC variants after the reaction with rDsrABL and sulfite they were analyzed via size exclusion chromatography. The analytical chromatography was performed using Äkta Purifier and a prepacked HiLoad 16/60 Superdex 75 prep grade column. The running buffer used was NaH_2PO_4 pH 8 150 mM NaCl. The DsrC solutions were concentrated to a volume of about 300 µl using Amicon Ultra 10K concentrator and applied to the column using a 500 µl loop.

3.4.5 Determination of Thiosulfate Concentration

The thiosulfate concentration of cell free culture supernatants was determined by means of a colorimetric test (Urban 1961). 200 µl sodium acetate (0.2 M, pH 4.8), 50 µl sodium cyanide (0.2 M) and 50 µl copper chloride (40 mM) were added to a sample of 650 µl (diluted 1:50). After vortexing the sample was transferred to a cuvette and 50 µl iron nitrate (300 g/L Fe(NO3)3 x 9 H2O, 22,1 % HNO3) were added. Afterwards the absorption at 460 nm was measured against 650 µl dH_2O treated the in the same manner as the samples. Samples containing thiosulfate (25 – 400 nmol) were used for calibration.

3.5 Enzymatic Activity Assays

All enzymatic activity assays were preformed in an anaerobic chamber (98% (v/v) N_2, 2% (v/v) H_2) at 30 °C in a final volume of 1 ml and were followed in a diode array spectrophotometer (Agilent 8453).

3.5.1 Enzymatic Reduction of Sulfite by rDsrABL

The enzymatic reduction of sulfite by rDsrABL was measured using methyl viologen, NADH or NADPH as electron donor. The assay mixtures contained 50 mM potassium phosphate buffer (pH 7.0 or 6.0, as needed), 1 mM methyl viologen (pre-reduced with zinc granules at 65 °C), NADH or NADPH, 3.5–50 µg/ml rDsrABL, and up to 15 µM reduced recombinant DsrC. Reactions were started by addition of sodium sulfite (up to 0.25 mM) if not stated otherwise. Methyl viologen and NAD(P)H oxidation were monitored at 585 nm (ε = 11.8 $mM^{-1}\,cm^{-1}$) and 340 nm (ε = 6.3 $mM^{-1}\,cm^{-1}$) (Bergmeyer, 1975; Ziegenhorn *et al.,* 1976), respectively. At concentrations exceeding 500 µM, NAD(P)H oxidation was followed

at 365 nm (ε = 3.4 mM^{-1} cm^{-1} for NADH and ε = 3.5 mM^{-1} cm^{-1} for NADPH (Bergmeyer, 1975) K_M and V_{max} values were calculated and figures were generated with GraphPad Prism 7.

To test if a bifurcation, in which electrons stemming from NADH can be used to reduce sulfite and DsrC in one partial reaction and ferredoxin in the other, 5 µM oxidized ferredoxin from *Clostridium tetenomorphum* were added to the reaction after NADH, rDsrABL and DsrC had been added. The reaction was started by addition of sodium sulfite.

3.5.2 NADH:Oxidoreductase Activity of rDsrABL

NADH-oxidizing activities of rDsrABL were measured by following the reduction of 300 µM thiazolyl blue tetrazolium bromide (MTT) at 578 nm (ε = 13 mM^{-1} cm^{-1}). MTT was dissolved in 75% (v/v) ethanol, 5% (v/v) Triton-X100 and 20% (v/v) H_2O. 50 mM potassium phosphate, pH 7.0 served as reaction buffer.

NAD^+-reducing activities of rDsrABL were measured by following the oxidation of 1 mM methyl viologen (pre-reduced with zinc granules at 65 °C) at 585 nm (ε = 11.8 mM^{-1} cm^{-1}).

3.5.3 NAD^+-Dependent Measurement of Ferredoxin Oxidation

The enzymatic oxidation of ferredoxin catalyzed by DsrL of the rDsrABL complex was measured using NAD^+ as electron acceptor. 50 mM potassium phosphate, pH 7.0 served as reaction buffer. First 8.3 µM ferredoxin from *C. tetanomorphum* were added to the reaction mixture, ferredoxin was then reduced by adding 10 µM sodium dithionite. Followingly 300 µM NAD^+ were added and the reaction was started with the addition of 8.4 µg rDsrABL. As the extinction coefficient of oxidized ferredoxin is higher (ε_{390} = 30 mM^{-1} cm^{-1}) than that of reduced ferredoxin (ε_{390} = 19 mM^{-1} cm^{-1}), ferredoxin reduction and re-oxidation was followed at 390 nm. Furthermore the reaction was followed at 340 nm to trace NAD^+ reduction.

3.5.4 Enzymatic Oxidation of DsrC-Bound Sulfur by rDsrABL

Persulfurated DsrC was used as substrate for the oxidation of DsrC-bound sulfur catalyzed by rDsrABL with several different potential electron acceptors. The assays were performed at pH 7 with 50 mM potassium phosphate as reaction buffer. The following electron acceptors with varying redox potentials were used in the given concentrations and traced

at the stated wavelengths respectively: 1 mM NAD^+ (E_0 = -320 mV) at 340 nm (ε = 6.3 mM^{-1} cm^{-1}), 300 µM MTT (E_0 = -110 mV) at 578 nm (ε = 13 mM^{-1} cm^{-1}), 1 mM ferricyanide (hexacyanidoferrat(III)) (E_0 = +360 mV) at 420 nm (ε = 0.9 mM^{-1} cm^{-1}) and 100 µM dichloroindophenol (E_0 = +220 mV) at 578 nm (ε = 7.6 mM^{-1} cm^{-1}) (Friedrich and Schink, 1993). For the assays with dichloroindophenol as artificial electron acceptor, 100 µM phenazine methosulfate (PMS) was used as electron shuttle. Up to 50 µg rDsrABL were added to the reaction mixture and the addition of upto 25 µM persulfurated DsrC should start the reaction.

4 Results

4.1 Heterologous Overexpression of rDsrAB from *Allochromatium vinosum*

For the structural and functional analysis of a protein it is essential to gain a sufficient amount of the protein in its isolated form. This can be achieved through purification from the organism the protein is originated from or through heterologous overexpression in a suitable production strain. The cultivation of *A. vinosum* under conditions, in which the expression of the dissimilatory sulfite reductase rDsrAB is upregulated, and the following purification of the protein complex are very time consuming and the protein yield is in relation to the expenditure of time quite low. Consequently rDsrAB fused to a Strep-tag was to be heterologously overexpressed in *E. coli* and purified by Strep-Tactin affinity chromatography.

4.1.1 Generation of an rDsrAB Overexpression Strain

The genes encoding for rDsrA and rDsrB, a*lvin_1251* and a*lvin_1252,* make up the beginning of the *dsr* operon in *A. vinosum*. The genes were amplified in two PCRs, with the primers DsrABstrepC'fw and DsrABstrepC'rev and with the primers DsrABstrepN'fw and DsrABstrepN'rev to create two PCR products encoding for rDsrAB, one in which rDsrB contains a C-terminal Strep-tag, while rDsrA contains an N-terminal Strep-tag in the other. The two different strategies were chosen to increase the probability of the Strep-tag being accessible without having a negative structural impact on the holoenzyme. The two inserts were cloned into the two plasmids pET22b and pBAD. Both plasmids encode for an ampicillin resistance needed for selection, contain a pBR322 origin of replication and a promoter region upstream of the multiple cloning site. In pET22b expression of the gene of interest is controlled by the T7 promoter and in pBAD by the araBAD promoter so that protein production can be specifically induced. The PCR product dsrABstrepC was cloned into pET22b via *Nde*I and *Hind*III (Figure 5A), while dsrABstrepN was cloned into pBAD, in the course of which pBAD was digested with *Nco*I and *Xba*I, while the insert was digested with *Bsp*HI and *Xba*I (Figure 5B). As *Nco*I cuts at the beginning of *rdsrB*, it could not by applied for the digestion of dsrABstrepN and *Bsp*HI, which generates identical sticky ends as *Nco*I, was used instead. As *Bsp*HI does not cut in the multiple cloning site of pBAD, but

at three other sites in the plasmid, it could not be used for the digestion of pBAD. Sequencing of pET22_dsrABstrepC and pBAD_dsrABstrepN showed that the generation of the two overexpression plasmids for rDsrAB had been successful.

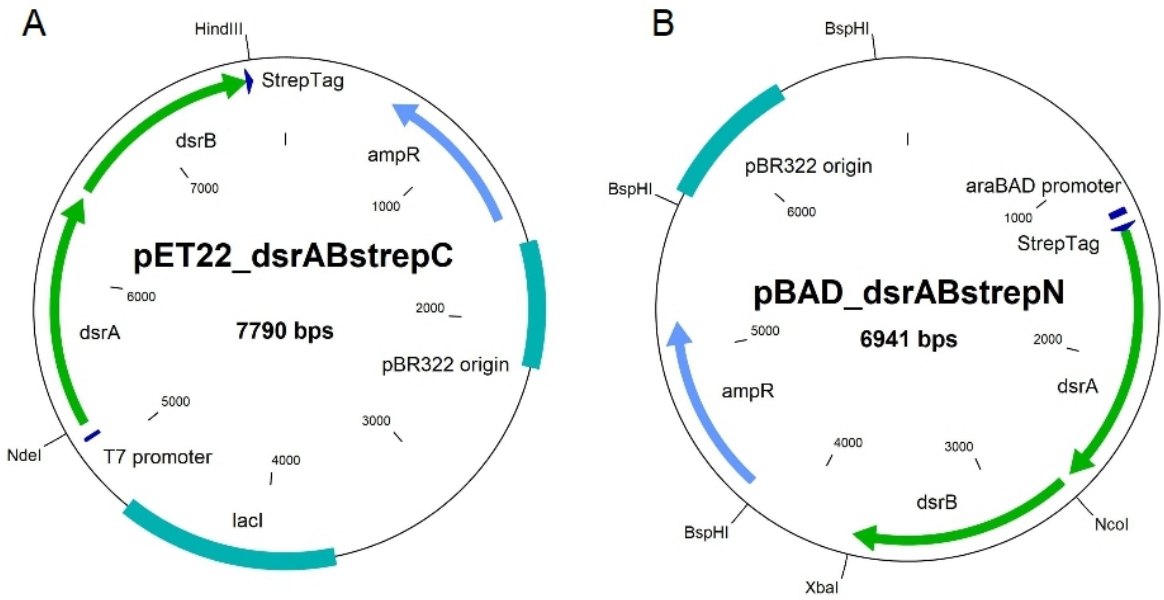

Figure 5: Recombinant plasmids pET22_dsrABstrepC and pBAD_dsrABstrepN for the production of rDsrAB from *A. vinosum*. (A) pET22_dsrABstrepC contains the genes *dsrA* and *dsrB* and encodes for a C-terminal Strep-tag. Gene expression is under the control of a T7 promoter. The gene *ampR* encodes for an ampicillin resistance needed for selection, *lacI* encodes for the lac repressor and the origin of replication is pBR322 origin. (B) pBAD_dsrABstrepN also contains the genes *dsrA* and *dsrB* and encodes for an N-terminal Strep-tag. Gene expression is under the control of a araBAD promoter. The gene *ampR* encodes for an ampicillin resistance needed for selection and the origin of replication is pBR322 origin.

The dissimilatory sulfite reductase of *A. vinosum* contains a siro(heme)amide cofactor, which is essential for its catalytic activity and possibly also for its structural assembly (Lübbe *et al.,* 2006). As *E. coli* also requires siroheme as cofactor of the assimilatory nitrite reductase and assimilatory sulfite reductase, it is able to synthesize siroheme from its precursor molecule uroporphyrinogen III, which is catalyzed by CysG (Spencer *et al.,* 1993). It is however probable that under standard cultivation conditions neither assimilatory nitrite nor sulfite reductase are expressed and consequently CysG will most probably not be expressed either. What is more, *E. coli* does not encode for DsrN, the enzyme needed for the final conversion from siroheme to siro(heme)amide (Lübbe *et al.,* 2006). In order to produce fully functional rDsrAB a coexpression with CysG and DsrN from *A. vinosum* was conducted.

For two different plasmids to remain stable in the same strain, they have to belong to two different plasmid incompatibility groups (Novick, 1987). For the coexpression of the siro(heme)amide synthesis genes the plasmid pACYCDuet-1 was chosen, as it has a p15A origin of replication and is thus in another plasmid incompatibility group as pET22B and pBAD. The gene expression in pACYCDuet-1 is under the control of a T7 promoter just as pET22b and pACYCDuet-1 encodes for a chloramphenicol resistance in contrast to pET22b and pBAD, which encode for an ampicillin resistance.

The genes *alvin_2598* and *alvin_1263* encode for CysG and DsrN respectively. Each gene was amplified by PCR, *cysG* with the primers CysG_SacI_for and CysG_NotI_rev and *dsrN* with the primers DsrN_NdeI_for and DsrN_XhoI_rev. The PCR product containing *cysG* was cloned into the first MCS of pACYCDuet-1 via *Sac*I and *Not*I and d*srN* was cloned into the second MCS via *Nde*I and *Xho*I (Figure 6). Sequencing of pACYCDuet_CysG+DsrN showed that the generation of coexpression plasmids had been successful.

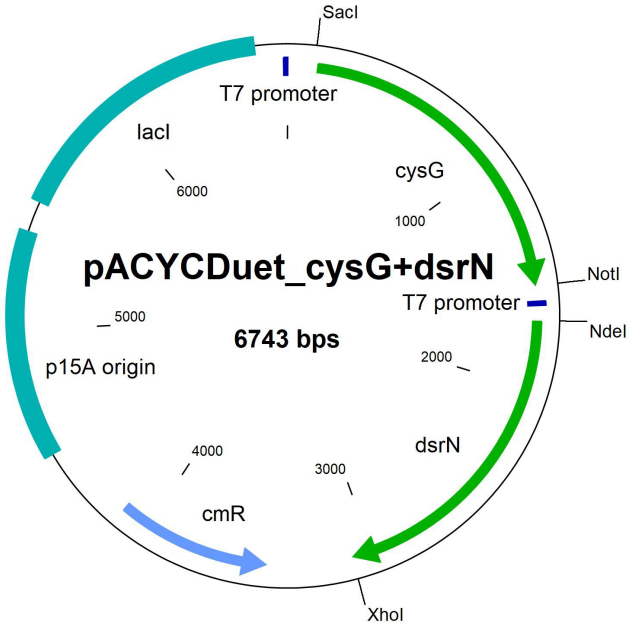

Figure 6: Recombinant plasmid pACYCDuet_cysG+dsrN for the production CysG and DsrN for siro(heme)amide synthesis. pACYCDuet_cysG+dsrN encodes for CysG and DsrN from *A. vinosum.* Gene expression is under the control of a T7 promoter. The gene *cmR* encodes for a chloramphenicol resistance needed for selection, *lacI* encodes for the lac repressor and the origin of replication is p15A origin.

4.1.2 Protein Expression

The plasmids pET22_dsrABstrepC and pBAD_dsrABstrepN encoding for the dissimilatory sulfite reductase rDsrAB from *A. vinosum* were to be transformed into a suitable production strain. The target protein complex does not only have the siro(heme)amide as prosthetic group, it also binds several iron-sulfur clusters. In *E. coli* the synthesis and assembly of iron-sulfur clusters is coordinated, inter alia, by proteins encoded in the *isc* operon (Johnson *et al.,* 2005). The transcription factor IscR is encoded in aforementioned operon and represses the expression of iron-sulfur cluster assembly proteins (Schwartz *et al.,* 2001). In order to enhance the iron-sulfur cluster load of recombinant proteins produced in *E. coli*, a strain lacking the *iscR* gene can be used for protein expression (Akhtar and Jones 2008). The protein complex rDsrAB loaded with iron-sulfur clusters and siro(heme)amide was to be produced in this strain, which will be called *E. coli* Δ*iscR* in the following. The plasmids pET22_dsrABstrepC and pBAD_dsrABstrepN were each transformed into competent *E. coli* Δ*iscR* cells via heat shock. Followingly competent *E. coli* Δ*iscR* pET22_dsrABstrepC cells and competent *E. coli* Δ*iscR* pBAD_dsrABstrepN cells were generated, in which pACYCDuet_cysG+dsrN was brought into.

The attempted overproduction was performed with iron ammonium citrate as iron source and cysteine as sulfur source (Kuchenreuther *et al.,* 2010) and was induced by addition of IPTG for rDsrAB from pET22_dsrABstrepC, CysG and DsrN and of arabinose for rDsrAB from pBAD_dsrABstrepN. In the shown results, cultivation was performed at 30 °C for 20 h under anaerobic conditions and pACYCDuet_cysG+dsrN was coexpressed with pET22_dsrABstrepC and pBAD_dsrABstrepN respectively. For the induction of protein production 0.1 mM IPTG and 0.0008 % arabinose were used. After harvesting the cells, they were lysed by ultrasonication and the cell debris as well as the soluble fraction was analyzed via SDS-PAGE and Western Blot (Figure 7). For the production strain containing pET22_dsrABstrepC and pACYCDuet_cysG+dsrN four distinct bands can be observed in the cell debris, two prominent bands running at approx. 37 kDa and 40 kDa and two slighter bands running at approx. 55 kDa and 57 kDa. For the production strain containing pBAD_dsrABstrepN and pACYCDuet_cysG+dsrN only three distinct bands are detectable in the cell debris at approx. 37 kDa, 55 kDa and 57 kDa. There is a great number of soluble proteins for both productions, with a few prominent bands running in proximity of the 40 kDa and 55 kDa marker proteins (Figure 7A). CysG has a molecular weight of

51.3 kDa, DsrN of 50.5 kDa, rDsrA of 46.8 kDa and rDsrB of 40 kDa, the fused Strep-tag to either rDsrA or rDsrB increases the molecular weight by 1.2 kDa. The above-mentioned bands in cell debris and soluble fraction could correlate with the to be produced proteins. However a Western Blot using antibodies against the Strep-tag showed that no signal could be detected in either production, while the positive control, HdrA fused to a Strep-tag, could be detected in the Western Blot (Figure 7B). Strep-Tactin affinity chromatography of the soluble proteins also resulted in no purified proteins (data not shown), which further indicates that no proteins fused to an accessible Strep-tag could be produced. A modification of the amount of inducing substances, temperature and incubation time after induction did not alter the results (data not shown).

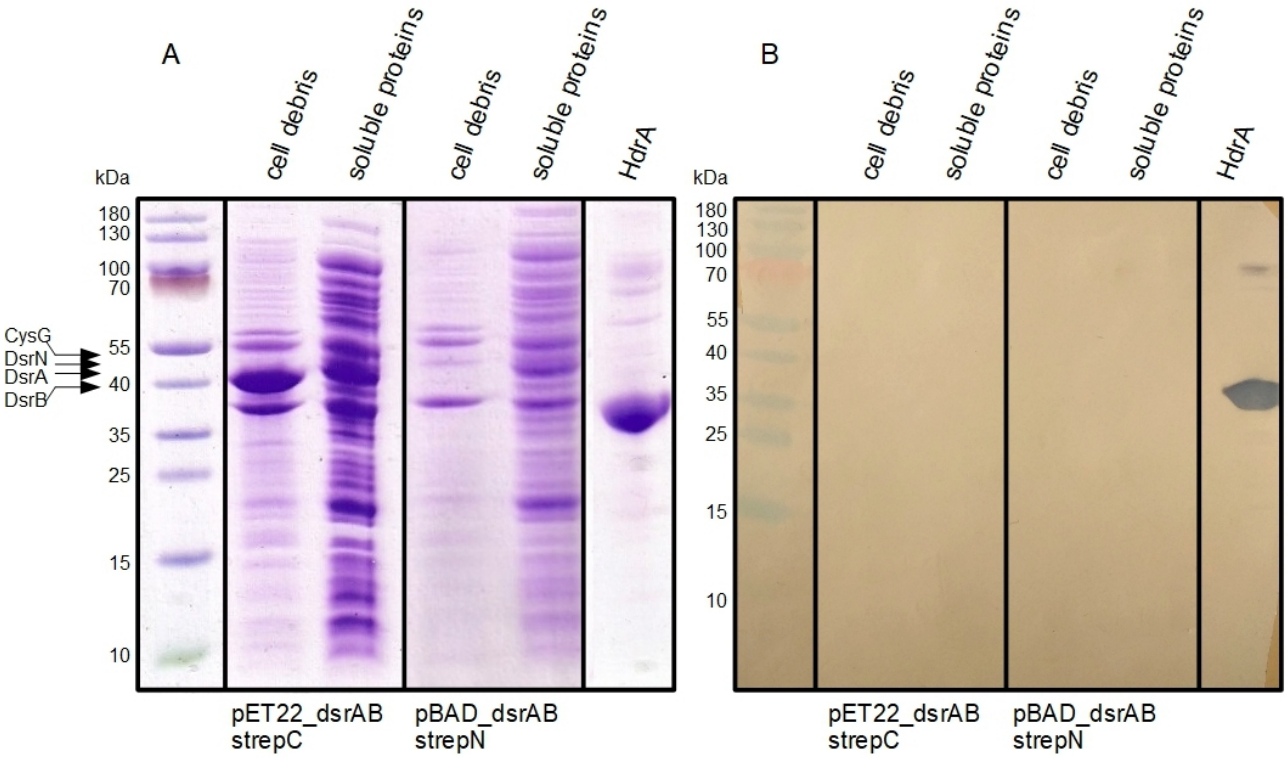

Figure 7: Analysis of rDsrAB production via SDS-PAGE and Western Blot. Heterologous production of rDsrAB was attempted in *E. coli* Δ*iscR* with pET22_dsrABstrepC and with pBAD_dsrABstrepN, which were each also equipped with pACYCDuet_cysG+dsrN. After cultivation and cell lysis, the cell debris and soluble proteins were separated and analyzed via SDS-PAGE (A) and Western Blot (B). For separation reducing 10 % Tricine SDS gels were used. A mouse anti-strep primary antibody and a goat anti-mouse secondary antibody were used to detect the Strep-tag fused to rDsrAB. Recombinant HdrA with a Strep-tag served as positive control. The PageRuler Protein Ladder from Thermo Scientific was applied as protein ladder.

4.2 Purification of rDsrAB from *Allochromatium vinosum* Δ*tsdA*

The purification of a protein from the organism it is originated from is often more time consuming and achieves lower protein yields than the heterologous production of a recombinant protein in *E. coli.* However it also has the advantage of obtaining the native protein without added affinity tags and it renders the potential of discovering possible interaction partners of the target protein by copurification. For the production of cell material containing rDsrAB, *A. vinsoum* was grown photolithoautotrophically on thiosulfate. Under these conditions expression of rDsrAB is upregulated, as the protein complex catalyzes a step in the oxidation of thiosulfate to sulfite. Due to the fact that TsdA can also use thiosulfate as a substrate for the oxidation to tetrathionate (Hensen *et al.,* 2006), the strain *A. vinsoum* Δ*tsdA* was used as production strain.

4.2.1 Purification of rDsrAB under Aerobic and Anaerobic Conditions

The purification of rDsrAB was performed under aerobic and anaerobic conditions in order to elucidate whether the purified protein complex is altered in its enzymatic activity, spectral properties and load with prosthetic groups under these different conditions. 50 g cells (wet weight) were gained from 30 l of *A. vinosum* Δ*tsdA* grown photolithoautotrophically on thiosulfate and used to purify the sulfite-generating rDsrAB complex under aerobic conditions. The first purification step was a hydrophobic interaction chromatography with a phenyl sepharose matrix, to which rDsrAB binds at high ammonium sulfate concentrations (Lübbe *et al.,* 2006). The soluble proteins of a 40 % ammonium sulfate precipitation were loaded onto an equilibrated phenyl sepharose column (40 ml). Unbound proteins were removed by a wash step with 40 % ammonium sulfate followed by a linear gradient to 0 % ammonium sulfate in ten column volumes (400 ml) (Figure 8A). As the interaction of the nonpolar protein surface regions with the hydrophobic matrix is dependent on the salt concentration, the bound proteins gradually eluted from the column during the linear decreasing ammonium sulfate gradient. Purification of rDsrAB was traced by UV/Vis spectroscopy taking advantage of the protein's characteristic absorption maxima at 392 and 595 nm (Schedel *et al.,* 1979). The rDsrAB complex eluted from 8–2.5 % ammonium sulfate.

Under anaerobic conditions the purification was carried out as mentioned above with the difference that the wash step was performed with 28 % ammonium sulfate to remove more undesired proteins before the elution step by linear gradient to 0 % ammonium sulfate in ten column volumes (Figure 8B). In this case rDsrAB eluted from 6–2.5 % ammonium sulfate.

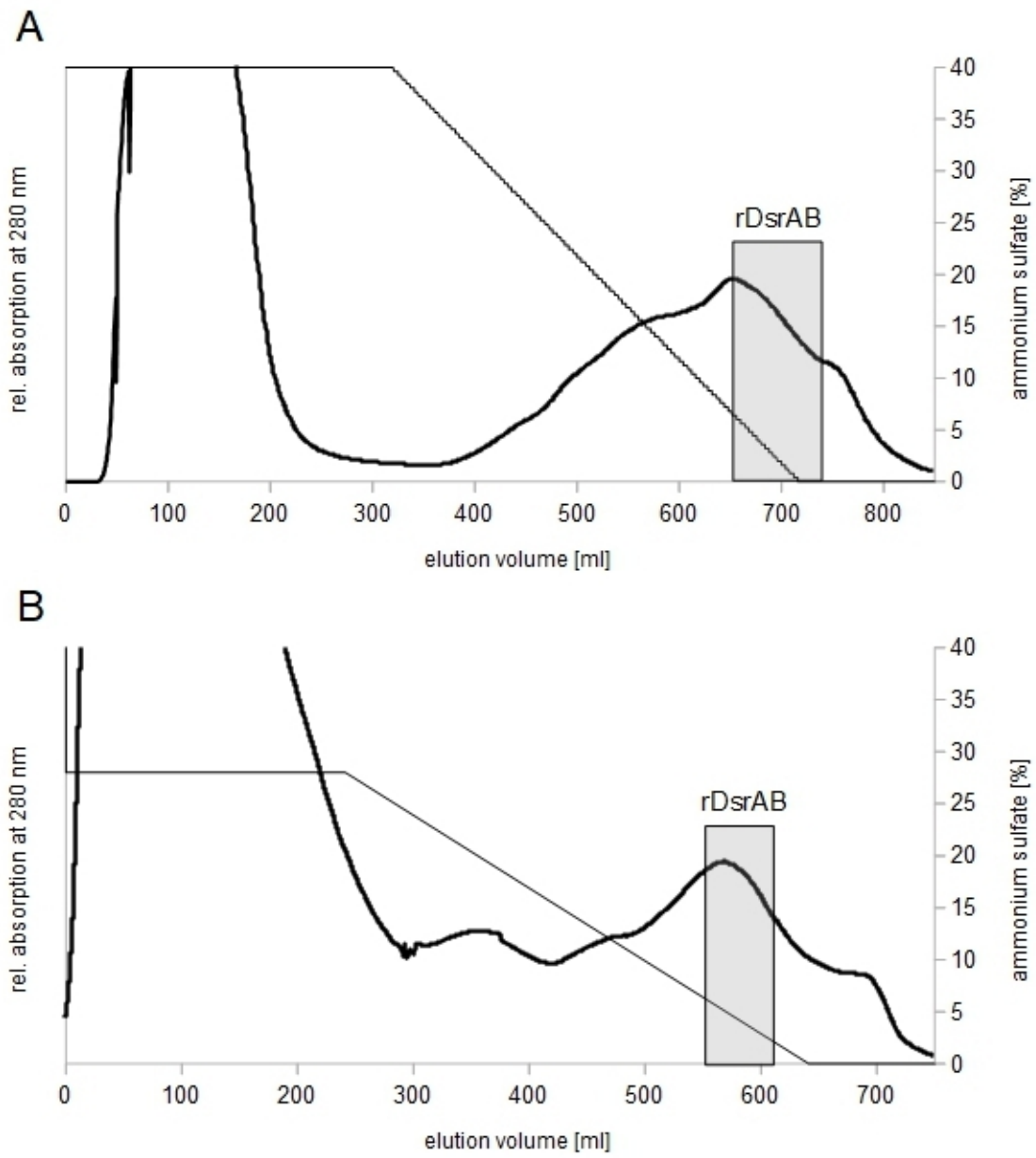

Figure 8: Characteristic elution profiles of rDsrAB purification step via hydrophobic interaction chromatography (Phenyl Sepharose 6 Fast Flow) under (A) aerobic and (B) anaerobic conditions. The relative absorption at 280 nm (thick black line) and the percentage of ammonium sulfate (thin black line) are plotted against the elution volume. They gray box indicates the elution region of rDsrAB.

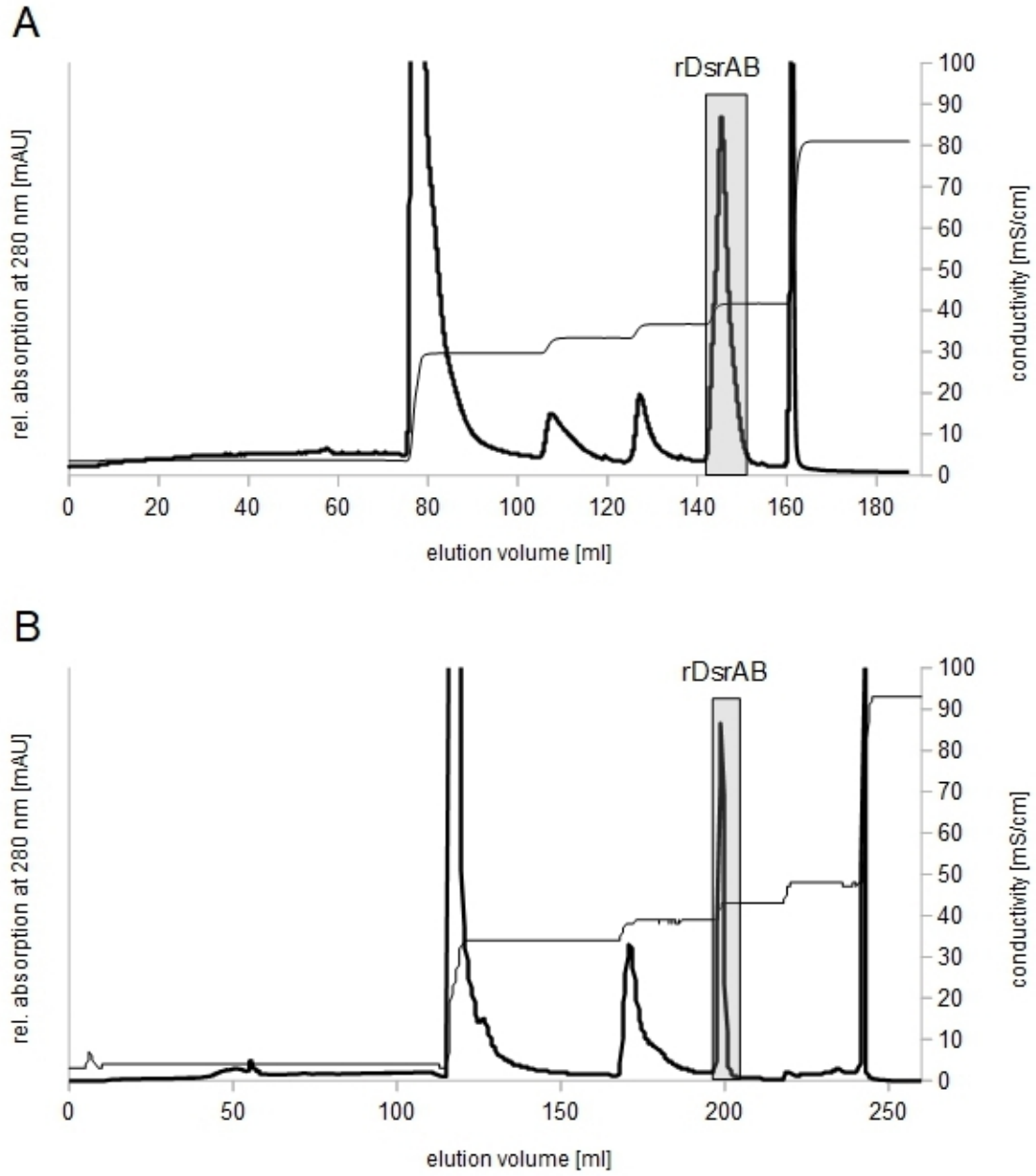

Figure 9: Characteristic elution profiles of rDsrAB purification step via anion exchange chromatography and (A) aerobic (Source 15Q) under (B) anaerobic (HiScreen Q HP) conditions. The relative absorption at 280 nm (thick black line) and the conductivity (thin black line) are plotted against the elution volume. The gray box indicates the elution region of rDsrAB.

The fractions containing rDsrAB were combined, dialysed and further purified via an anion exchange chromatography. The dialysed fractions were loaded onto a 12 ml Source 15Q column for the aerobic purification and onto a 4.7 ml HiScreen Q HP column for the

anaerobic purification. The columns were washed with 300 mM NaCl followed by an increase of NaCl in 50 mM steps, which led to an increase of conductivity. When conductivity was above 40 mS/cm rDsrAB eluted from the column (Figure 9A&B). Followingly the fractions containing rDsrAB were combined, concentrated and stored under anaerobic conditions.

Analysis via SDS-PAGE revealed that not only two bands of 40 kDa and 45 kDa correlating to rDsrB and rDsrA respectively, but also two further bands of about 55 kDa and 70 kDa could be detected in both the aerobic and the anaerobic purification (Figure 10). The contaminating band running at about 55 kDa was identified as the Glutamine synthetase Alvin_3000 by mass spectrometric analysis of tryptic peptides (Appendix, Table 7), while the 70 kDa band was assumed to correspond to the 72 kDa NADH:acceptor oxidoreductase DsrL, which is also encoded in proximity to rDsrAB in the *dsr* operon. The comparative analysis of rDsrAB purification displays that the copurification with DsrL is independent on aerobic or anaerobic conditions.

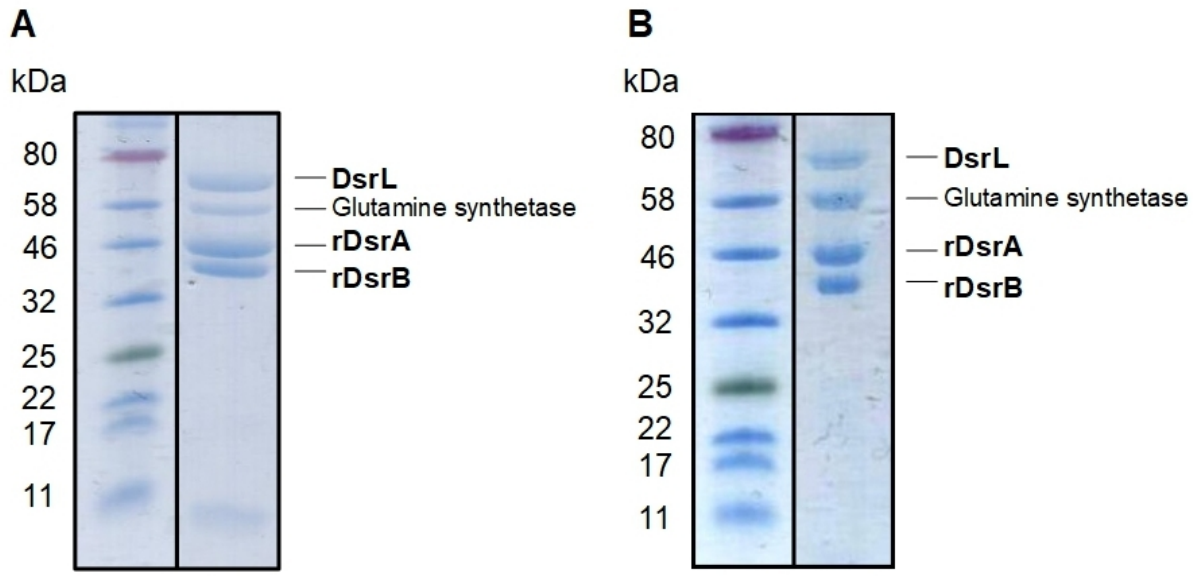

Figure 10: SDS-PAGE of the rDsrAB purifications after hydrophobic interaction chromatography and anion exchange chromatography under (A) aerobic and (B) anaerobic conditions. The Color Prestained Protein Standard, Broad Range from NEB was used as protein standard. The purified proteins were separated via reducing 12.5 % Tricine SDS gels.

4.2.2 Interaction of rDsrAB with DsrL

The copurification of the reverse acting dissimilatory sulfite reductase rDsrAB with the NADH:oxidoreductase DsrL was a first indication that these proteins specifically interact and build up a sulfite-generating rDsrABL complex in *A. vinosum*. For further evidence the preparations were analyzed via Blue Native polyacrylamide gel electrophoresis (Figure 11), which allows the separation of native proteins based only on their mass. The advantage of an analysis via native PAGE is that the conformation of proteins and protein complexes with regard to their oligomerization and interaction partners can be visualized.

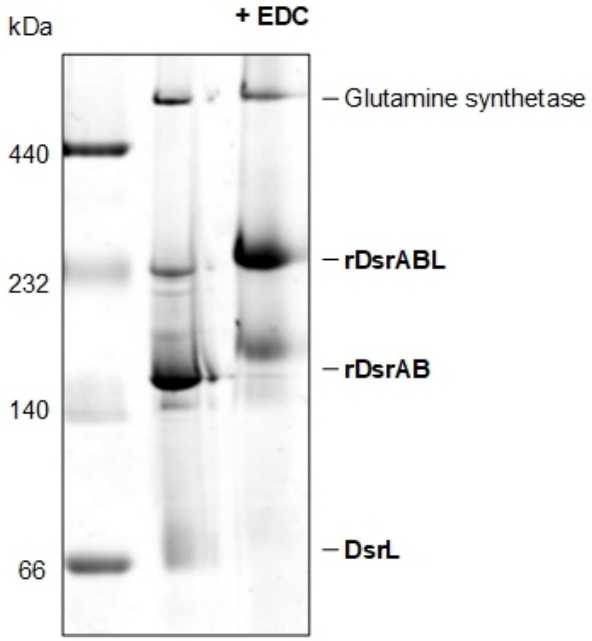

Figure 11: Analysis of rDsrABL purification via Blue Native PAGE. The HMW marker was used as protein standard. Purified rDsrABL was analyzed with and without pretreatment with EDC.

In the Blue Native PAGE of the rDsrAB purification the main band detectable has an estimated size of 170 kDa (Figure 11), which correlates with the calculated mass of a $rDsrA_2B_2$ heterotetramer (173 kDa) and indeed analysis of tryptic peptides via mass spectrometry confirmed the presence of rDsrA and rDsrB but not DsrL (Appendix, Table 8). A minor band was shown to contain rDsrA, rDsrB and DsrL (Appendix, Table 9) and ran at a calculated size of 283 kDa, indicating that rDsrAB interacts with DsrL and that they potentially form an rDsrABL complex. Furthermore a diffuse band at about 72 kDa was detectable, which likely consists of DsrL monomers. An additional minor band running at a

calculated size of 554 kDa represents the dodecameric glutamine synthetase (Eisenberg *et al.,* 2000) (Appendix, Table 10).

After preincubation with the cross-linker EDC (1-ethyl-3-(3-dimethylaminopropyl) carbodiimid) the migration pattern was altered (Figure 11). The 170 kDa band and the diffuse 72 kDa band, consisting of rDsrAB and DsrL respectively, substantially disappeared, while the 283 kDa band representing rDsrABL gained intensity. There was no alteration of the minor band consisting of the glutamine synthetase. These results confirm the assumed specific interaction of rDsrAB and DsrL, strongly portend the formation of an rDsrABL complex and demonstrate that the contaminating glutamine synthetase does not interact with rDsrABL nor with DsrL.

4.2.3 UV/Vis Spectroscopy of rDsrABL Purifications

A UV/Vis spectrum can provide useful information regarding the quality and quantity of prosthetic groups with spectral properties of a protein or protein complex. The purified rDsrABL complex contains several prosthetic groups, namely siro(heme)amid coordinated via [4Fe4S] clusters of rDsrAB, FAD ligated by DsrL and further [4Fe4S] clusters of both rDsrAB and DsrL. All of the aforementioned bear spectral properties and at least FeS cluster assembly is dependent on the exclusion of oxygen. Accordingly a comparative spectral analysis of the aerobic and anaerobic purifications of rDsrABL was performed (Figure 12).

In both the aerobically and anaerobically purified rDsrABL absorption maxima at 280 nm, 392 nm, 595 nm and 724 nm were detectable (Figure 12). The maximum at 280 nm represents the protein peak, while the 392 nm, 595 nm and 724 nm maxima are characteristic for rDsrAB (Schedel *et al.,* 1979). The two spectra of interest were normalized to 750 nm and to the 280 nm peak. No qualitative differences between the aerobic and anaerobic purifications of rDsrABL are detectable. The 392 nm absorption of the anaerobic purification is slightly higher than that of the aerobic purification. This is presumably due to a higher relative concentration of rDsrAB and consequently also of siro(heme)amide in the purification.

Neither the reduction with dithiothreitol (DTT) nor the oxidation with ferricyanide led to qualitative changes of the spectrum (data not shown). FAD has several absorption maxima between 350 nm and 500 nm, however siroheme has an about tenfold higher extinction

coefficent at e.g. 450 nm (Schedel *et al.,* 1979; Aliverti *et al.,* 1999), therefor the detection of FAD is prevented by the presence of the siro(heme)amide.

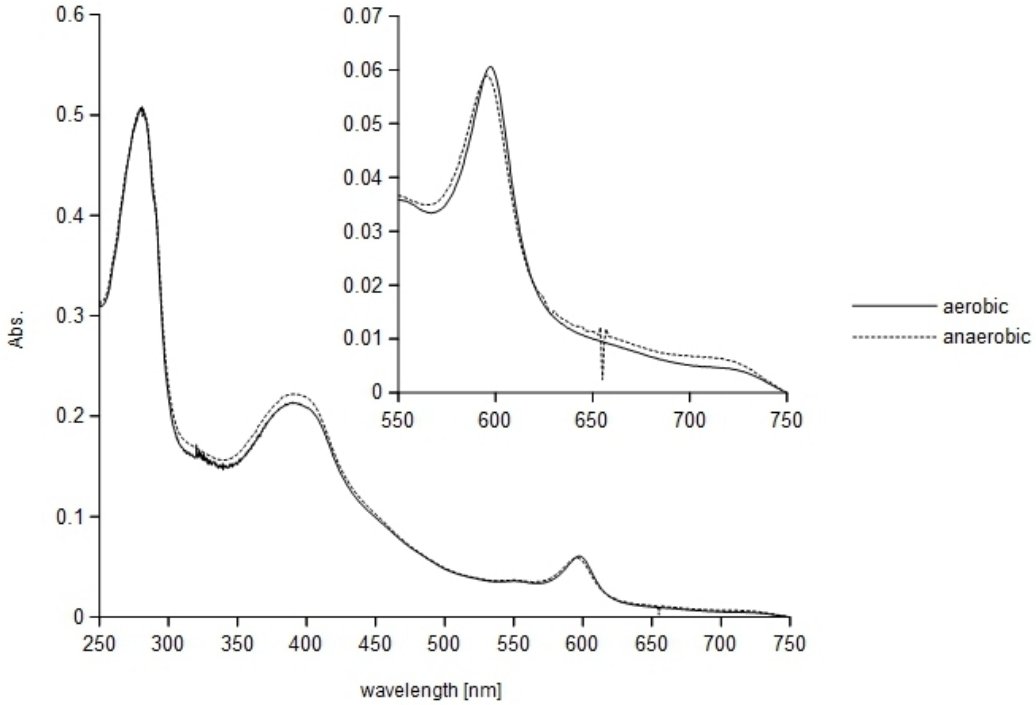

Figure 12: UV/Vis absorption spectra of purified rDsrABL. The spectra of rDsrABL purified under aerobic (solid line) and anaerobic conditions (dotted line) were recorded at RT in a 50 mM potassium phosphate pH 7.0 buffer. The two spectra were normalized to 750 nm and to the 280 nm peak. The inset shows a blowup of the 550 to 750 nm region.

4.3 Enzymatic Activity of rDsrABL

The physiological activity of *A. vinosum* rDsrAB is predicted to be the oxidation of DsrC-bound sulfur to sulfite (Stockdreher *et al.,* 2012). Interaction of DsrAB from the sulfate reducers *A. fulgidus* and *D. vulgaris* with DsrC has been shown previously (Oliveira *et al.,* 2008; Santos *et al.,* 2015), however no structural or kinetic data exists for the interaction of rDsrAB with DsrC from a sulfur oxidizer. The copurification of rDsrAB with the NADH:oxidoreductase DsrL also implies a functional interaction, which is to be tested. In the following the enzymatic activity of rDsrAB from *A. vinosum* will be characterized with a special focus on the potential interaction partners DsrL and DsrC. All assays were performed under anoxic conditions.

4.3.1 Reduction of Sulfite with rDsrABL in Presence of DsrC

For rDsrAB from the sulfur oxidizer *A. vinosum* sulfite reductase activity with methyl viologen has been described (Schedel *et al.,* 1979). Furthermore DsrAB from the archaeal sulfate reducer *Archaeoglobus fuldigus* is known to show an increased sulfite reduction rate, when the sulfur-binding protein DsrC is added to the reaction (Santos *et al.,* 2015). In order to elucidate whether this also holds true for the dissimilatory sulfite reductase of a sulfur oxidizer, recombinant DsrC from *A. vinosum* was added to the reaction with methyl viologen as artificial electron donor. Without DsrC a sulfite reduction rate of 0.14 U/mg protein was measured, while the reaction with 7.5 µM DsrC displayed an initial fast reaction rate of 2.0 U/mg, which then slowed to a rate of 0.22 U/mg (Figure 13). Hence in the following rDsrABL-catalyzed sulfite reduction was measured in the presence of DsrC.

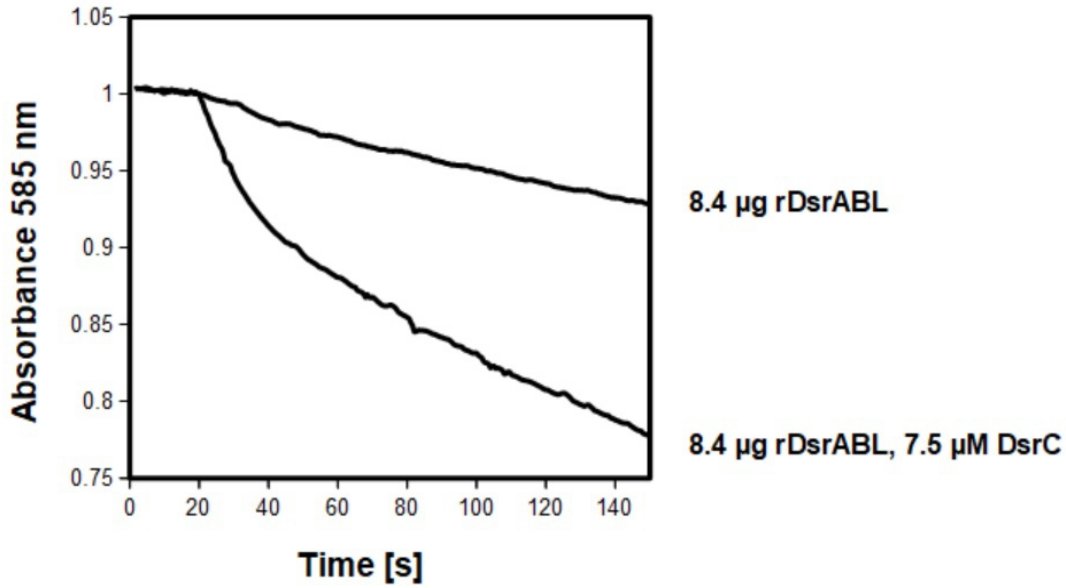

Figure 13: Effect of DsrC on sulfite reduction by *A. vinosum* rDsrABL with methyl viologen. Reactions contained 250 µM sulfite, 8.4 µg rDsrABL and were measured with and without 7.5 µM *A. vinosum* DsrC at pH 7. Methyl viologen was used as artificial electron donor and its oxidation was followed at 585 nm (ε_{585}= 11.8 mM^{-1} cm^{-1}).

Through application of varying substrate concentrations, it could be demonstrated that the specific activity of rDsrABL is dependent on the amount of sulfite added to the reaction (Figure 14A). The specific activity of rDsrABL is at its maximum with 250 µM and 150 µM sulfite and it slightly decreases until 25 µM sulfite. At lower sulfite concentrations like

6.25 µM and 3.125 µM only mere fractions of the maximum specific activity could be measured. Michaelis-Menten kinetics could be applied when the specific activity of rDsrABL was plotted against the sulfite concentration with the program Graph Pad Prism 7 (Figure 14B). This demonstrated a quite low K_M for sulfite (13.5 ± 2.1 µM) and a high V_{max} (1728 ± 62 mU/mg).

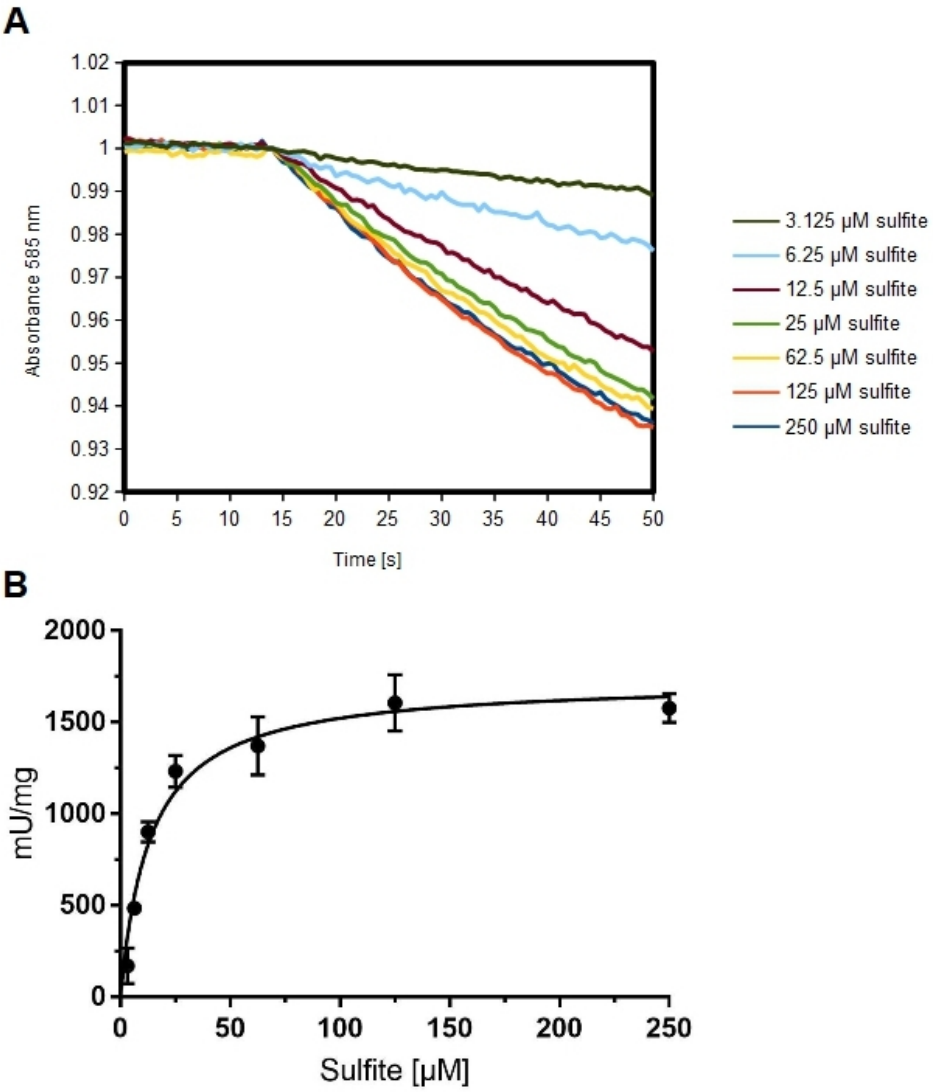

Figure 14: Activity of rDsrABL from *A. vinosum* with varying sulfite concentrations. Assays were measured in the presence of 3.75 µM DsrC at pH 7, with methyl viologen (ε_{585}= 11.8 mM^{-1} cm^{-1}) as artificial electron donor and with sulfite concentrations from 3.125-250 µM. (A) Representative traces are shown and (B) triplicates of the specific activity of rDsrABL were plotted against the sulfite concentration. Michaelis-Menten kinetics model was applied by Graph Pad Prism 7.

4.3.2 Electron Transfer via DsrL of the Purified rDsrABL Complex

As DsrL is an iron-sulfur flavoprotein, it theoretically has the capability of transferring electrons from an electron donor to an electron acceptor in an enzymatic reaction. The copurification of DsrL with rDsrAB and their tight interaction indicate that DsrL could mediate the electron flow needed for sulfite reduction. The iron-sulfur flavoprotein DsrL from *A. vinosum* was shown to exhibit NADH:oxidoreductase activity (Löffler *et al.,* 2020), it is therefor probable that the rDsrABL complex can transfer electrons to and receive electrons from NADH via DsrL.

4.3.2.1 NADH:Oxidoreductase Activity of DsrL from rDsrABL

For recombinant DsrL an NADH:oxidoreductase activity was verified and demonstrated to be independent on the FeS clusters of DsrL, as activity could be measured with anaerobically and aerobically purified DsrL (Löffler *et al.,* 2020). To ascertain that DsrL from the purified rDsrABL complex also exhibits NADH:oxidoreductase activity, it was tested whether electron transfer from NADH to the artificial electron acceptor MTT (thiazolyl blue tetrazolium bromide) and from the artificial electron donor methyl viologen to NAD^+ is possible via rDsrABL (Figure 15).

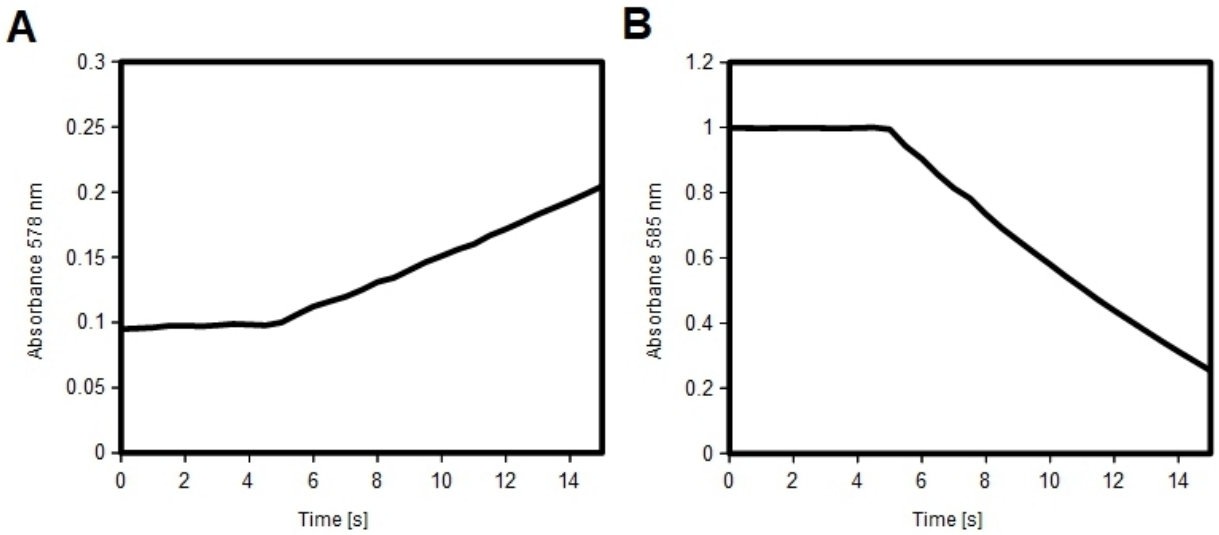

Figure 15: NADH:oxidoreductase activity of rDsrABL. (A) The assay contained 1 mM NADH, 0.3 mM MTT (ε_{578}= 13 mM^{-1} cm^{-1}) and 7.6 µg rDsrABL. Reduction of MTT was followed at 578 nm. (B) The assay contained 1 mM methyl viologen (ε_{585}= 11.8 mM^{-1} cm^{-1}), 1 mM NAD^+ and 7.6 µg rDsrABL. Oxidation of methyl viologen was followed at 585 nm. Both assays were preformed at pH 7 and rDsrABL was added after 5 s.

Electrons stemming from NADH could be transferred to MTT via rDsrABL with a specific activity of 5.9 U/mg (Figure 15A) and NAD^+ could be reduced with electrons stemming from methyl viologen in a rDsrABL dependent manner with an about 9-fold higher specific activity of 49.3 U/mg (Figure 15B). The strong preference for NAD^+ reduction was also observed in recombinant DsrL from *A. vinosum* (Maria Löffler, personal communication). After reconstitution of FeS clusters in rDsrABL NADH:oxidoreductase activity was not increased (data not shown).

4.3.2.2 Electron Transfer from NAD(P)H unto rDsrAB Mediated by DsrL

As the activity of rDsrABL as NADH:oxidoreductase had been confirmed, the next step was to determine whether electrons stemming from NADH could be transferred via DsrL onto rDsrAB and finally be used for sulfite reduction.

As a control experiment it was tested if recombinant DsrL alone could catalyze NADH-dependent sulfite reduction in the presence of DsrC (Figure 16). Apart from a slight background reaction no activity could be observed in this assay. Addition of rDsrABL however resulted in the reduction of sulfite and the reduction rate increased with an increasing amount of the catalyst rDsrABL from 10 µM/min with 23 µg rDsrABL to 25 µM/min with 92 µg rDsrABL (Figure 16).

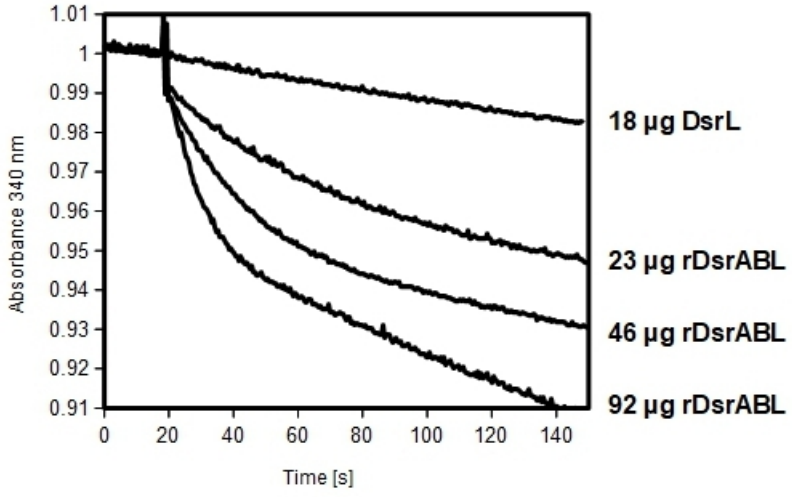

Figure 16: Potential of DsrL and of rDsrABL for NADH-dependent sulfite reduction. Assays contained 150 µM NADH, 250 µM sulfite, 7.5 µM DsrC and either 18 µg DsrL or varying amounts of rDsrABL. All assays were performed at pH 7 and NADH oxidation was followed at 340 nm (ε_{340}= 6.3 mM^{-1} cm^{-1}).

With NADH as electron donor the K_M for sulfite (15.9 ± 3.1 µM) was determined to be in the same range as that observed for rDsrABL with methyl viologen as electron donor (Figure 17A, Figure 14B). Consequently the affinity towards the substrate sulfite is not altered when electrons stem from NADH and are transferred via DsrL onto rDsrAB. The affinity towards the new substrate NADH (78.5 ± 21.0 µM) (Figure 17B) is also very close to that determined for recombinant DsrL in assays with NADH and the artificial electron acceptor MTT (86.7 ± 17.0 µM) (Löffler *et al.,* 2020). However V_{max} was with 254 ± 17.6 mU/mg substantially lower than V_{max} measured with methyl viologen as artificial electron donor for sulfite reduction. The in Figure 16 and Figure 17 displayed results were obtained with aerobically purified rDsrABL. Activity measured with rDsrABL purified under anoxic conditions and the aerobically purified protein complex reconstituted *in vitro* with FeS clusters was in the same range as the here described activity (data not shown).

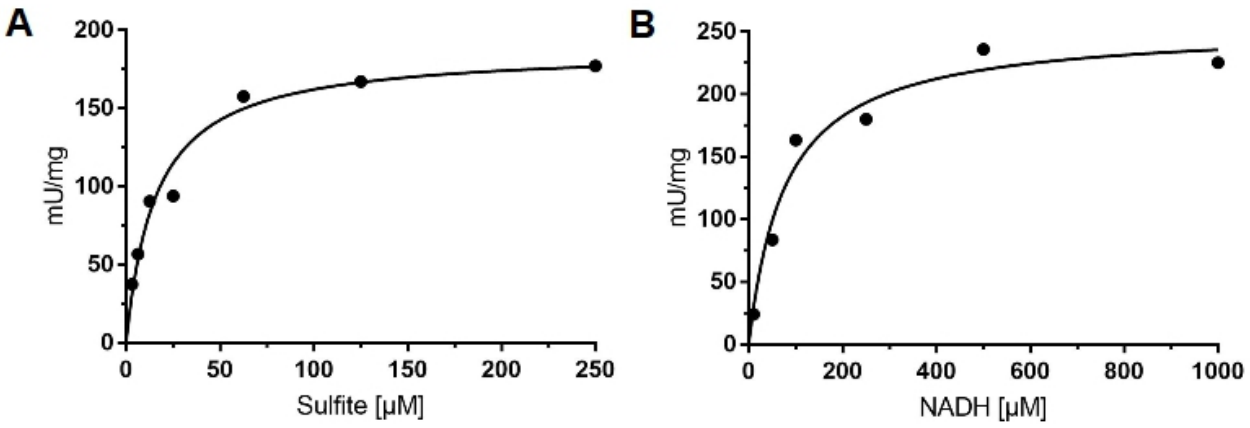

Figure 17: NADH-dependent sulfite reduction catalyzed by rDsrABL. (A) Assays contained 150 µM NADH, 3.75 µM DsrC and sulfite concentrations from 3.125-250 µM. NADH oxidation was followed at 340 nm (ε_{340}= 6.3 mM^{-1} cm^{-1}). (B) Assays contained 250 µM sulfite, 3.75 µM DsrC and varying NADH concentrations (10-1000 µM). For NADH concentrations from 10-250 µM, absorbance was measured at 340 nm, for 500 µM and 1000 µM at 365 nm (ε_{365}= 3.4 mM^{-1} cm^{-1}). All assays were measured at pH 7.

Furthermore the NADH-dependent sulfite reduction rate of aerobically purified rDsrABL was compared to that of aerobically purified rDsrABL, which was preincubated with recombinant DsrL for 15 min at 30 °C (Figure 18). As the recombinant DsrL is fully loaded with FAD and FeS clusters, it could presumably enable a more efficient electron transfer from NADH onto rDsrAB and thus lead to a higher sulfite reduction rate. The results of Figure 18 however demonstrate that this is not the case. The sulfite reduction rates of solely rDsrABL and of rDsrABL preincubated with DsrL are in the same range.

NADPH was tested as alternative electron donor for rDsrABL. With NADPH the specific activity at pH 7 was under 20% of that observed with NADH, however the activity could be increased 3-fold when the pH was shifted to 6 (data not shown).

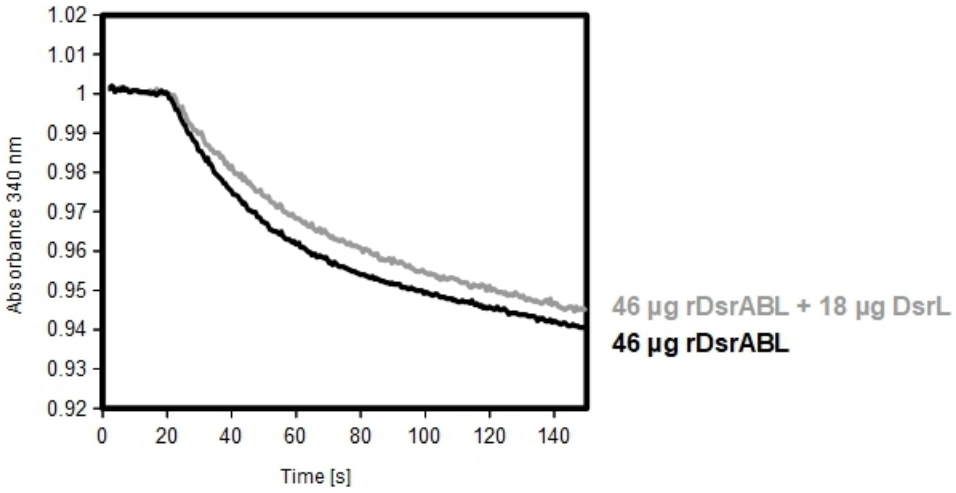

Figure 18: Impact of recombinant DsrL on NADH-dependent sulfite reduction catalyzed by rDsrABL. Both assays contained 150 µM NADH, 250 µM sulfite and 7.5 µM DsrC. The reaction catalyzed by 46 µg rDsrABL (black curve) is compared to the reaction catalyzed by 46 µg rDsrABL, which was preincubated with 18 µg recombinant DsrL for 15 min at 30 °C (gray curve). The assays were performed at pH 7 and NADH oxidation was followed at 340 nm (ε_{340}= 6.3 mM^{-1} cm^{-1}).

4.3.2.3 Electron Transfer Between rDsrABL and Ferredoxin

The iron-sulfur flavoprotein DsrL is closely related to NfnB, the large subunit of the NADH-dependent reduced ferredoxin:NADP oxidoreductase NfnAB from *Thermotoga meritima* (Demmer *et al.,* 2015). The structurally and functionally characterized protein complex NfnAB catalyzes a reversible electron bifurcation, in which two electrons stemming from NADPH are used to reduce ferredoxin and NAD^+. The large subunit NfnB binds NADPH, the bifurcating FAD and reduces ferredoxin, while the reduction of NAD^+ occurs at NfnA (Demmer *et al.,* 2015).

There are several structural similarities between DsrL and NfnB, namely an iron-sulfur cluster binding domain, two Rossmann type nucleotide-binding domains, one binding FAD and the other $NAD(P)^+$ (Löffler *et al.,* 2020). Additionally DsrL has a carboxyl-terminal ferredoxin domain binding two [4Fe4S] clusters, which is not found in NfnB. It has already been demonstrated that DsrL can bind, receive electrons from and transfer electrons to

NADH and NAD^+ respectively. Electron transfer to another protein complex is also possible, similar to the described electron transfer from NfnB to NfnA. Possibly DsrL can also interact with ferredoxin and the FAD bound can likewise enable bifurcation.

To discover whether an electron transfer between DsrL of the rDsrABL complex and ferredoxin is possible, reduced ferredoxin ($E^{0'}$ = ~ -400 mV) from *Clostridium tetanomorphum* was used as a potential electron donor for DsrL-catalyzed NAD^+ reduction (Figure 19). The reaction was followed at 340 nm to measure NAD^+ reduction and at 390 nm to display ferredoxin reduction and re-oxidation, as the extinction coefficient of oxidized ferredoxin is higher (ε_{390} = 30 $mM^{-1}\,cm^{-1}$) than that of reduced ferredoxin (ε_{390} = 19 $mM^{-1}\,cm^{-1}$).

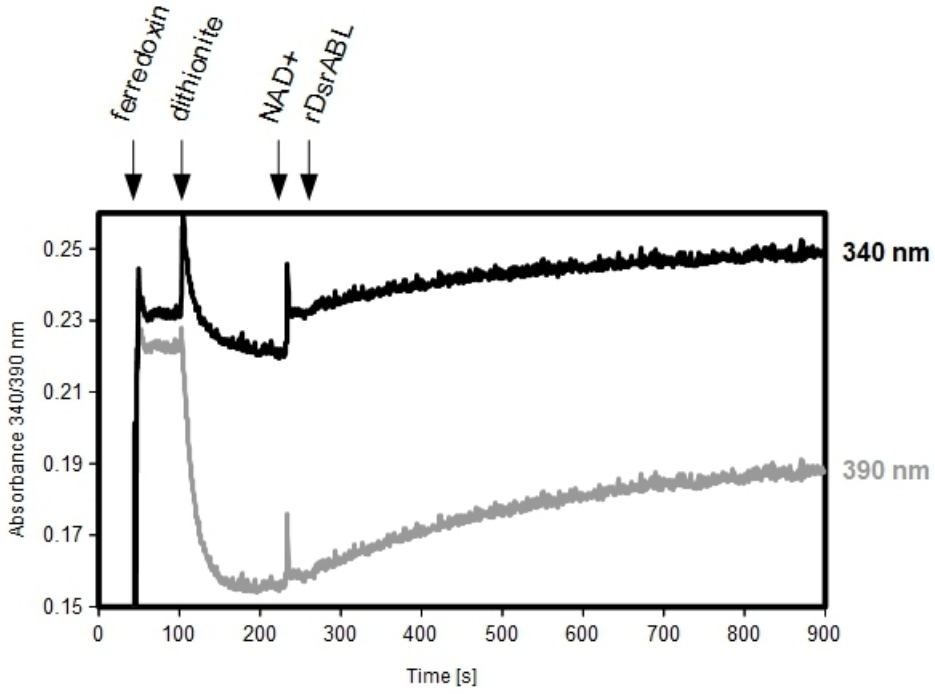

Figure 19: Reduced ferredoxin as electron donor for DsrL-catalyzed NAD^+ reduction. The reaction was followed at 340 nm (black curve) and 390 nm (gray curve). The assay contained 8.3 µM ferredoxin, 10 µM sodium dithionite, 300 µM NAD^+ and 8.4 µg rDsrABL and was performed at pH 7.

As the assay contained 8.3 µM ferredoxin, absorbance at 390 nm was expected to be at 0.25 with fully oxidized ferredoxin. Absorbance was at 0.22, which indicates that the applied ferredoxin was not fully oxidized. After addition of an equimolar amount of the reductant sodium dithionite, the absorbance decreased to about 0.155, which is very close

to the expected 0.157 for fully reduced ferredoxin. The addition of NAD^+ led to no substantial increase of 390 nm absorbance, indicating that the redox status of ferredoxin was not altered. When rDsrABL was added to the reaction, absorbance at 390 nm gradually increased from 0.155 to 0.19 displaying a partial re-oxidation of ferredoxin. Simultaneously absorbance at 340 nm also increased, indicating a reduction of NAD^+ to NADH (Figure 19).

The presented results were obtained with aerobically purified rDsrABL. Assays containing *in vitro* FeS cluster reconstituted rDsrABL provided similar results (data not shown). Taken together these results demonstrate that reduced ferredoxin can function as electron donor for DsrL-catalyzed NAD^+ reduction.

Based on the assumption that DsrL is, in homology to NfnB, the subunit enabling bifurcation, one electron stemming from NADH ($E^{0'}$ = -320 mV) could be transferred onto rDsrABL to reduce sulfite and DsrC, as has been already demonstrated, while the other electron is used to reduce ferredoxin. In case of an electron bifurcation, the first partial reaction, in which sulfite and DsrC are reduced, should proceed with an increased activity rate, while the second partial reaction of ferredoxin reduction would be generally enabled (Kaster *et al.,* 2011). To address this hypothesis, NADH-dependent sulfite reduction catalyzed by rDsrABL in the presence of DsrC was performed with and without oxidized ferredoxin and the assays were traced at 340 nm (Figure 20A) and 390 nm (Figure 20B), in order to follow NADH oxidation and ferredoxin reduction respectively. As a control an assay without the catalyzing enzyme complex rDsrABL, but with ferredoxin is also displayed (Figure 20). Regarding the oxidation of NADH, no substantial difference between the assays with and without ferredoxin can be observed (Figure 20A). The curve depicting the control reaction without rDsrABL clearly shows a lower NADH oxidation rate than the reactions with rDsrABL and can be considered as the background reaction. The absorbance at 390 nm is quite low for the reaction without ferredoxin, as it is only accountable to the very slight absorbance of NADH at 390 nm (Figure 20B, dark gray curve). In the course of the reaction, the dark gray curve, which resembles the NADH-dependent sulfite reduction without ferredoxin, shows a slight decrease in absorbance at 390 nm of about 0.01, which can be traced back to the oxidation of NADH. Both the black and the light gray curve, resembling the reaction with rDsrABL and ferredoxin and the control with only ferredoxin respectively, display a distinctly higher absorbance at 390 nm,

which can be attributed to NADH and to ferredoxin. The absorbance decreased from 0.2 to about 0.18 in the course of time, which is a slightly higher decrease than measured for the curve without ferredoxin. This indicates a partial reduction of ferredoxin, but as it occurred in both the assay with and without rDsrABL, it does not seem to be a specific phenomenon. The assays were also performed with NADPH as electron donor at pH 6 and pH 7 with the same outcome (data not shown). These results give no indication for an electron bifurcation of rDsrABL, in which electrons deriving from NAD(P)H can be used to reduce sulfite and DsrC in one partial reaction and ferredoxin in another.

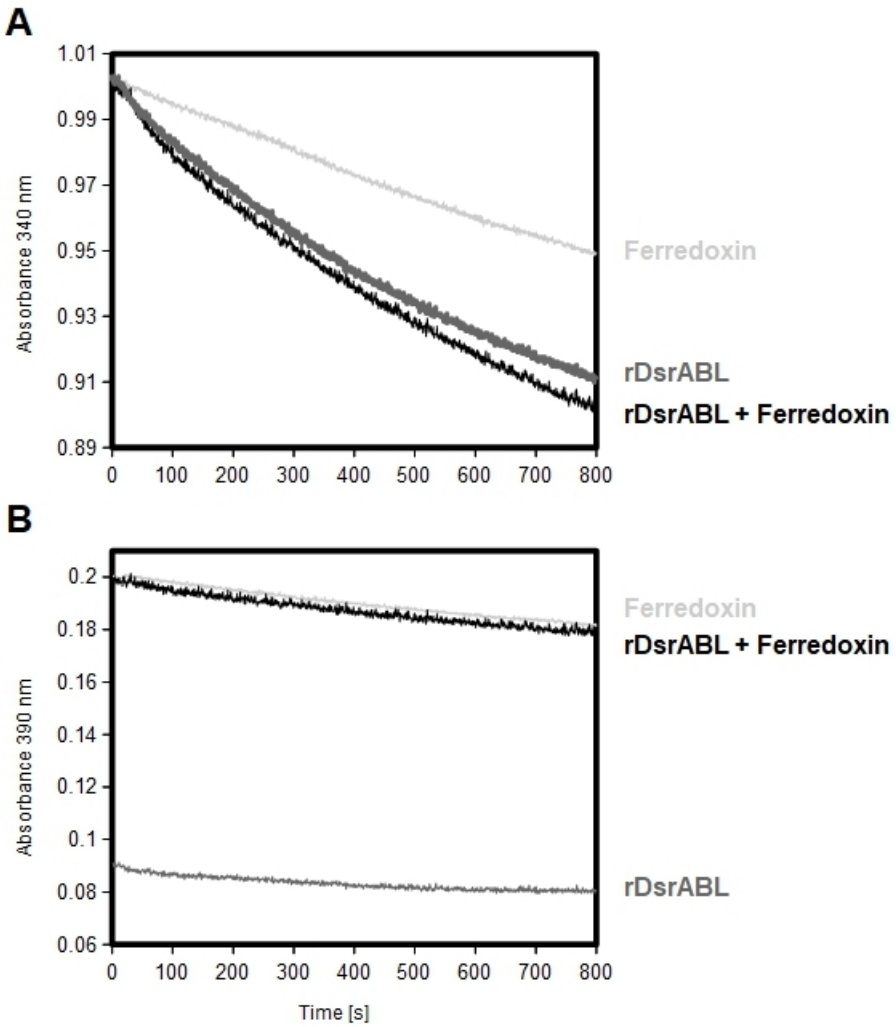

Figure 20: Potential electron bifurcation of rDsrABL. All assays contain 150 µM NADH, 10 µM DsrC and 250 µM sulfite. Reactions with 50.4 µg rDsrABL (dark gray curve), with 50.4 µg rDsrABL and 5 µM ferredoxin (black curve) and with 5 µM ferredoxin (light gray curve) are compared. Absorbance was followed at 340 nm (A) and 390 nm (B). All assays were performed at pH 7.

4.3.3 Interaction of rDsrABL with DsrC in *A. vinosum*

The 12-14 kDa protein DsrC occurs in sulfur oxidizers and sulfite reducers and is characterized by its highly conserved carboxyl-terminus, which forms a flexible arm and contains two strictly conserved cysteines (Cort *et al.,* 2001; Cort *et al.,* 2008; Oliveira *et al.,* 2008). One cysteine is the penultimate residue at the C-terminus (Cys_A) and the other lays eleven residues upstream (Cys_B). DsrC was shown to physiologically interact with the dissimilatory sulfite reductase DsrAB in sulfate reducers (Oliveira *et al.,* 2008; Santos *et al.,* 2015). The results presented in 4.3.1 already demonstrate that DsrC from the sulfur oxidizer *A. vinosum* interacts with rDsrABL in the dissimilatory sulfur metabolism as well. In the following this interaction will be investigated in more detail.

4.3.3.1 Consumption of DsrC in Sulfite Reduction

The NADH-dependent sulfite reduction rate of rDsrABL without the sulfur-binding protein DsrC lays at 21.7 mU/mg. In the presence of DsrC the activity of rDsrABL in the initial fast phase is increased more than ten-fold to 229 mU/mg (Figure 21).

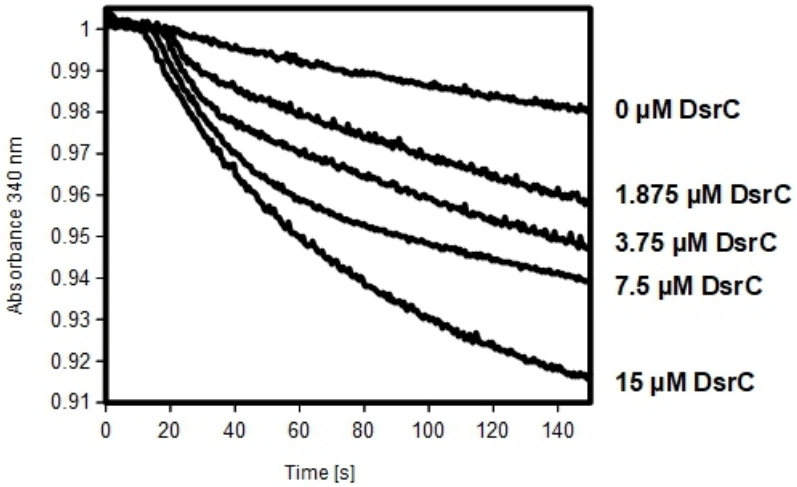

Figure 21: Role of DsrC in rDsrABL-catalyzed NADH-dependent sulfite reduction. All assays contained 150 µM NADH, 250 µM sulfite, 46 µg rDsrABL and varying concentrations of DsrC and were performed at pH 7. NADH oxidation was followed at 340 nm (ε_{340}= 6.3 mM^{-1} cm^{-1}).

The length of this initial fast phase is dependent on the amount of DsrC added to the reaction, indicating that the sulfur-binding protein is consumed during the reaction and functions as a co-substrate. By calculating the difference in absorbance at 340 nm from

the beginning to the end of the fast phase, the consumption of NADH can be determined. This resulted in a NADH:DsrC ratio of about 1:1.17, which is very close to one NADH per DsrC, indicating that two electrons are needed for the consumption of one DsrC.

4.3.3.2 Interaction of DsrC with rDsrABL and with Sulfite

In an enzymatic reaction it can be of relevance in which order the enzyme and its substrates are added to the *in vitro* assay, especially when the enzyme has several interaction partners. It can possibly be beneficial for the reaction rate, when the enzyme is preincubated with a certain interaction partner or two co-substrates are preincubated. For the NADH-dependent sulfite reduction catalyzed by rDsrABL in the presence of the co-substrate DsrC, the enzyme was either preincubated with sulfite or with DsrC or the two co-substrates sulfite and DsrC were preincubated before starting the reaction by addition of rDsrABL (Figure 22).

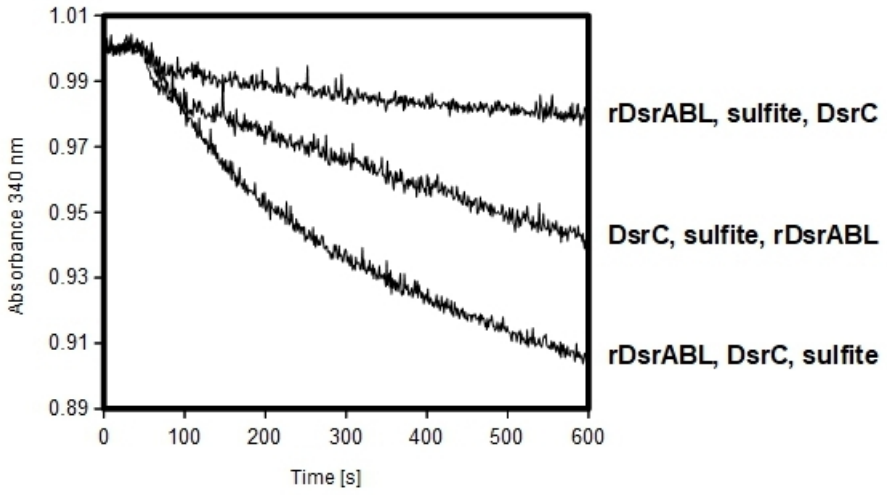

Figure 22: Sulfite reduction rate dependent on the order of substrates added. Assays contained 250 µM NADH, 92 µg rDsrABL, 15 µM DsrC and 250 µM sulfite. NADH was always added first, then either rDsrABL and sulfite were preincubated and DsrC was added last or DsrC and sulfite were preincubated and rDsrABL was added last or rDsrABL and DsrC were preincubated and sulfite was added last. All assays were performed at pH 7 and preincubation lasted for at least 1 min. NADH oxidation was followed at 340 nm (ε_{340}= 6.3 mM^{-1} cm^{-1}).

The highest sulfite reduction rate could be attained when sulfite was added last and rDsrABL could initially interact with only DsrC. When DsrC and sulfite were preincubated and rDsrABL was added last, sulfite reduction rate was only at 52% and when rDsrABL

initially interacted with sulfite and DsrC was added last, sulfite reduction rate was even lower at 20%. Taken together these results indicate that the NADH-dependent sulfite reduction rate is highest, when rDsrABL and DsrC initially interact and sulfite is added last.

4.3.3.3 Influence of Conserved DsrC Cysteines on Sulfite Reduction Rate

The sulfur-binding protein DsrC has two strictly conserved cysteine residues located on its flexible carboxyl-terminal arm. For the sulfate reducer *Desulfovibrio vulgaris* it has been shown, that this flexible arm extends into the interface between DsrA and DsrB, bringing Cys_A very close to the substrate binding site of DsrAB (Oliveira *et al.,* 2008). In order to elucidate whether both cysteines or only one cysteine – and in that case which of the two – is essential for the initially increased sulfite reduction rate of rDsrABL from a sulfur oxidizer, wild type DsrC from *A. vinosum* (DsrC WT) and cysteine exchange variants of DsrC were examined (Figure 23, Figure 24).

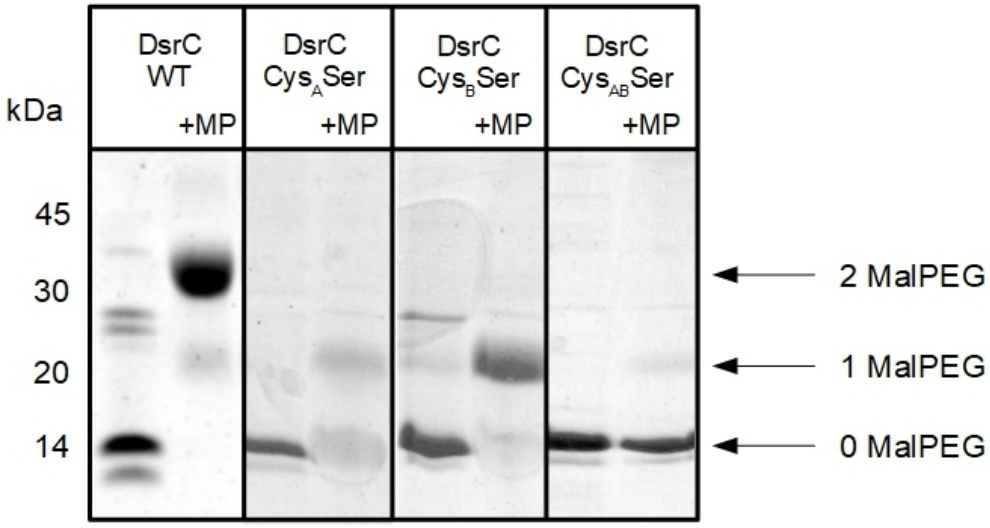

Figure 23: Analysis of *A. vinosum* DsrC variants via MalPEG gel shift assay. Wild type DsrC (DsrC WT) and DsrC variants (DsrC Cys_ASer, DsrC Cys_BSer and DsrC Cys_{AB}Ser) were reduced with 5 mM DTT (dithiothreitol) at 30 °C for 30 min (first lane) and treated with 1 mM MalPEG at 30 °C for 15 min afterwards (second lane). 10 µg protein were applied per lane onto a non-reducing 12.5 % Tricine SDS-PAGE.

While DsrC WT has both conserved cysteines of the C-terminal arm, in DsrC Cys_ASer the penultimate cysteine is exchanged by a serine and in DsrC Cys_BSer the cysteine eleven residues upstream is exchanged by a serine. The double variant DsrC Cys_{AB}Ser has both its cysteines exchanged by serines. In order to analyze the DsrC variants before and after

the reaction with rDsrABL and sulfite, gel shift assays with the labeling reagent MalPEG (methoxy-polyethylene glycol maleimide) were performed. MalPEG selectively binds to free thiol groups, such as the SH group of the amino acid cysteine, covalently (Lu and Deutsch 2001). The molecular mass of the labeled protein is increased by about 10 kDa per accessible SH group and this rise of molecular mass can be detected by SDS-PAGE.

SDS-PAGE analysis of DsrC WT and of the DsrC variants demonstrated that all variants were mainly in their monomeric form after reduction with DTT (dithiothreitol), as for each variant a predominant band at 14 kDa is present in the first lane (Figure 23). All DsrC proteins also show a more faint band slightly below the 14 kDa band, which can be accounted to recombinant DsrC without the amino-terminal His-tag. The longer recombinant DsrC is stored the likelier the degradation of the heterologously added His-tag is (data not shown). For DsrC WT another faint double band can be detected between 25–28 kDa, representing a dimer with and without His-tag. For the DsrC variant Cys_BSer, which only contains Cys_A, the band representing the dimer can also be detected. Treatment of the reduced DsrC proteins with MalPEG led to a gel shift (Figure 23, second lane). The wild type protein shifted to about 34 kDa, which represents the monomer with two MalPEGs, indicating that one MalPEG per cysteine can be found. A much slighter band can be detected at about 24 kDa, which represents the monomer with one MalPEG. For DsrC Cys_ASer and DsrC Cys_BSer the 14 kDa monomer bands also shift to 24 kDa, indicating that one MalPEG is bound to each variant. For DsrC $Cys_{AB}Ser$ no gel shift occurs, as there is no cysteine accessible for MalPEG.

To ascertain which of the two strictly conserved cysteines is essential for the increased sulfite reduction rate, activity of rDsrABL in the presence of DsrC WT, of the DsrC variants and without DsrC was compared (Figure 24A). The lowest sulfite reduction rate was achieved without DsrC, followed by a slightly higher rate in the reactions with the variants DsrC Cys_ASer and DsrC $Cys_{AB}Ser$. The reactions with DsrC WT and DsrC Cys_BSer show the highest sulfite reduction rate and both display an initial fast phase (Figure 24A). Taken together the reactions with DsrC containing Cys_A proceed rapidly and in a similar manner, while the reactions with DsrC lacking Cys_A have a lower sulfite reduction rate. The reaction rate without DsrC at all is the lowest, thus DsrC without Cys_A still leads to an increased sulfite reduction rate, which seems to be independent on Cys_B.

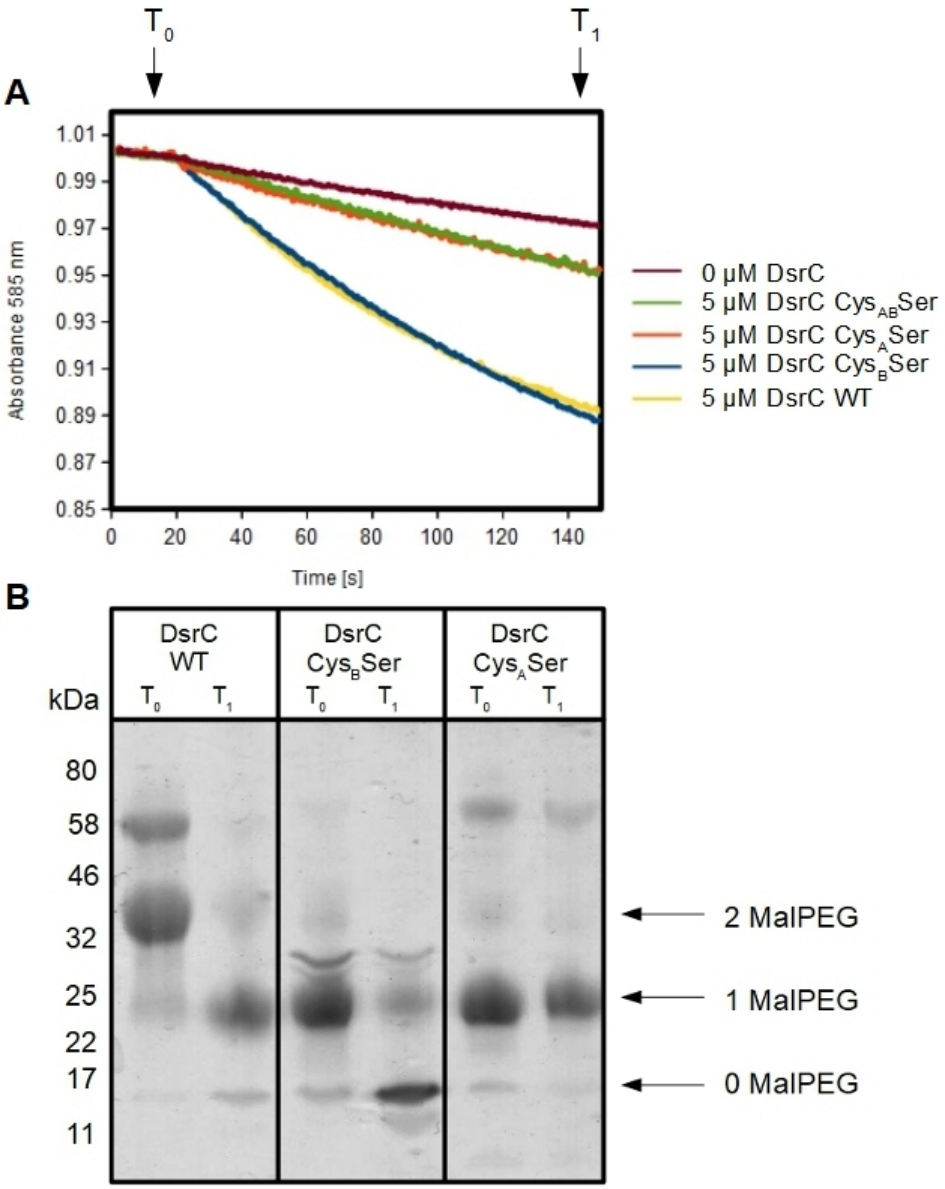

Figure 24: Effect of DsrC variants on sulfite reduction by rDsrABL. (A) All assays contained 17.2 µg rDsrABL and 250 µM sulfite. Methyl viologen was used as artificial electron donor and its oxidation was followed at 585 nm (ε_{585}= 11.8 mM^{-1} cm^{-1}). The reactions contained either no DsrC or 5 µM DsrC WT or DsrC variants. Samples were taken at T_0 and T_1, incubated for 15 min at 30 °C with 1 mM MalPEG and (B) loaded onto a non-reducing 12.5 % Tricine SDS gel. The Color Prestained Protein Standard, Broad Range from NEB was used as protein standard.

MalPEG analysis of DsrC WT shows that, before the reaction with rDsrABL and sulfite, both cysteines were accessible, as two MalPEGs could bind to the monomer (Figure 24B). The slighter band at 58 kDa represents the DsrC WT dimer with two MalPEGs bound. After the reaction the predominant band coincides with the monomer with one MalPEG. There is also a fainter band resembling the monomer with no MalPEG bound. MalPEG

analysis of the DsrC variant Cys_BSer, with which a similar sulfite reduction rate could be observed, showed that before the reaction Cys_A was accessible for MalPEG, as the main band resembles a DsrC monomer with one MalPEG. A very small portion has no bound MalPEG or appears as a dimer (28 kDa band). After the reaction Cys_A is no longer accessible for MalPEG, as the 24 kDa band shifts to the 14 kDa band. The DsrC variant Cys_ASer binds one MalPEG before and after the reaction with rDsrABL and sulfite, thus the accessibility of Cys_B does not seem to change in the course of the reaction.

As both cysteines in DsrC Cys_{AB}Ser are exchanged by serine, no MalPEG can bind (Figure 23) and thus no sample was taken before and after the reaction with rDsrABL and sulfite. In conclusion Cys_A is essential for the increased sulfite reduction rate of DsrC and it is in some way modified in the reaction making it inaccessible for MalPEG binding afterwards.

DsrC proteins from sulfate reducers and from sulfur oxidizers have several homologies both in amino acid sequence and structure (Oliveira *et al.,* 2008; Cort *et al.,* 2008; Venceslau *et al.,* 2014), as the alignment of DsrC from sulfate reducer *D. vulgaris* and sulfur oxidizer *A. vinosum* exemplary displays (Figure 25A).

Throughout the amino acid sequence identities can be found and especially the carboxyl-terminus containing the two conserved cysteines shows a high similarity with the last ten residues being identical (Figure 25A). In addition to the two highly conserved cysteines of the carboxyl-terminus, DsrC from *D. vulgaris* has another cysteine, which is not conserved (Cys26). To determine whether DsrC from a sulfate reducer can interact with a sulfite reductase from a sulfur oxidizer, DsrC Cys26Ala from *D. vulgaris* was added to sulfite reduction catalyzed by rDsrABL from *A. vinosum* (Figure 25B). The DsrC variant with an exchange of Cys26 by alanine was chosen to simplify MalPEG gel shift analysis. With DsrC Cys26Ala from *D. vulgaris* the sulfite reduction rate was in the same range as in the reaction without DsrC, while activity could be strongly increased through addition of DsrC from *A. vinosum.* Before the reaction DsrC Cys26Ala was accessible for two MalPEGs, which did not change due to the reaction with rDsrABL and sulfite (Figure 25C). These results indicate that DsrC from a sulfate reducer, even though it shows great similarities especially in the carboxyl-terminal arm, cannot simply adopt the function of DsrC from a sulfur oxidizer.

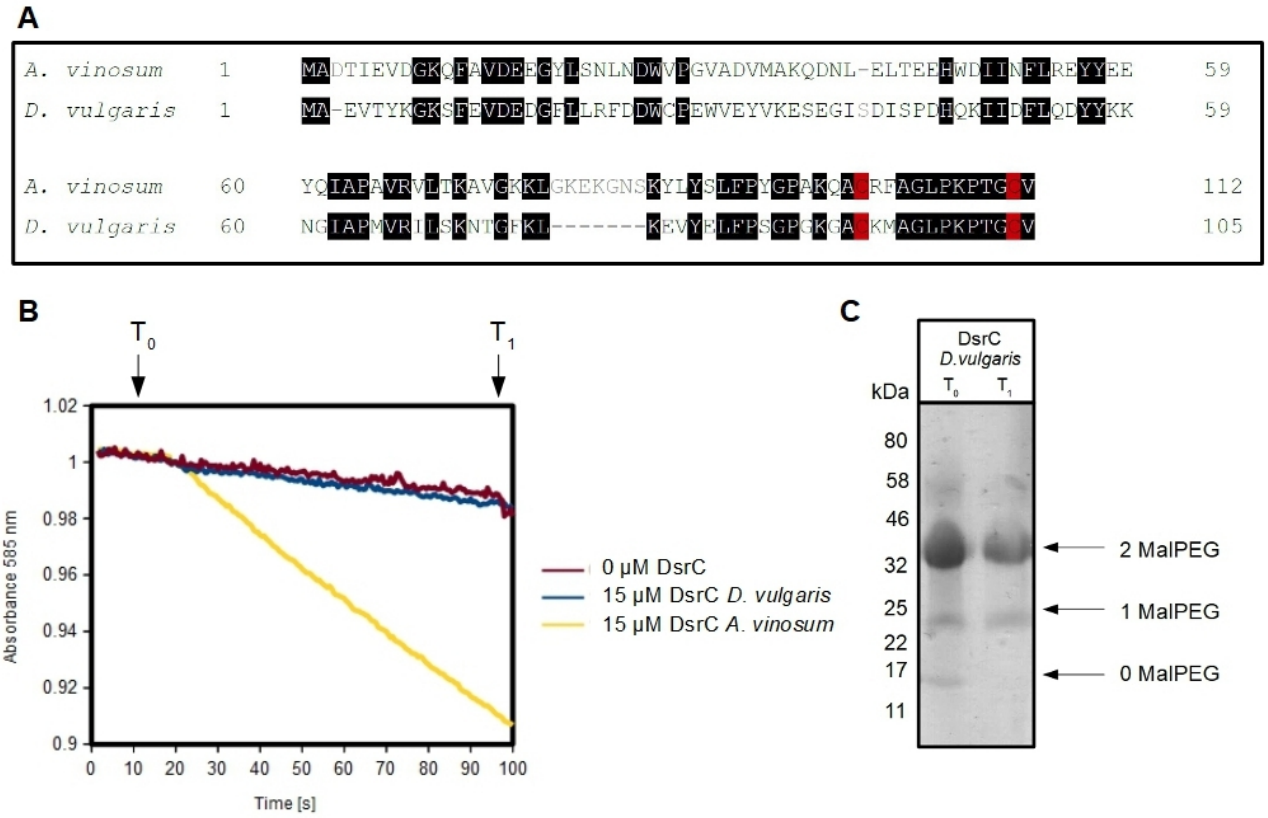

Figure 25: Effect of DsrC from *D. vulgaris* on sulfite reduction by rDsrABL. (A) DsrC from *A. vinosum* and *D. vulgaris* are compared via sequence alignment. Cys_A and Cys_B are marked in red. (B) All assays contained 17.2 µg rDsrABL and 250 µM sulfite. Methyl viologen was used as artificial electron donor and its oxidation was followed at 585 nm (ε_{585}= 11.8 mM^{-1} cm^{-1}). The reactions contained either no DsrC or 15 µM DsrC from *A. vinosum* or 15 µM DsrC Cys26Ala from *D. vulgaris*. Samples were taken at T_0 and T_1, incubated for 15 min at 30 °C with 1 mM MalPEG and (C) loaded onto a non-reducing 12.5 % Tricine SDS gel. The Color Prestained Protein Standard, Broad Range from NEB was used as protein standard.

4.3.3.4 Analysis of DsrC After the rDsrABL-Catalyzed Sulfite Reduction

In the sulfur-binding protein DsrC from *A. vinosum* the penultimate residue of the strictly conserved carboxyl-terminal arm Cys_A was shown to be essential for the increased sulfite reduction rate in the rDsrABL-catalyzed reaction. DsrC is consumed in the reaction, which seems to be due to some kind of modification of Cys_A. In order to elucidate what happens to Cys_A in the course of the reaction, sulfite reduction catalyzed by rDsrABL was traced in the presence of DsrC WT and of DsrC Cys_BSer respectively (Figure 26A, Figure 27A). The assays were preformed with 250 µM sulfite (standard condition) and 25 µM sulfite comparatively, while samples for the MalPEG gel shift analysis of DsrC were taken in the course of the reaction (Figure 26B, Figure 27B).

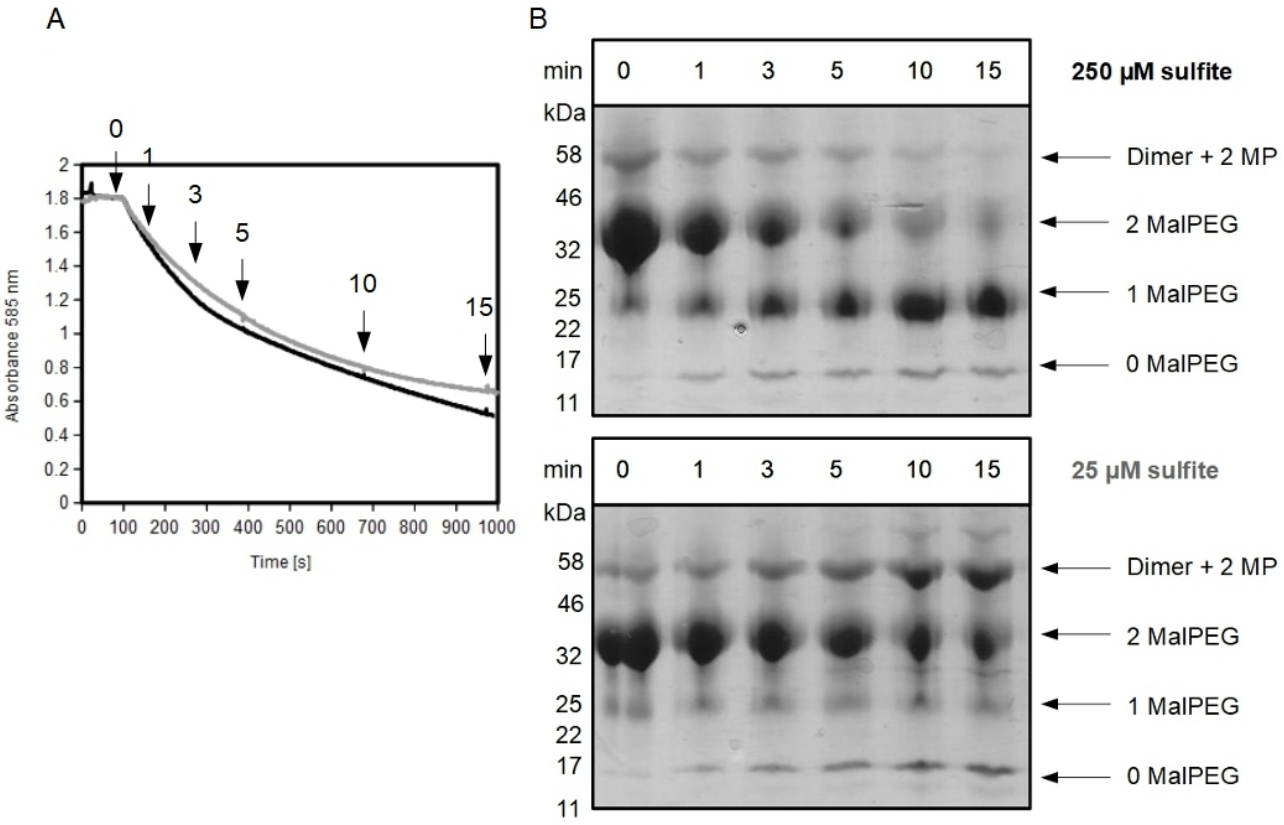

Figure 26: Analysis of DsrC WT over the course of the reaction with rDsrABL dependent on the sulfite concentration. (A) Methyl viologen was used as artificial electron donor and its oxidation was followed at 585 nm (ε_{585}= 11.8 mM^{-1} cm^{-1}). Both assays contained 25 µM DsrC WT and either 250 µM sulfite and 8.4 µg rDsrABL (black curve) or 25 µM sulfite and 16.8 µg rDsrABL (gray curve). Samples were taken at 0, 1, 3, 5, 10 and 15 min as indicated in (A). The samples were incubated at 30 °C for 15 min with 1 mM MalPEG and (B) loaded onto a non-reducing 12.5 % Tricine SDS gel. The Color Prestained Protein Standard, Broad Range from NEB was used as protein standard.

By tracing the redox status of DsrC WT in the assay with 250 µM sulfite, it can be observed that during the course of the reaction the 34 kDa band (monomer with two MalPEG) gradually becomes fainter, while the 24 kDa band (monomer with one MalPEG) increases in intensity. Before the reaction a small portion of DsrC WT is present as dimer (58 kDa band, dimer with two MalPEG) and almost no portion is present as monomer without any MalPEG bound. This also changes in the course of the reaction, the dimer band loses intensity, while the monomer band gains intensity.

The gel shift pattern substantially changes when the assays are preformed with 25 µM sulfite instead of 250 µM sulfite. The band resembling the monomer with two MalPEGs bound also gradually decreases, but not to such a high degree as in the assay with 250 µM sulfite and it mainly shifts to the 58 kDa band resembling the dimer with two

MalPEGs bound. The intensity of the monomer with one MalPEG band (24 kDa) does not noticeably change in the course of the reaction, while the monomer without MalPEG band (14 kDa) gains intensity to a similar degree as observed for the assay with 250 µM sulfite.

Sulfite reduction catalyzed by rDsrABL in the presence of the DsrC variant Cys_BSer proceeds in a similar manner to the reaction with DsrC WT regardless of the sulfite concentration (Figure 27A). The variant however only has only one cysteine, which simplifies MalPEG analysis of DsrC in the course of the reaction (Figure 27B).

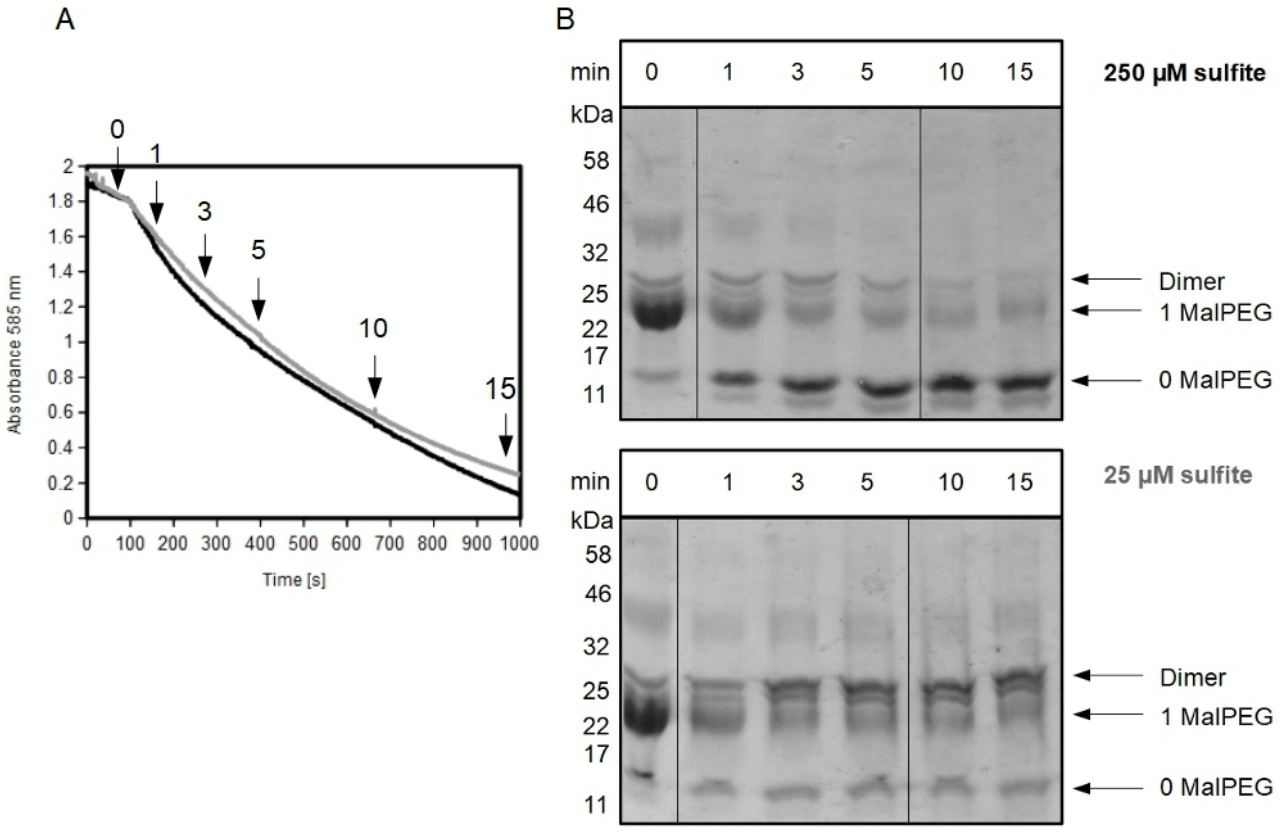

Figure 27: Analysis of DsrC Cys_BSer over the course of the reaction with rDsrABL dependent on the sulfite concentration. (A) Methyl viologen was used as artificial electron donor and its oxidation was followed at 585 nm (ε_{585}= 11.8 mM^{-1} cm^{-1}). Both assays contained 25 µM DsrC Cys_BSer and either 250 µM sulfite and 8.4 µg rDsrABL (black curve) or 25 µM sulfite and 16.8 µg rDsrABL (gray curve). Samples were taken at 0, 1, 3, 5, 10 and 15 min as indicated in (A). The samples were incubated at 30 °C for 15 min with 1 mM MalPEG and (B) loaded onto a non-reducing 12.5 % Tricine SDS gel. The Color Prestained Protein Standard, Broad Range from NEB was used as protein standard.

Before the 250 µM sulfite are added to the reaction mixture, Cys_A of DsrC Cys_BSer is accessible for MalPEG, as the predominant band resembles the monomer with one MalPEG bound. There are also two more faint bands resembling the dimer (28 kDa) and the monomer without MalPEG (14 kDa). In the course of the reaction the dimer and monomer with one MalPEG bands gradually lose intensity, while the monomer without MalPEG bound gains intensity. This demonstrates that Cys_A is modified during the reaction, insofar that it is no longer accessible for MalPEG.

In the reaction with 25 µM sulfite the gel shift pattern is different, just as observed for the reaction with DsrC WT. The dimer band gains intensity while the monomer band with one MalPEG loses intensity. The intensity of the monomer band without MalPEG does not substantially increase in the course of time. Taken together the analysis of DsrC WT and DsrC Cys_BSer over the course of the reaction with rDsrABL with high and low sulfite concentrations, demonstrate that Cys_A is modified insofar that it is no longer accessible for MalPEG, when the sulfite concentration is high. When the concentration is lower, Cys_A is in parts still accessible for MalPEG and in parts a intermolecular disulfide bond between two Cys_A residues leads to the generation of DsrC dimers.

To verify whether the formation of dimers after the reaction with rDsrABL and a low concentration of sulfite is genuine or only an artifact due to treatment with MalPEG, samples of DsrC WT and DsrC Cys_BSer were taken after the reaction with rDsrABL and 250 µM sulfite and 25 µM sulfite respectively. These were analyzed via size exclusion chromatography to distinguish their oligomerization status (Figure 28).

Analysis of DsrC WT (Figure 28A) and DsrC Cys_BSer (Figure 28C) after the reaction with rDsrABL and 250 µM sulfite revealed that both proteins elude from the column in two peaks, the first with an elution volume of about 65 ml and the second at about 76 ml, which correlate to a molecular weight of 35 kDa and 16 kDa respectively. For both proteins the 76 ml peak, representing the DsrC monomer is substantially higher than the dimer peak. The elution profiles of DsrC WT (Figure 28B) and DsrC Cys_BSer (Figure 28D) after the reaction with 25 µM sulfite also show these two peaks, however the size ratios are inverse. Here the dimer peaks are distinctly higher than the monomer peaks. Taken together the analysis via size exclusion chromatography revealed that the DsrC dimer formation after the reaction with rDsrABL and 25 µM sulfite is authentic.

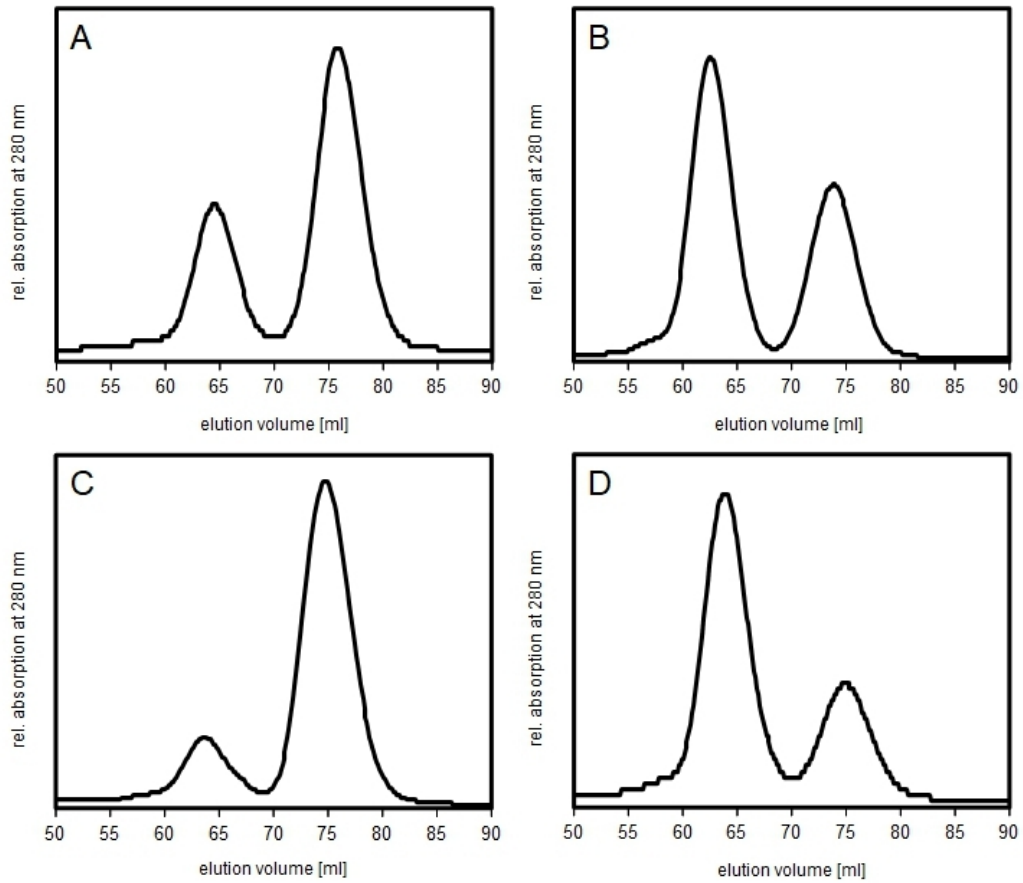

Figure 28: Elution profile of DsrC WT and DsrC Cys_BSer in size exclusion chromatography after reaction with rDsrABL dependent on sulfite concentration. DsrC WT was analyzed via size exclusion chromatography after reaction with rDsrABL an 250 µM sulfite (A) and 25 µM sulfite (B) respectively. The DsrC variant Cys_BSer was also analyzed with 250 µM sulfite (C) and 25 µM sulfite (D). Prepacked HiLoad Superdex 75 prep grade was used for size exclusion chromatography.

To elucidate what exactly happens to Cys_A of DsrC in the reaction with rDsrABL and sulfite, DsrC was analyzed via MALDI-TOF mass spectrometry. A possible modification would be the persulfuration of Cys_A leading to an additional mass of 32 Da. Another unknown modification is expected, as Cys_A is not accessible for MalPEG after the rDsrABL-catalyzed reaction with 250 µM sulfite and MalPEG would be able to bind to a persulfurated Cys_A.

The MALDI-TOF mass spectrometric analysis of reduced DsrC WT (Figure 29A) and DsrC Cys_BSer (Figure 29D) display the unmodified proteins with 14639 Da and 14622 Da respectively. However both spectra also contain at least two further smaller peaks with a mass increase of 37-38 Da and 2 x 37-38 Da. This seems to be an unspecific modification

of the DsrC proteins, which might be traced back to an accumulation of potassium ions, which have a mass of 39 Da and were present in the reaction buffer. This unspecific modification has to be taken into account, when interpreting the mass spectra of DsrC proteins after the reaction with rDsrABL and sulfite.

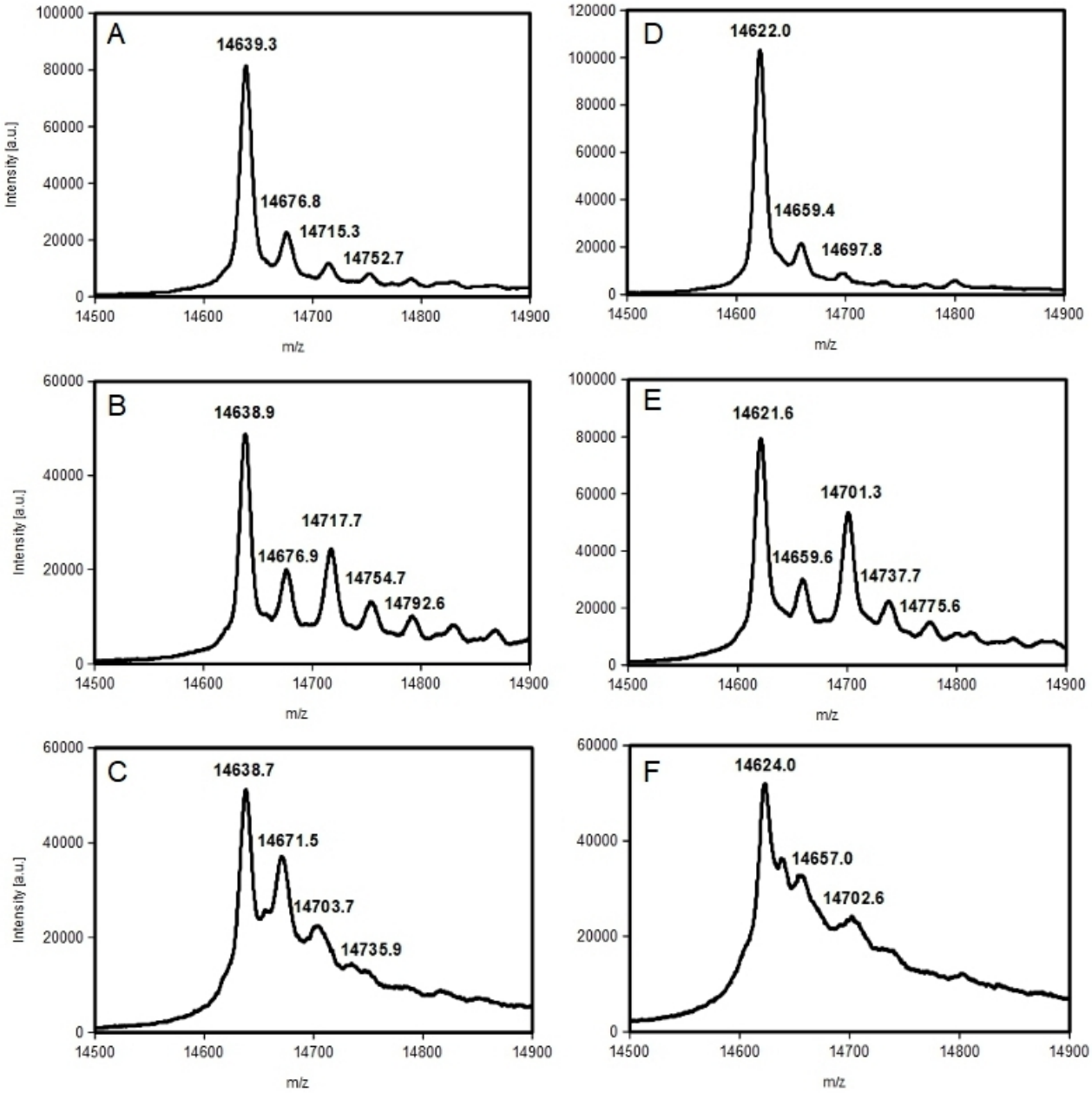

Figure 29: DsrC modification analyzed via MALDI-TOF mass spectrometry. Reduced DsrC WT (A) and DsrC Cys_BSer (D) were analyzed as a control. The DsrC proteins were analyzed after the rDsrABL catalyzed reaction with 250 µM sulfite (DsrC WT – B; DsrC Cys_BSer – E) and with 25 µM sulfite (DsrC WT – C; DsrC Cys_BSer – F). The theoretically calculated masses for His-tagged DsrC WT and DsrC Cys_BSer are 14638.5 Da and 14622.4 Da respectively.

When 250 µM sulfite are added to the reaction, the mass spectra of DsrC WT (Figure 29B) and of DsrC Cys_BSer (Figure 29E), differ from the mass spectra of the reduced proteins (Figure 29A+D). The peak for unmodified DsrC is still detectable in both cases and a smaller peak with an additional mass of about 38 Da is also present. However the next peak shows a mass increase of about 80 Da to the unmodified protein instead of 74-76 Da (2 x 37-38 Da) as detectable for the reduced proteins. This peak is relatively higher than the 74-76 Da peak in the controls. Moreover the DsrC proteins with the 80 Da modification seem to be further modified in the same manner as the reduced DsrC proteins, as multiple mass increases of 37-38 Da are also detectable in addition to the 80 Da modification.

The mass spectrum of DsrC WT after the rDsrABL-catalyzed reaction with 25 µM sulfite contains a peak for unmodified DsrC and in addition peaks with a mass increase of about 32 Da, as expected for persulfurated DsrC (Figure 29C). Up to three additional sulfur atoms bound to DsrC WT can be detected. For DsrC Cys_BSer an additional mass of 33 Da can be detected after the reaction with 25 µM sulfite, which can also be traced back to the persulfuration of Cys_A (Figure 29F). However a small peak with an additional mass of about 80 Da can also be detected here.

Further controls without rDsrABL were executed to determine whether the observed effects are dependent on the rDsrABL-catalyzed reaction or if they are merely chemical modifications (Figure 30).

The controls with 250 µM sulfite and without rDsrABL (Figure 30A+C) display very similar results to the assays with 250 µM sulfite and with rDsrABL (Figure 29B+E). Thus the observed mass increase of 80 Da seems to be independent on the reaction with rDsrABL. The mass spectra of DsrC in the controls with 25 µM sulfite and without rDsrABL (Figure 30B+D) resemble those of the reduced DsrC proteins (Figure 29A+D). Accordingly the observed persulfuration of Cys_A is dependent on the rDsrABL catalyzed reaction. DsrC dimers were also detected in all MALDI-TOF mass spectra, however the resolution was not high enough to detect considerable differences in mass. Taken together these results indicate that Cys_A is persulfurated in the reaction with rDsrABL and sulfite. When the sulfite concentration is low, dimer formation is favored and when the sulfite concentration is high, a modification of Cys_A, which is independent on the reaction with rDsrABL, can be observed. This modification makes Cys_A inaccessible for MalPEG (Figure 26B,

Figure 27B) and leads to a mass increase of 80 Da (Figure 29B+E, Figure 30A+C), which can presumably be traced back to a sulfonate group (-SO_3^-) bound to Cys_A of DsrC. There are no indications from MalPEG gel shift analysis nor from mass spectrometry that DsrC from *A. vinosum* forms a intramolecular trisulfide between Cys_A and Cys_B as has been demonstrated for DsrC from *A. fulgidus* (Santos *et al.,* 2015).

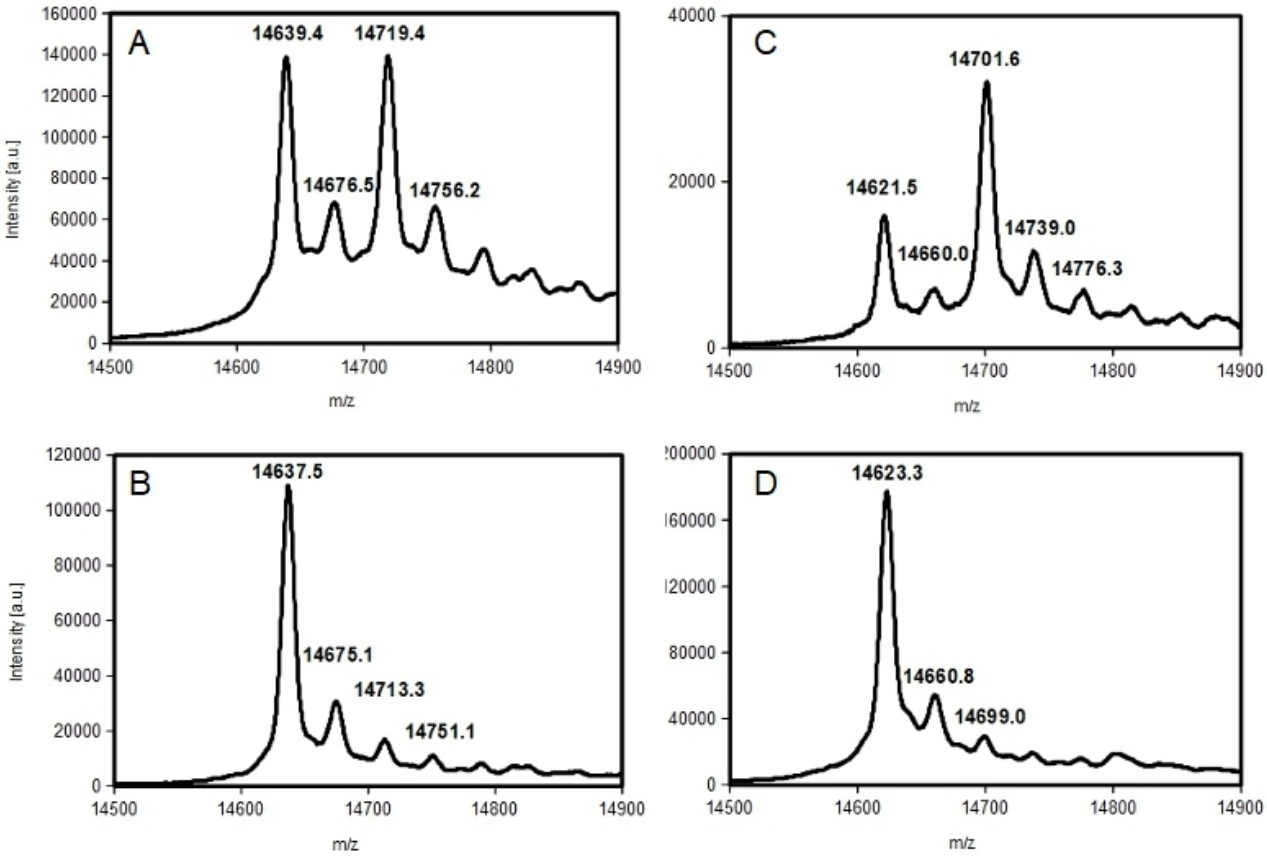

Figure 30: DsrC controls without rDsrABL analyzed via MALDI-TOF mass spectrometry. The DsrC proteins were analyzed after the incubation with 250 µM sulfite (DsrC WT – A; DsrC Cys_BSer – C) and with 25 µM sulfite (DsrC WT – B; DsrC Cys_BSer – D). The theoretically calculated masses for His-tagged DsrC WT and DsrC Cys_BSer are 14638.5 Da and 14622.4 Da respectively.

4.3.4 Activity of rDsrABL in Sulfur Oxidation

The reverse dissimilatory sulfite reductase rDsrAB from *A. vinosum* is known to be essential for the oxidation of stored sulfur to sulfite in the cytoplasm (Pott and Dahl, 1998; Dahl *et al.,* 2005). A so far unknown carrier molecule transfers sulfur from the periplasmic sulfur deposits into the cytoplasm, where the zero-valent sulfur passes as a persulfide

between multiple proteins and finally to the active site of rDsrAB, where it is oxidized to sulfite. It is most probable that DsrC stands at the end of this extensive cascade of protein persulfides (Stockdreher *et al.,* 2012) and not only functions as a (co-)substrate in sulfite reduction by DsrAB (Santos *et al.,* 2015), but also as a substrate, in form of sulfur-bound DsrC, in sulfur oxidation by rDsrAB. The here proven interaction of DsrC and rDsrABL from *A. vinosum* (4.3.3) also strongly encourages this hypothesis.

4.3.4.1 Possible Substrates for Sulfur Oxidation by rDsrABL

The penultimate residue of the flexible carboxyl-terminal arm of DsrC Cys_A is essential for the interaction of DsrAB and DsrC in sulfite reduction and also plays a substantial role in the sulfur trafficking system of sulfur oxidizers, as sulfane sulfur is transferred from DsrEFH onto Cys_A of DsrC (Stockdreher *et al.,* 2012). Potentially, persulfurated DsrC (DsrC-Cys_A-S^-), as final product of the cytoplasmic sulfur relay system, serves as the substrate for rDsrAB in sulfur oxidation. Another candidate for the potential substrate is a DsrC trisulfide, in which a sulfur atom is bridging Cys_A and Cys_B of the carboxyl-terminal arm, as this is the released product of sulfite reduction in the sulfate reducer *A. fulgidus* (Santos *et al.,* 2015). In this chapter potential substrates for sulfur oxidation by rDsrABL are to be generated.

DsrC can be persulfurated chemically by incubation with NaHS and the persulfuration occurs at Cys_A (Stockdreher *et al.,* 2012). In one approach DsrC WT was incubated with NaHS and in another it was added to the rDsrABL-catalyzed reaction with 25 µM sulfite and thereafter the proteins were analyzed by MalPEG gel shift assay (Figure 31).

The DsrC proteins were first treated with MalPEG to determine their accessibility for MalPEG and then reduced with DTT. The reductant is able to reduce perthiols, however not fully able to reduce the covalent bond between MalPEG and the thiol group of cysteine. Therefor samples were taken before and after the treatment with DTT. Consequently, one can distinguish between MalPEG bound to a thiol of cysteine and MalPEG bound to a perthiol of cysteine.

The analysis of reduced DsrC WT serves as a control and displayes that MalPEG binds to both cysteines (Figure 31). After reduction with DTT, the intensity of the monomer with two MalPEG band slightly decreases and the bands monomer with one MalPEG and monomer without MalPEG slightly gain intensity. This demonstrates that the reductant DTT, in the

applied concentration and incubation time, does not lead to a full reduction of the thiol MalPEG bond, but does slightly alter the gel pattern.

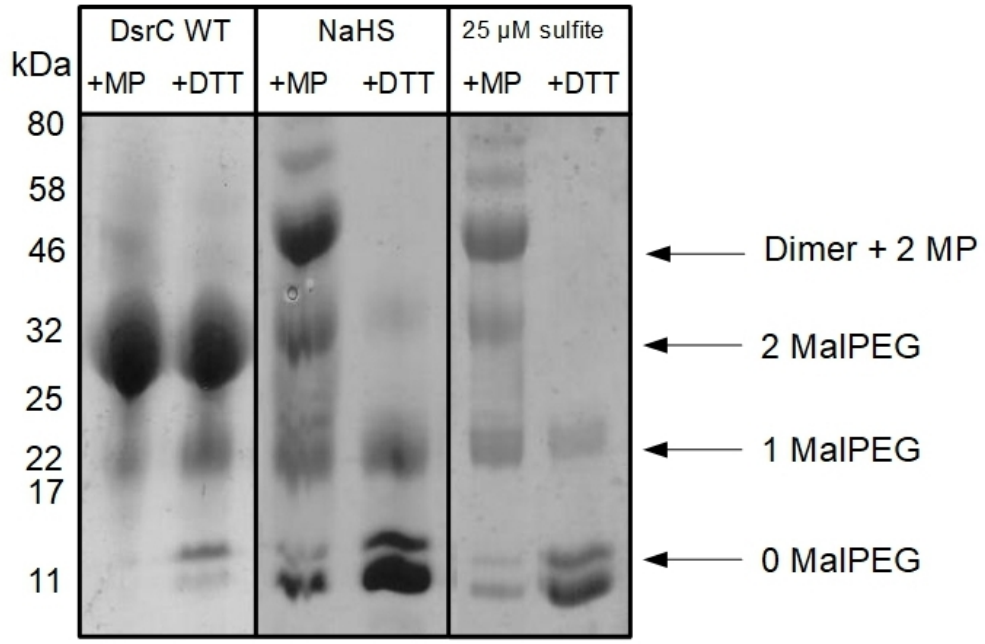

Figure 31: Analysis of potential DsrC substrates for sulfur oxidation by rDsrABL. DsrC WT was analyzed via MalPEG gel shift assay as a control. Reduced DsrC WT was treated with 2 mM NaHS for 1 h at 30 °C and analyzed via MalPEG assay (NaHS). Also analyzed was the DsrC WT product of rDsrABL-catalyzed sulfite reduction with 25 µM sulfite. The DsrC WT proteins were treated with 1 mM MalPEG for 15 min at 30 °C (+MP) and then treated with 5 mM DTT for 30 min at 30 °C (+DTT). A sample was taken after treatment with MalPEG (first lane) and another after further treatment with DTT (second lane). The samples were loaded onto a non-reducing 12.5 % Tricine SDS gel. The Color Prestained Protein Standard, Broad Range from NEB was used as protein standard.

After the incubation with NaHS, the results of the MalPEG assay are quite different. The predominant band resembles the DsrC dimer with two MalPEG, but there are also bands resembing the monomer with two, one and no MalPEG bound. Reduction with DTT strongly alters the gel pattern. The main band is the monomer without MalPEG and a smaller portion of DsrC is present as monomer with one MalPEG. Accordingly MalPEG was mainly bound to perthiols. The DsrC protein after the reaction with rDsrABL and 25 µM sulfite displays a very similar gel shift pattern, also indicating that MalPEG is mainly bound to perthiols.

Taken together these two methods led to the generation of a DsrC persulfide. However, it was not possible to produce an *A. vinosum* DsrC trisulfide.

4.3.4.2 Possible Electron Acceptors for Sulfur Oxidation by rDsrABL

Cytoplasmic oxidation of stored sulfur is known to be catalyzed by rDsrAB in *A. vinosum* Pott 1998 #77}(Dahl *et al.,* 2005) with DsrC-bound sulfur as its potential substrate. It is however unclear, where the electrons of this oxidation flow to. As a tight interaction of and electron flow between rDsrAB and the NADH:oxidoreductase DsrL could be demonstrated in this work, it is probable that electrons of sulfur oxidation are transferred from rDsrAB onto DsrL. The NADH:oxidoreductase could use these electrons to reduce NAD^+ to NADH. However assays with persulfurated DsrC, rDsrABL and NAD^+ demonstrated no reduction of NAD^+. As the redox potential of NADH/NAD^+ (E^0 = -320 mV) is quite low, the oxidation of persulfurated DsrC might not be sufficient to reduce NAD^+ *in vitro*. Thus artificial electron acceptors were tested to elucidate if the oxidation of the selected substrate is generally possible. DsrL can transfer electrons from NADH to MTT (4.3.2.1 NADH:Oxidoreductase Activity of DsrL from rDsrABL) and MTT accordingly has a higher redox potential (E^0 = -110 mV) than NADH/NAD+. Further electron acceptors with a very high redox potential were chosen, namely ferricyanide (E^0 = +360 mV) and dichloroindophenol (E^0 = +220 mV). However no activity could be measured with chemically persulfurated DsrC, nor with the DsrC product of the reaction with rDsrABL and a low sulfite concentration.

5 Discussion

The microbial processes of sulfur dissimilation belong to the most ancient metabolic pathways of life, they have strongly contributed to the evolution of the biogeochemical sulfur cycle and still shape it today (Canfield, 1999; Fike *et al.,* 2015). Sulfite reductases are key enzymes in the biogeochemical sulfur cycle, as they occur in pathways of dissimilatory sulfur metabolism and also play a central role in the assimilation of sulfate (Dhillon *et al.,* 2005). In this study the reverse-acting dissimilatory sulfite reductase rDsrAB from the sulfur oxidizer *A. vinosum* was shown to interact with DsrL to form the sulfite-generating rDsrABL complex and to interact with the substrate-binding protein DsrC. The rDsrABL complex was characterized both structurally and biochemically.

5.1 Comparison of rDsrABL of *Allochromatium vinosum* to Further Sulfite and Nitrite Reductases

The reverse-acting dissimilatory sulfite reductase of *A. vinosum* was first purified over forty years ago and shown to reduce sulfite and to contain a heme-like prosthetic group (Schedel *et al.,* 1979). A few years before this heme-like prosthetic group was discovered in the assimilatory NADPH-sulfite reductase purified from *E. coli* and termed siroheme (Murphy *et al.,* 1973; Murphy and Siegel, 1973). With the newly gained insights from this study rDsrABL will be compared to other siroheme-containing reductases with regard to production, structure, phylogeny and activity.

Importance of the Siroheme-[4Fe4S] Cofactor for Sulfite and Nitrite Reductase Production

Sirohemes are iron-tetrahydroporphyrins with eight carboxylate side chains and enable multi-electron reductions, in which as many as six electrons are transferred to an enzyme-bound substrate before the product is released (Murphy *et al.,* 1974). In all enzymes containing siroheme as prosthetic group, it is directly linked to a [4Fe4S] cluster, which presumably shuttles electrons onto the acceptor substrate (Crane and Getzoff, 1996). As such, they can be found in assimilatory sulfite and nitrite reductases (aSir and aNir), where they enable the catalysis of the six electron reductions from sulfite to sulfide and nitrite to ammonium respectively. Siroheme is also present in the cytoplasmic dissimilatory nitrite

reductases of *E. coli* and *Klebsiella pneumoniae* (Mohan and Cole, 2007), in dissimilatory sulfite reductases (dSir) of sulfate reducers and in reverse-acting dissimilatory sulfite reductases of sulfur oxidizers (Crane and Getzoff, 1996).

In the biosynthesis of siroheme uroporphyrinogen III is an important precursor molecule and it is also an intermediate in the biosynthesis of heme, chlorophyll and vitamin B12 (Stroupe *et al.,* 2003). In several bacteria, like *E. coli* and *Salmonella enterica*, the homodimeric enzyme CysG catalyzes siroheme synthesis (Spencer *et al.,* 1993; Stroupe *et al.,* 2003). CysG contains two structurally independent modules, enabling it to catalyze the four reactions, which transform uroporphyrinogen III into siroheme und making it a multifunctional enzyme (Warren *et al.,* 1994). The first module is a bismethyltransferase and catalyzes two SAM-dependent methylations at C2 and C7 of the macrocyclic ring (Warren *et al.,* 1990), while the second is a dual-function dehydrogenase-chelatase catalyzing NAD^+-dependent dehydrogenation to generate sirohydrochlorin and iron chelation to finally form siroheme (Warren *et al.,* 1994). The *E. coli* assimilatory sulfite reductase is encoded by *cysJ* and *cysI*, which are part of the cysteine regulon. As such their transcription is enhanced in the presence of the cysteine precorsor *N*-acethyl-L-serine (Ostrowski and Kredich, 1989). Although its name suggests it, CysG is not encoded in the cysteine regulon, but in the nitrate regulon, meaning it is expressed constitutively at low levels and overexpressed in response to nitrate or nitrite (Peakman *et al.,* 1990). The overexpression of recombinant *E. coli* NADPH-sulfite reductase revealed that the coexpression of siroheme synthetase CysG was necessary to overcome limitations of the siroheme cofactor (Wu *et al.,* 1991). The assembly of the structurally complex holoenzyme even seems to depend on the presence of cellular siroheme (Askenasy *et al.,* 2015). It consists of two subunits, a flavin-binding flavoprotein and an iron-containing hemoprotein, which assemble to form $\alpha_8\beta_4$ holoenzyme (Siegel and Davis, 1974). When expressed alone the flavoprotein is octameric and the hemoprotein is monomeric (Zeghouf *et al.,* 1998; Wu *et al.,* 1991). The N-terminus of the hemoprotein is required for the complex formation with the octameric flavoprotein subunits (Askenasy *et al.,* 2015). When the hemoprotein does not bind the siroheme nor the [4Fe4S] cluster, it builds an inactive tetrameric form, which is proposed to be assembly deficient (Askenasy *et al.,* 2015). This would ensure that inactive holoenzymes are not formed, when the siroheme synthetase CysG is limited due to the differential transcriptional regulation of the aSir and the

siroheme cofactor. Taken together the assembly of the holoenzyme is dependent on the full cofactor load of the hemoprotein and its interaction with the flavoprotein.

In the attempt to heterologously produce rDsrAB from *A. vinosum* in *E. coli*, it was also coexpressed with the siroheme synthetase CysG and additionally with the siroamidase DsrN (Figure 7), as the cofactor of rDsrAB was identified as siroamide, an amidated siroheme (Lübbe *et al.,* 2006). The two subunits rDsrA and rDsrB were to be expressed in two approaches, in one an N-terminal Strep-tag was fused to rDsrA and in the other a C-terminal Strep-tag was attached to rDsrB (Figure 5). However, in a Western Blot against the Strep-tag, it could neither be detected in the cell debris nor in the soluble fraction (Figure 7). The protein bands running between 35 and 55 kDa in the SDS-PAGE of the rDsrAB production could represent rDsrA (47 kDa) and rDsrB (40 kDa), but it seems improbable that both the N-terminal Strep-tag of rDsrA and the C-terminal Strep-tag of rDsrB would be inaccessible for an antibody against the Strep-tag. More likely, the proteins were not expressed correctly and degraded, so that the Strep-tags were not detectable. One reason for the unsuccessful overexpression of rDsrAB could be the absence of the iron-sulfur flavoprotein DsrL in the production. DsrL was shown to interact with rDsrAB both structurally and functionally in an rDsrABL complex (Figure 11, Figure 16) and may also contribute to its assembly in analogy to the flavoprotein in the aSir of *E. coli* (Askenasy *et al.,* 2015). This hypothesis is challenged by the fact that many sulfate reducers, which encode for the homologous DsrAB complex, do not encode for DsrL, indicating that the flavoprotein is not the universal protein essential for assembly of (r)DsrAB. Other *dsr* gene products however are worth considering and will be discussed, inter alia, in the following chapter.

Structure and Phylogeny of Siroheme-Containing Reductases

Among the siroheme-containing reductases, which all contain at least one conserved binding motif for their prosthetic group siroheme-[4Fe4S] (C-X_5-C-X_n-C-X_3-C) (Ostrowski *et al.,* 1989), various structures can be found. The assimilatory sulfite reductase of *D. vulgaris* is monomeric and of low molecular weight (24 kDa), while the well investigated NADPH-dependent aSir of *E. coli* consists of a flavo- and a hemoprotein, which form an $\alpha_8\beta_4$ holoenzyme (Figure 32) (Crane and Getzoff, 1996; Dhillon *et al.,* 2005). The assimilatory ferredoxin-dependent sulfite and nitrite reductases of organisms able of

oxygenic photosynthesis, like plants, algae and cyanobacteria, are soluble monomeric enzymes with a molecular mass of 60 – 66 kDa and only one siroheme-[4Fe4S] binding site (Figure 32) (Hase *et al.,* 2006). The most common dissimilatory sulfite reductase DsrAB consists of two structurally related subunits building an $\alpha_2\beta_2$ formation (Fauque *et al.,* 1990; Dahl *et al.,* 1993), while the dissimilatory sulfite reductase of e.g. *Salmonella* ArsABC consists of a ferredoxin protein (AsrA), a flavoprotein (AsrB) and a hemoprotein (AsrC) (Figure 32) (Huang and Barrett, 1991).

Sulfite reductase hemoproteins and nitrite reductases are homologous proteins and presumably have evolved from a common ancestral peptide, as amino acid sequence identities between these proteins indicate (Ostrowski *et al.,* 1989). Concerning the evolution of sulfite reductases, it has been proposed that the last common ancestor of assimilatory and dissimilatory sulfite reductases is a monomeric sulfite reductase bearing one siroheme-[4Fe4S] binding motif and is of similar structure as the assimilatory type low molecular sulfite reductase from *D. vulgaris* (Dhillon *et al.,* 2005). Sequence and structure of the *E. coli* assimilatory sulfite reductase hemoprotein indicate that it emerged from a duplication event of the ancestral sulfite reductase gene. The resulting gene product forms a pseudodimer with only one functional siroheme-[4Fe4S] binding site, while the second is degenerated (Crane *et al.,* 1995; Dhillon *et al.,* 2005). The two structurally related subunits of dissimilatory sulfite reductases, DsrA and DsrB, each have a siroheme-[4Fe4S] binding site and additionally include a ferredoxin domain, which binds an additional [4Fe4S] cluster (Dahl *et al.,* 1993). The hemoprotein AsrC of the dissimilatory sulfite reductase AsrABC also contains a ferredoxin domain in addition to its siroheme-[4Fe4S] binding motif. Presumably a ferredoxin gene was inserted into the gene of the ancestral monomeric sulfite reductase and the duplication of this ancestral gene led to the formation of the two structurally related subunits DsrA and DsrB (Dahl *et al.,* 1993), while AsrC is a modern example of a monomeric dissimilatory sulfite reductase with a ferredoxin domain (Dhillon *et al.,* 2005). Taken together the model of sulfite reductase evolution includes at least two independent duplication events, one before and one after the insertion of a ferredoxin gene into the ancestral sulfite reductase gene, leading to the modern assimilatory and dissimilatory sulfite reductases respectively (Dhillon *et al.,* 2005).

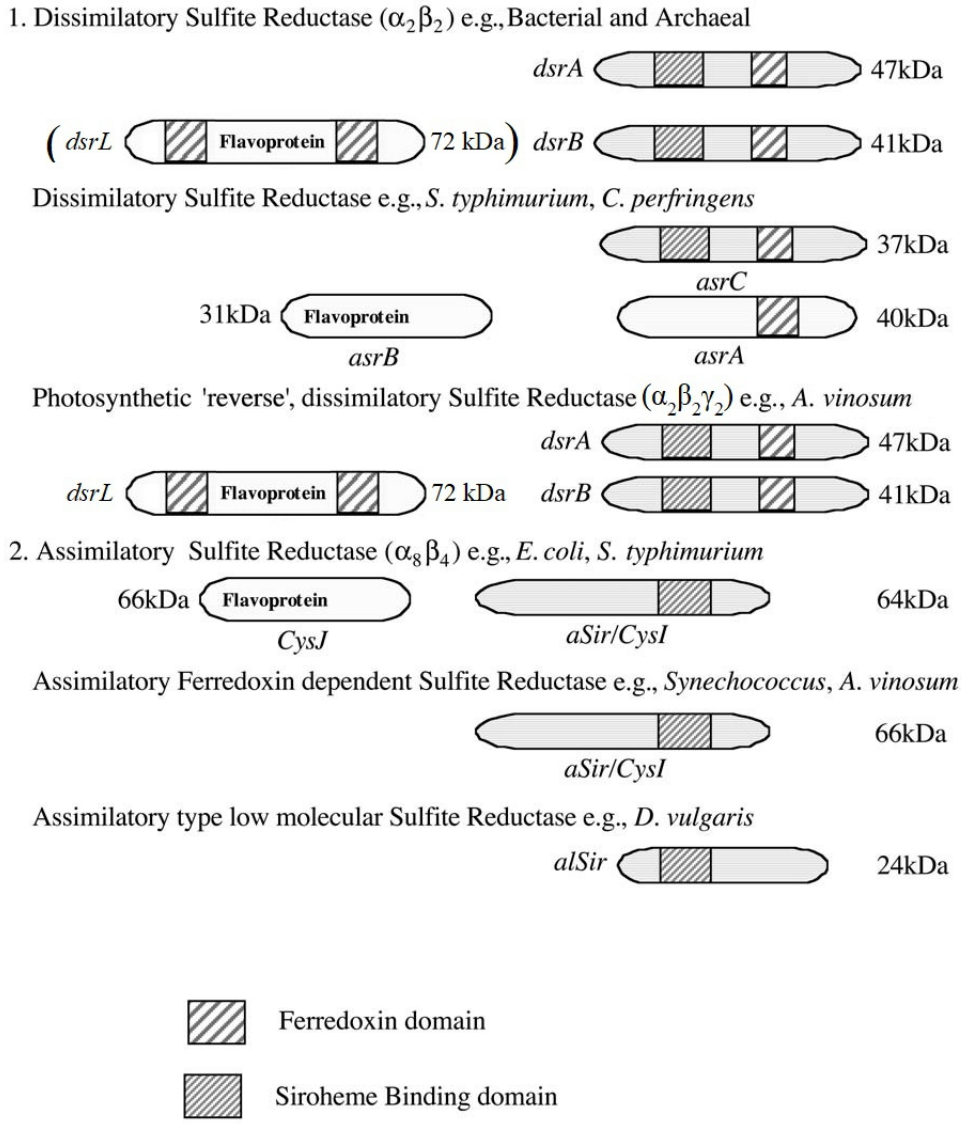

Figure 32: Graphical overview of protein domains involved in the electron transport during sulfite reduction and sulfur oxidation. Modified after Dhillon *et al.* (2005).

Several recombinant assimilatory sulfite and nitrite reductases from bacteria and plants can be produced successfully in *E. coli*. The complex NADPH-dependent aSir of *E. coli* can be produced heterologously, as it belongs to the production strains own proteins (Wu *et al.,* 1991). Most of the other recombinantly produced siroheme-containing reductases are monomeric assimilatory sulfite or nitrite reductases (Nakayama *et al.,* 2000; Schnell *et al.,* 2005; Tripathy *et al.,* 2007). Furthermore the dissimilatory sulfite reductase from *Salmonella* ArsABC has been overexpressed in *E. coli*, which enabled the latter to reduce sulfite to hydrogen sulfide (Huang and Barrett, 1991). The recombinant production of the $\alpha_2\beta_2$ holoenzyme DsrAB however seems to be more difficult. This is supported by the fact

that biochemically and structurally analyzed DsrAB complexes from the sulfate-reducers *Desulfovibrio gigas, D. vulgaris* and *A. fulgidus* were all obtained from their originated organisms and not produced heterologously (Hsieh *et al.,* 2010; Oliveira *et al.,* 2008; Schiffer *et al.,* 2008; Santos *et al.,* 2015). The rDsrAB investigated in this study was also purified from the sulfur oxidizer *A. vinosum* (4.2), as heterologous production in *E. coli* was not successful (Figure 7).

The *dsrAB* genes can be found in phylogenitically distinct bacteria and archaea uniting them in the functional group of microorganisms with a dissimilatory sulfur metabolism (Loy *et al.,* 2008). Three different DsrAB protein families can be delineated: the bacterial DsrAB of microbes capable of reducing sulfate, sulfite and/or organosulfonates, the bacterial rDsrAB of sulfur oxidizers and the archaeal DsrAB from sulfite reducers of the *Pyrobaculum* species (Molitor *et al.,* 1998). Members of the archaeal genus *Archaeoglobus* encode for bacterial DsrAB and have presumably acquired the genes in an ancient lateral gene transfer (Loy *et al.,* 2008). However, the main evolutionary process responsible for the distribution of *dsrAB* is vertical transmission, while lateral gene transfer (LGT) relatively plays a minor role (Loy *et al.,* 2008). Therefore the aforementioned duplication of an ancestral *dsr* gene likely occurred prior to the diversification of the *Archaea* and *Bacteria* domains (Molitor *et al.,* 1998). The ancestral DsrAB is postulated to have functioned in reductive direction, while a functional split of the bacterial DsrAB presumably led to the emergence of the reverse-acting DsrAB (Molitor *et al.,* 1998; Loy *et al.,* 2008).

When considering (r)DsrAB, it is important to note that organisms encoding for this sulfite reductase, also encode for a whole set of further Dsr proteins. DsrC and minimally DsrMK of the DsrMKJOP complex belong to the core set of Dsr proteins, which are encoded in the genomes of all organisms encoding for (r)DsrAB (Grein *et al.,* 2013; Venceslau *et al.,* 2014). The DsrMKJOP complex of *A. vinosum* was found to copurify with the sulfite-generating rDsrAB complex and the sulfur-binding protein DsrC (Dahl *et al.,* 2005) and in *D. vulgaris* the subunits of DsrAB are tightly bound to DsrC forming an $\alpha_2\beta_2\gamma_2$ complex (Oliveira *et al.,* 2008). These findings indicate a tight functional interaction between (r)DsrAB, DsrC and the DsrMKJOP complex. Possibly one or several of these obligatory Dsr proteins also play a role in (r)DsrAB assembly and would be required in a heterologous production of the dissimilatory sulfite reductase in *E. coli.* Especially DsrC,

which was shown to bind in a cleft between DsrA and DsrB close to the catalytic site of the sulfite reductase in *D. vulgaris* (Oliveira *et al.,* 2008) could potentially enable the assembly of the two subunits.

The iron-sulfur flavoprotein DsrL is, as mentioned above, most probably not required for (r)DsrAB assembly, as it is not encoded in all organisms containing *(r)dsrAB*. Nonetheless *dsrL* is included in the genome of all sulfur oxidizers encoding for rDsrAB, where its gene product is absolutely essential for the oxidation of stored sulfur (Lübbe *et al.,* 2006), and it is also included in genomes of several sulfate and sulfite reducers (Anantharaman *et al.,* 2018). In this study the DsrL homodimer was shown to form an $\alpha_2\beta_2\gamma_2$ complex with rDsrAB of *A. vinosum* and to functionally interact with the sulfite reductase (Figure 11, Figure 16) (Löffler *et al.,* 2020). The finding that a dissimilatory sulfite reductase interacts with a flavoprotein is quite plausible, as many siroheme-containing reductases interact with flavoproteins (Figure 32) (Dhillon *et al.,* 2005). A further common interaction partner of monomeric assimilatory sulfite and nitrite reductases are ferredoxin proteins (Hase *et al.,* 2006). The hemoprotein AsrC of the *Salmonella* dSir even interacts with a flavoprotein and a ferredoxin protein to form the AsrABC holoenzyme (Huang and Barrett, 1991). Interestingly DsrL is not only a flavoprotein, it also has a C-terminal ferredoxin domain, indicating that rDsrAB interacts with a flavoprotein and a ferredoxin just like shown for the DsrA and DsrB homologous hemoprotein AsrC (Figure 32).

Catalytic Properties of Siroheme-Containing Reductases

The six electron reductions of sulfite to hydrogen sulfide and nitrite to ammonia are catalyzed by sulfite and nitrite reductases, which both bind a siroheme-[4Fe4S] cofactor in their active site (Murphy *et al.,* 1974). Although siroheme-containing reductases occur in various sizes and oligomeric states, they all share a characteristic cofactor binding site, which presumably ensures the efficient transfer of multiple electrons to the substrate through the direct linkage of an [4Fe4S]-cluster to the siroheme (Crane and Getzoff, 1996). It has been demonstrated for several sulfite and nitrite reductases, that they can use both sulfite and nitrite as substrates, but with varying affinity and turnover rates (Crane and Getzoff, 1996). For the *E. coli* sulfite reductase a K_M value of 4.3 µM for sulfite and an almost 200-fold higher K_M value (800 µM) for nitrite were determined, demonstrating that sulfite is clearly the preferred substrate. However, after substrate saturation higher

turnover rates were reached with nitrite (3100 NADPH/min/enzyme) compared to sulfite (1850 NADPH/min/enzyme) (Siegel *et al.,* 1974). Comparison of catalytic data obtained from further assimilatory sulfite and nitrite reductases demonstrates that both enzyme classes show a greater V_{max} with the substrate nitrite than with sulfite. Furthermore the affinity towards sulfite is higher for sulfite reductases, while the affinity towards nitrite is higher for nitrite reductases (Krueger and Siegel, 1982; Crane and Getzoff, 1996).

The dissimilatory sulfite reductase of *A. fulgidus* can also reduce both sulfite and nitrite, however the specific activity for sulfite reduction is substantially higher than for nitrite reduction (Parey *et al.,* 2010). Interestingly sulfite reduction rate of DsrAB with methyl viologen as artificial electron donor can be strongly increased, when DsrC is added to the reaction (1278 ± 2 mU/mg with and 82 ± 2 mU/mg without DsrC), while the affinity towards sulfite is not affected (K_M: 12 ± 3 µM with and 11 ± 4 µM without DsrC) (Santos *et al.,* 2015). Results obtained in this study demonstrate that rDsrABL from *A. vinosum* has similar catalytic properties, although its physiological activity is clearly distinct from that of DsrAB from a sulfate reducer. Sulfite reduction rate is also higher in the presence of DsrC (1728 ± 62 mU/mg) than without it (140 mU/mg) (Figure 13) and the K_M towards sulfite (13.5 ± 2.1 µM) (Figure 14) is in the same range as determined for DsrAB from *A. fulgidus* (Santos *et al.,* 2015). Consequently the interaction of (r)DsrAB with DsrC, a gene product encoded in all organisms containing *dsrAB* (Venceslau *et al.,* 2014), seems to be generally valid. The capability of rDsrABL to reduce the alternate substrate nitrite has not been tested, but in the light of the homology between *A. vinosum* rDsrAB and *A. fulgidus* DsrAB (Hipp *et al.,* 1997) and their similar catalytic properties with sulfite as substrate, rDsrABL is most probably also able to reduce nitrite. While DsrAB from *A. fulgidus* cannot use NAD(P)H as electron donor for sulfite reduction, it could be demonstrated in this study that the rDsrABL complex from *A. vinosum* can receive electrons from NAD(P)H via the FAD-containing DsrL and use them to reduce sulfite (Figure 16). While the K_M towards sulfite (15.9 ± 3.1 µM) is not altered, the specific activity in the presence of DsrC is substantially lower (254 ± 17.6 mU/mg) when NADH is used as electron donor instead of methyl viologen (1728 ± 62 mU/mg) (Figure 17A, Figure 14B). The assimilatory sulfite reductase from *E. coli*, which also consists of a siroheme-containing subunit and an FAD-containing subunit, likewise shows a greater activity with methyl viologen than with NADPH as electron donor (Siegel *et al.,* 1974). This indicates that electron transfer between the

flavoprotein and the hemoprotein can be limiting in the reduction of sulfite at the catalytic site of the hemoprotein (Siegel *et al.,* 1982). The electrons from methyl viologen can be directly transferred onto the siroheme of the aSir hemoprotein and of rDsrAB, while the electrons from NAD(P)H have to be transferred via the FAD of the aSir flavoprotein and DsrL onto the siroheme-containing subunit, before they can be used to reduce sulfite. Interestingly in ferredoxin-dependent sulfite and nitrite reductases the electron transfer from reduced ferredoxin to the siroheme-containing subunit does not seem to be limiting, as their specific activity is higher with ferredoxin than with methyl viologen as electron donor (Krueger and Siegel, 1982).

5.2 The Role of Iron-Sulfur Flavoprotein DsrL in the (r)Dsr Pathway

The iron-sulfur flavoprotein DsrL of *A. vinosum* is essential for the oxidation of stored sulfur catalyzed by rDsrAB (Lübbe *et al.,* 2006). It has been shown recently that *dsrL* is not only present in the genome of sulfur oxidizers, but also in the *dsr* operons of some sulfate and sulfite reducers (Anantharaman *et al.,* 2018). Up to now it was unclear in which manner DsrL contributes to the dissimilatory sulfur metabolism. In the present study its interaction with rDsrAB from *A. vinosum* was demonstrated both structurally and functionally (4.2.2, 4.3.2.2). The impact these findings have on our understanding of the (r)Dsr pathway in both sulfur oxidizers and sulfate reducers will be discussed in the following.

Structure and Function of DsrL as NAD(P)H:Oxidoreductase

DsrL belongs to the FAD and FeS cluster-containing pyridine nucleotide: disulfide oxidoreductase protein family along with proteins such as glutathione reductase and thioredoxin reductase (Dahl *et al.,* 2005). DsrL contains two Rossmann-type binding domains, one binding FAD and the other binding $NAD(P)^+$ (Figure 33) (Löffler *et al.,* 2020). A helical domain at the N-terminus binds two [4Fe4S] clusters, while a ferredoxin-like domain at the C-terminus potentially binds two further [4Fe4S] clusters (Löffler *et al.,* 2020). The C-terminal domain is connected to the rest of the protein through a linker domain (Figure 33).

Although DsrL is a homolog of the small subunit of bacterial glutamate synthases (GltD) and was thought to deliver glutamine needed by DsrN for siroheme amidation, it does not

exhibit glutamate synthase activity (Lübbe *et al.,* 2006). Recombinant DsrL does however exhibit NAD(P)H:oxidoreductase activity just as GltD, which transfers electrons from NAD(P)H to an acceptor protein or protein domain (Vanoni and Curti, 1999; Löffler *et al.,* 2020). The purification of the rDsrABL complex from *A. vinosum* gave the opportunity to compare the catalytic properties of DsrL from the rDsrABL complex and of recombinant DsrL.

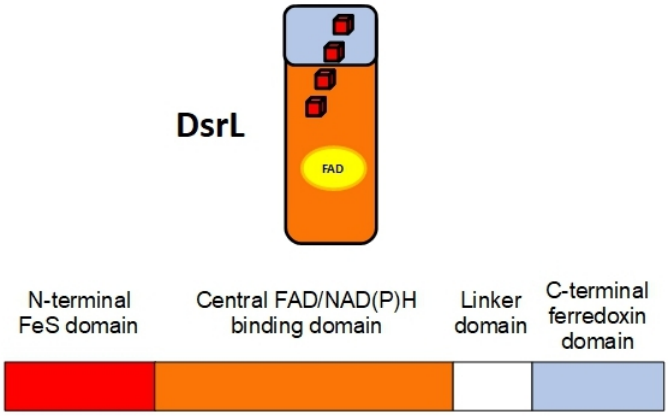

Figure 33: Schematic overview of DsrL structure. DsrL consists of an N-terminal FeS-domain (red), a central FAD/substrate-binding domain (orange) and a C-terminal ferredoxin domain (light blue), which is connected via a linker domain (white). Prosthetic groups are indicated as follows: FAD (yellow ellipse), [4Fe4S]-clusters (red boxes). Modified after Löffler *et al.* (2020).

NAD(P)H:oxidoreductase activity could also be observed for DsrL from the rDsrABL complex of *A. vinosum*, as the protein was able to transfer electrons from NADH to the artificial electron acceptor MTT and to reduce NAD^+ with electrons from the artificial electron donor methyl viologen (Figure 15). The specific activity was however about 9-fold higher for NAD^+ reduction in comparison to NADH oxidation (49.3 U/mg and 5.9 U/mg). This catalytical preference was also observed for recombinant DsrL from *A. vinosum* (Wallerang *et al.,* 2020). The K_M values towards NADH for DsrL of the purified rDsrABL complex (78.5 ± 21.0 µM) and for recombinant DsrL (86.7 ± 17.0 µM) are in the same range (Löffler *et al.,* 2020). These findings indicate that neither the interaction with its physiological partner rDsrAB nor the Strep-tag added to recombinant DsrL alter its catalytic properties substantially. DsrL from *A. vinosum* can also use NADPH as a substrate, however at a physiological pH of 7, specific activity is considerably lower and the K_M value

towards NADPH is much higher than when NADH is used as substrate (Löffler *et al.,* 2020). Similar catalytic tendencies can be observed when $NADP^+$ is used as a substrate instead of NAD^+ (Wallerang *et al.,* 2020). On the whole the oxidation of NAD^+ seems to be the preferred reaction for DsrL from the sulfur oxidizer *A. vinosum* under *in vivo* conditions. Interestingly this catalytical bias is also found in DsrL from sulfur oxidizers of the phylum *Chlorobi* such as *Chlorobaculum tepidum* but cannot be confirmed for DsrL from the thiosulfate reducer *Desulfurella amilsii* (Wallerang *et al.,* 2020). DsrL from *D. amilsii* shows no reactivity with NAD^+ or NADH, but only with $NADP^+$ and NADPH. An alignment of several DsrL sequences from organisms associated with reduction of sulfur compounds and organisms associated with oxidation of sulfur compounds revealed that the reducers have three highly conserved residues (Y-R-R) in the Rossmann-type binding motif for $NAD(P)^+$, while the residues are not conserved in the oxidizers (Wallerang *et al.,* 2020). The two adjacent arginines are also conserved in another member of the disulfide oxidoreductase superfamily, the DsrL homolog NfnB, where they were shown to bind the phosphate of $NADP^+$ via hydrogen bonds (Demmer *et al.,* 2015).

Taken together DsrL from oxidizers preferably reduces NAD^+ while DsrL from reducers preferably reacts with $NADP^+$/NADPH. The finding of conserved residues in the Rossmann-type binding motif of DsrL from reducers give a plausible explanation for the different catalytical preferences of DsrL from oxidizers and reducers.

DsrL and (r)DsrAB Work Together as NAD(P)H:Sulfite Oxidoreductase

The copurification of the reverse-acting dissimilatory sulfite reductase of *A. vinosum* with the NAD(P)H:oxidoreductase DsrL demonstrated their structural interaction (Figure 10) and was a first indication for a functional interaction. The interaction of a flavoprotein with NAD(P)H:oxidoreductase activity and a siroheme-containing sulfite reductase is quite common (Figure 32) (Dhillon *et al.,* 2005). In the assimilatory sulfite reductase of *E. coli* the flavoprotein subunits enable electron transfer from NADPH via bound FAD and FMN cofactors to the catalytically active siroheme of hemoprotein subunits and finally onto sulfite (Crane *et al.,* 1997). A well characterized homolog of DsrL is NfnB, the large subunit of the NADH-dependent reduced ferredoxin:NADP oxidoreductase NfnAB (Demmer *et al.,* 2015). Electrons stemming from NADPH are transferred via NfnB onto ferredoxin and NfnA, which then reduces NAD^+ (Figure 34A). In the present study it could be

demonstrated that DsrL enables electron transfer from NAD(P)H onto a protein acceptor just as was shown for the flavoprotein of aSir and for NfnB of the NfnAB complex. Electrons deriving from NAD(P)H were transferred via DsrL onto rDsrAB and used to reduce sulfite (Figure 16, Figure 34B). DsrL alone could not catalyze NADH-dependent reduction of sulfite, proving that the complete rDsrABL complex is needed for NAD(P)H:sulfite oxidoreductase activity. As mentioned above the specific activity of rDsrABL was substantially lower with NADH than with methyl viologen as electron donor (Figure 17A, Figure 14B), which indicates that electron transfer from NADH via DsrL onto rDsrAB might be a limiting factor in the reduction of sulfite. As the specific activity with NADH was not increased when recombinant DsrL was added to the reaction (Figure 18), DsrL concentration does not seem to be limiting. Furthermore the reaction was preformed with aerobically purified, iron-sulfur reconstituted and with anaerobically purified rDsrABL with similar results. This indicates that the load with prosthetic groups is not the limiting factor either. As a higher specific activity with methyl viologen than with NADPH was also observed for aSir of *E. coli*, the limiting electron transfer from NAD(P)H via FAD of the flavoprotein onto the siroheme of the hemoprotein could be a general phenomenon (Siegel *et al.,* 1982).

At a physiological pH of 7 the specific activity of sulfite reduction catalyzed by rDsrABL with NADH as electron donor was over 5-fold higher than with NADPH, which is consistent with catalytical preferences observed for recombinant DsrL from sulfur oxidizers (Löffler *et al.,* 2020; Wallerang *et al.,* 2020). Furthermore the specific activity of DsrL from *A. vinosum* is substantially higher for NAD^+ reduction than for NADH oxidation (Figure 15). Taken together DsrL of sulfur oxidizers presumably functions as NAD^+ reductase, transferring electrons stemming from sulfite formation catalyzed by rDsrAB onto NAD^+ (Figure 34C). DsrL proteins from organisms associated with reduction of sulfur compounds presumably interact with NADPH and not with NADH as could be shown for DsrL from the thiosulfate reducer *D. amilsii* (Wallerang *et al.,* 2020). This theory is supported by the fact that in the $NAD(P)^+$ binding motif three residues (Y-R-R) are highly conserved in DsrL from reducers and in NfnB, where they were shown to bind the phosphate of $NADP^+$ (Demmer *et al.,* 2015; Wallerang *et al.,* 2020). Thus in reducers DsrL presumably functions as physiological electron donor for sulfite reduction catalyzed by DsrAB, by transferring electrons from NADPH to DsrAB and finally onto sulfite (Figure 34B).

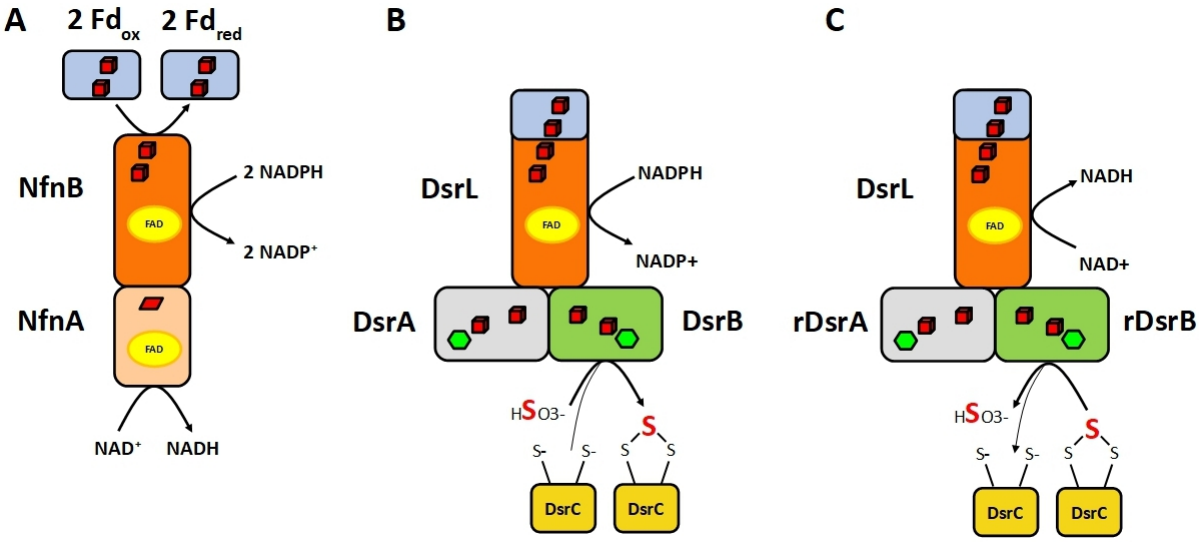

Figure 34: Schematic overview of the reactions catalyzed by NfnAB (A), DsrABL (B) and rDsrABL (C). The (r)DsrABL complex is depicted as heterotrimer and not as the heterohexamer isolated from *A. vinosum* for better clarity and comparability to the NfnAB complex. Similarity of NfnB and the major part of DsrL as well as that of ferredoxin (Fd) and the C-terminal domain of DsrL is highlighted by identical colors (orange and light blue, respectively). Prosthetic groups are indicated as follows: FAD (yellow ellipse), [4Fe4S] clusters (red boxes), [2Fe2S] cluster (red parallelogram), siroheme (green hexagon). Modified after Löffler *et al.,* (2020).

These findings have a considerable impact on our understanding of the dissimilatory sulfur metabolism of both oxidizers and reducers. For those organisms, which encode DsrL and are associated with dissimilatory reduction of sulfur compounds, a very plausible candidate for the long sought-for electron donor for DsrAB is found. The finding that DsrAB interacts with a NAD(P)H:oxidoreductase with an additional ferredoxin domain, can also be beneficial in the search for the unknown electron donor in reducers not encoding for DsrL, as it might have similar properties as DsrL. For autotrophic sulfur oxidizers the postulated direct transfer of electrons stemming from the oxidation of stored sulfur into the nicotinamide adenine dinucleotide pool via rDsrABL (Figure 34C) would be a big advantage, as it reduces the need for energy-consuming reverse electron flow for the production of reducing equivalents needed for CO_2 fixation (Löffler *et al.,* 2020). When the electron donor has a more positive redox potential than $NAD(P)^+$/NAD(P)H, microorganisms have to use energy at the expense of the proton motive force to reduce $NAD(P)^+$. The reduction potential of the rDsrABL-catalyzed reaction ($DsrC_{ox}$-S + 3 H_2O → HSO_3^- + $DsrC_{red}$ + 3 H^+ + 2 e^-) alone is possibly too positive to directly reduce NAD^+. Perhaps an additional input of electrons from an electron donor with a lower redox

potential is needed, meaning that the dissimilatory sulfur oxidation would involve electron bifurcation to reduce NAD^+.

Potential Activity of DsrL as Bifurcating Subunit

As DsrL shows great homologies to NfnB, the bifurcating subunit of the NADH-dependent reduced ferredoxin:NADP oxidoreductase NfnAB, it can possibly also enable electron bifurcation. In the following the general mechanism of electron bifurcation, the specific process of flavin-based electron bifurcation in NfnAB and the potential activity of DsrL as bifurcating subunit will be discussed.

Next to the two well characterized mechanisms of biological energy conservation, substrate-level phosphorylation and electron transport-linked phosphorylation, a third mechanism exists named electron bifurcation (Herrmann *et al.,* 2008). In this energy conservation mechanism exergonic and endergonic redox reactions are simultaneously coupled to bypass thermodynamic barriers for the endergonic reaction and to minimize free energy loss for the exergonic reaction (Peters *et al.,* 2016). In the cell an endergonic reaction does not occur spontaneously, as it requires energy, while an exergonic reaction releases free energy, which is lost unless it is sustained via energy-conserving mechanisms. Bifurcating enzymes directly couple either the reduction of a low and a high potential electron acceptor to the oxidation of a donor with intermediate potential or the oxidation of a low and a high potential electron donor to the reduction of an acceptor with intermediate potential, the latter also being called electron confurcation (Figure 35). There are two types or electron bifurcation, the quinone- and the flavin-based electron bifurcation (QBEB/FBEB). While the first papers on FBEB were only published quite recently (Herrmann *et al.,* 2008; Li *et al.,* 2008), QBEB was already discovered 45 years ago (Mitchell 1975).

In the following the focus will be laid on flavin-based electron bifurcation, in which the bifurcating enzyme complex contains multiple electron transfer centers including FeS clusters and flavins, whereby a flavin is the site of bifurcation (Herrmann *et al.,* 2008). While FeS clusters transfer single electrons and pyridine nucleotides are two-electron donors or acceptors, flavin cofactors like FAD and FMN have intermediate redox properties. The flavoquinone is the fully oxidized form (ox = 0), which can be partially reduced with one electron to the flavosemiquinone (ox = -1) and the fully reduced form is

called flavohydroquinone (ox = -2) (Buckel and Thauer, 2018). FBEB can only occur if the flavosemiquinone is not stable, as then the reducing power of flavohydroquinone is lower than that of the unstable flavosemiquinone (Nitschke and Russell, 2012). This means the first electron stemming from flavohydroquinone is transferred to an acceptor with a higher redox potential in an exergonic reaction, while the second electron is structurally prevented from also following the exergonic path. The second electron stemming from the unstable flavosemiquinone with strong reducing power can then be transferred to an acceptor of lower redox potential (Nitschke and Russell, 2012).

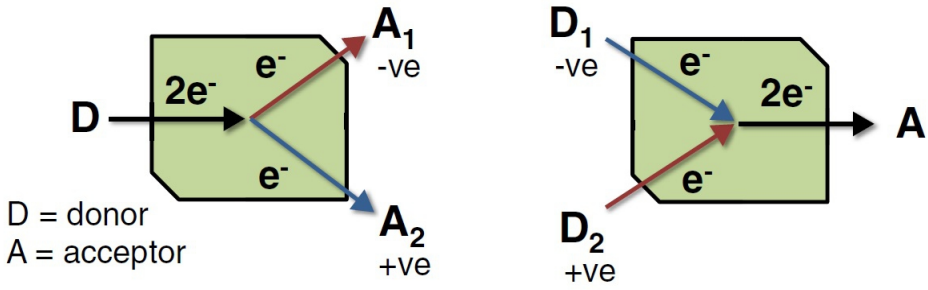

Figure 35: Electron transfer in bifurcating enzymes. Left: Electron bifurcation in which a two-electron donor (D) of intermediate reduction potential simultaneously provides electrons to electron acceptors with more negative (A_1) and more positive (A_2) potentials. Right: Electron confurcation in which a two-electron acceptor (A) of intermediate reduction potential simultaneously accepts electrons from electron donors with more negative (D_1) and more positive (D_2) potentials. (Peters *et al.,* 2016)

The low potential electron donor or acceptor of several electron bifurcations and confurcations respectively is ferredoxin (Li *et al.,* 2008; Kaster *et al.,* 2011; Demmer *et al.,* 2015; Weghoff *et al.,* 2015). Ferredoxins are iron-sulfur proteins, which function as electron carriers and link various biochemical pathways (Atkinson *et al.,* 2016). They build a structurally diverse group of proteins, which contain one or two iron-sulfur clusters as redox active cofactor. Reduced ferredoxins belong to the strongest soluble reductants found in nature, as they have a typical midpoint potential of approximately -420 mV (Knaff, 1996). In archaea, bacteria and eukaryotes ferredoxins interact with a vast number of proteins and are involved in various metabolic pathways such as carbon fixation, nitrate and sulfate assimilation, photosynthesis and energy conservation (Atkinson *et al.,* 2016). The interaction partners of ferredoxins in energy conservation pathways are bifurcating

enzymes, such as the NADH-dependent reduced ferredoxin:NADP oxidoreductase NfnAB (Demmer *et al.,* 2015).

NfnAB catalyzes a reversible electron bifurcation, in which four electrons from two NADPH molecules are used to reduce two ferredoxins and NAD^+ (Figure 34A) (Demmer *et al.,* 2015). Thereby NfnB binds NADPH, reduces ferredoxin and transfers electrons to NfnA, which reduces NAD^+. Thus NfnB is the bifurcating subunit of the NfnAB complex and binds the bifurcating FAD, while the FAD of NfnA transfers two electrons onto NAD^+. The homologous proteins DsrL and NfnB have several structural elements in common: an N-terminal FeS cluster binding domain and two Rossmann-type nucelotide-binding domains of which one binds FAD and the other $NAD(P)^+$ (Figure 34) (Löffler *et al.,* 2020). However, DsrL has a C-terminal extension consisting of a linker domain and a ferredoxin-like domain (Figure 33), which NfnB lacks. The sequence identifies of DsrL and NfnB especially in the central FAD/NAD(P)H binding domain suggest that DsrL could also enable flavin-based electron bifurcation.

In the present study it could be demonstrated that DsrL can interact with ferredoxin from *Clostridium tetanomorphum*, as electrons stemming from reduced ferredoxin could be transferred via DsrL of the rDsrABL complex onto NAD^+ (Figure 19). However assays with NAD(P)H as the electron donor of intermediate reduction potential for the simultaneous reduction of ferredoxin and sulfite/DsrC were unsuccessful (Figure 20). Oxidized ferredoxin could not be reduced by rDsrABL and the reduction of sulfite in the presence of DsrC did not proceed faster in the presence of oxidized ferredoxin. Thus electron transfer between ferredoxin and DsrL could be detected, but the results give no indication for an electron bifurcation, in which electrons stemming from NAD(P)H can be used to reduce sulfite and DsrC in the exergonic reaction and ferredoxin in the endergonic reaction.

Clostridial ferredoxin and alvin-like ferredoxin, as it occurs in *A. vinosum*, both bind two [4Fe4S] clusters, nevertheless they show structural differences (Atkinson *et al.,* 2016). Consequently it is possible that ferredoxin from *C. tetanomorphum* is not an ideal interaction partner for DsrL from *A. vinosum*, which is supported by the fact that electron transfer detected in Figure 19 occurs at a very slow rate. Thus the exiting question whether DsrL enables electron bifurcation in the dissimilatory sulfur metabolism will have to be investigated in further studies.

For sulfate reducers the involvement of electron bifurcation in dissimilatory sulfur metabolism would mean that two electrons stemming from NADPH could be simultaneously used to reduce sulfite in the presence of DsrC and to reduce the low potential ferredoxin. Reduced ferredoxins with their strong reducing power have an important role in the cell, as they drive electrochemical H^+ and Na^+ pumps and enable difficult reductions (Buckel and Thauer, 2013). In sulfur oxidizers the oxidation of reduced ferredoxin could enable the electron transfer from DsrC-bound sulfur onto NAD^+ and therefore link the dissimilatory sulfur metabolism to the production of reducing equivalents needed for the fixation of CO_2.

5.3 DsrC Plays a Central Role in (r)Dsr Metabolism

DsrC belongs to the core set of proteins encoded in organisms which contain *dsrAB* (Grein *et al.,* 2013; Venceslau *et al.,* 2014). The small protein (12-14 kDa) binds no prosthetic groups and is characterized by a highly conserved C-terminal arm containing two strictly conserved cysteine residues (Cort *et al.,* 2001; Cort *et al.,* 2008; Oliveira *et al.,* 2008). DsrC was shown to tightly interact with DsrAB from sulfate reducers both structurally and functionally (Oliveira *et al.,* 2008; Santos *et al.,* 2015). In the present study a functional interaction between the sulfite-generating rDsrABL complex from *A. vinosum* and DsrC has been demonstrated for the first time. In the following characteristics of DsrC and the key role it plays in both reductive and oxidative dissimilatory sulfur metabolism will be outlined.

Structure and Distribution of DsrC and DsrC-like Proteins

DsrC structures from both sulfate reducers and sulfur oxidizers reveal its globular form with a protruding C-terminal arm (Cort *et al.,* 2001; Mander *et al.,* 2005; Cort *et al.,* 2008). The main part of the globular protein is made up of five α-helices, whereby the flexible C-terminal arm is attached to helix α5. Between helices α3 and α4 a helix-turn-helix(HTH)-like structural motif can be found (Cort *et al.,* 2001; Cort *et al.,* 2008). HTH domains are common DNA-binding motifs in transcriptional regulator proteins, as they mediate interaction between proteins and nucleic acids, but they are also associated with protein-protein interactions (Aravind *et al.,* 2005). The HTH motif in DsrC could allow the small protein to regulate transcription of the *dsr* operon, which is supported by the fact that DsrC

binds to the putative *dsr* promotor region upstream of the *dsrA* gene in *A. vinosum* (Grimm *et al.,* 2010). Alternatively or additionally the HTH motif could enable the interaction of DsrC with its large number of physiological interaction partners like the DsrEFH complex (Stockdreher *et al.,* 2012), DsrK of the DsrMKJOP complex (Grein *et al.,* 2010) and (r)DsrAB (Oliveira *et al.,* 2008; Santos *et al.,* 2015) (4.3.3).

An essential part of DsrC is its flexible C-terminal arm, which harbors two highly conserved cysteine residues (Cort *et al.,* 2001; Cort *et al.,* 2008; Oliveira *et al.,* 2008). One cysteine is the penultimate residue at the C-terminus (Cys_A) and the other lays eleven residues upstream (Cys_B). Cys_A was shown to be absolutely essential for the functional interaction of DsrC with DsrAB from sulfate reducer *A. fulgidus* (Santos *et al.,* 2015) and with rDsrABL from sulfur oxidizer *A. vinosum* (Figure 24). The product of sulfite reduction catalyzed by DsrAB from *A. fulgidus* in the presence of DsrC is a trisulfide in which the reduced sulfur atom is bridged between Cys_A and Cys_B of DsrC.

Along with several other DsrC-like proteins, which are partly also present in organisms not associated with dissimilatory sulfur metabolism, DsrC belongs to the DsrC/TusE/RpsA superfamily (Venceslau *et al.,* 2014). The proteins of this family can be divided into three groups. DsrC proteins have two conserved cysteines at the C-terminus ($Cys_BX_{10}Cys_A$ motif), TusE proteins only have one conserved cysteine namely Cys_A and DsrC-like proteins lacking Cys_A or lacking both cysteines are termed as regulatory sulfur-related proteins (RspA). The RspA proteins could be involved in gene regulation, as they also harbor the HTH motif possibly enabling DNA-protein interaction (Venceslau *et al.,* 2014). TusE of *E. coli* is part of a sulfur relay system for the thiouridylation of tRNAs together with the sulfur transferases TusA and TusBCD (Ikeuchi *et al.,* 2006). After receiving activated sulfur from the cysteine desulfurase IscS, TusA transfers sulfane sulfur onto TusD of the TusBCD complex. From TusD sulfur is transferred onto Cys_A of the DsrC homolog TusE, which then interacts with thiouridylase MnmA for 2-thiouridine formation. For its activity as sulfur transferase TusE obviously only requires Cys_A and not Cys_B.

Interestingly DsrC of sulfur oxidizers interacts with a protein complex homologous to TusBCD, the DsrEFH complex (Stockdreher *et al.,* 2012). DsrEFH also receives sulfane sulfur from a TusA protein and transfers it further onto DsrC (Stockdreher *et al.,* 2014). Furthermore DsrC from sulfur oxidizers, which encode for DsrEFH, and TusE proteins from

organisms, which encode for TusBCD, share a seven-residue insertion in the HTH-motif, which DsrC proteins from sulfate reducers lack (Cort *et al.,* 2008). Consequently this region could be essential for the protein-protein interaction of DsrC with DsrEFH and of TusE with TusBCD.

Not only the two characteristic cysteines, but also several further residues are conserved in the flexible arm of DsrC proteins (Venceslau *et al.,* 2014). Despite the high similarity of their C-terminal arms DsrC from sulfate reducer *D. vulgaris* cannot takeover the role of DsrC from *A. vinosum* in sulfite reduction catalyzed by rDsrABL from *A. vinosum* (Figure 25B). This could also be due to the above-mentioned differences in the HTH-like motif, where DsrC from *A. vinosum* has a seven residue insertion in comparison to DsrC from *D. vulgaris* (Figure 25A) (Cort *et al.,* 2008; Venceslau *et al.,* 2014).

Role of DsrC in Reductive and Oxidative Dissimilatory Sulfur Metabolism

DsrC was first found to be tightly associated with DsrAB from *D. vulgaris* almost 30 years ago, as the small protein was copurified with and did not dissociate from the two subunits DsrA and DsrB (Pierik *et al.,* 1992). The crystal structure of the $\alpha_2\beta_2\gamma_2$ complex revealed that the flexible C-terminal arm of DsrC is located in a cleft between DsrA and DsrB, so that Cys_A is in proximity of the catalytic site, where sulfite binds to the siroheme-[4Fe4S] cofactor (Oliveira *et al.,* 2008). The association of DsrC with (r)DsrAB from other sulfate reducers like *A. fulgidus* or from sulfur oxidizers like *A. vinosum* does not seem to be as strong, as (r)DsrAB can be purified without DsrC (Schiffer *et al.,* 2008)(Figure 10). However, DsrC from both above-mentioned organisms was shown to functionally interact with (r)DsrAB (Santos *et al.,* 2015) (4.3.3) and the site of interaction is with high probability the same as detected for DsrC from *D. vulgaris* (Oliveira *et al.,* 2008).

Both DsrC and its homolog TusE are characterized by a conserved Cys_A residue, but DsrC has an additional conserved cysteine eleven residues upstream (Cys_B), which TusE lacks (Venceslau *et al.,* 2014). Its function in DsrC from sulfate reducers was revealed, when the product of sulfite reduction catalyzed by DsrAB was shown to be a DsrC trisulfide with a sulfur atom bound to Cys_A and Cys_B and when the proposed reaction mechanism was unraveled (Figure 3)(Santos *et al.,* 2015). At the catalytic site sulfite is partially reduced by two electrons stemming from DsrAB, the resulting S^{II} intermediate then reacts with Cys_A of DsrC to a sulfenic acid (Cys_A-S-OH). Rearrangement of the C-terminal arm brings the two

cysteines in proximity of each other and Cys_B reduces the S^I intermediate to an S^0 product, in which the zero-valent sulfur is bridged between Cys_A and Cys_B. Thereafter the DsrC trisulfide is proposed to be reduced at the DsrMKJOP complex to sulfide and reduced DsrC (Santos *et al.,* 2015). Thereby DsrK is presumably the subunit at which the DsrC trisulfide is reduced, as it is homologous to HdrD, the catalytic subunit of the membrane-bound HdrDE complex of methanogens, which catalyzes heterodisulfide reduction (Heiden *et al.,* 1994). In analogy to the substrate of the reaction taking place in methanogens, DsrC has already been designated as the “bacterial heterodisulfide” (Venceslau *et al.,* 2014).

DsrC-bound sulfur is the proposed substrate for rDsrAB from sulfur oxidizers and in the present study a functional interaction between these proteins from *A. vinosum* could be demonstrated (4.3.3). Furthermore DsrC from *A. vinosum* was shown to interact with DsrK of the DsrMKJOP complex and with DsrE of the DsrEFH complex (Grein *et al.,* 2010; Stockdreher *et al.,* 2012). In the present study the functional interaction of DsrC and rDsrABL from *A. vinosum* was investigated in detail. The sulfite reduction rate of rDsrABL is increased when reduced DsrC is added to the reaction resulting in an initial fast phase of the reaction, which later decreases to a slow phase (Figure 21). The length of this fast phase is dependent on the amount of DsrC added to the reaction, demonstrating that DsrC is consumed in the course of the reaction. This is consistent with data gained from similar reactions with DsrC and DsrAB from sulfate reducer *A. fulgidus* (Santos *et al.,* 2015).

Reactions with NADH as electron donor for rDsrABL-catalyzed sulfite reduction in the presence of DsrC showed that approximately one molecule NADH is oxidized donating two electrons, when one molecule DsrC is consumed (Figure 21). This is also consistent with the proposed reaction mechanism for dissimilatory sulfite reduction, in which two electrons are transferred from DsrAB onto sulfite and the additional two electrons needed for the reduction to a DsrC trisulfide stem from the reduced DsrC itself (Santos *et al.,* 2015).

The increase in sulfite reduction rate is clearly dependent on Cys_A of DsrC, as variants lacking Cys_A did not increase the reaction rate in a biphasic manner, while the results obtained with a variant lacking only Cys_B were similar to those obtained in the presence of the DsrC WT protein (Figure 24A). The sulfite reduction rate was only slightly increased in the presence of DsrC proteins lacking either only Cys_A or lacking both Cys_A and Cys_B in

comparison to the reaction without DsrC (Figure 24A). Interestingly this increase was not biphasic but persistent, indicating that these DsrC variants are not consumed in the reaction but contribute to its slightly increased rate in a different manner. As DsrC binds in proximity of the active site of rDsrABL it could slightly modify it, so that sulfite can be processed faster. This is supported by the fact that the NADH-dependent sulfite reduction rate is higher, when rDsrABL and DsrC are preincubated before sulfite is added than when rDsrABL is preincubated with sulfite before DsrC is added (Figure 22). Furthermore this slight increase of sulfite reduction rate is not observed in the presence of DsrC from the sulfate reducer *D. vulgaris.* Although it has both conserved cysteines in its C-terminal arm, it does not even have a comparable effect on rDsrABL-catalyzed sulfite reduction as *A. vinosum* DsrC, which lacks both cysteines. This is possibly due to its different HTH motif, which does not enable it to bind to rDsrAB from *A. vinosum*.

Although many similarities between sulfite reduction in the presence of DsrC catalyzed by DsrAB from sulfate reducers and by rDsrABL from a sulfur oxidizer could be observed, differences were also detected. In the *in vitro* assays with rDsrABL and DsrC from *A. vinosum* the product of sulfite reduction is not a DsrC trisulfide (4.3.3.4). The interpretation of the data concerning the DsrC product after reaction with rDsrABL is quite complex, as firstly it is not the physiological reaction of the sulfur oxidizing organism these proteins are originated from and secondly the nonphysiological *in vitro* conditions have an influence on the DsrC product.

On the whole the product of sulfite reduction catalyzed by rDsrABL in the presence of DsrC seems to be a DsrC persulfide. After the reaction with rDsrABL and 25 µM sulfite, DsrC WT was analyzed via MALDI-TOF mass spectrometry and was shown to bind up to three sulfur atoms (+32 Da, +64 Da, +96 Da) (Figure 29C). Thereby the clearest peaks were observed for DsrC binding no or one sulfur (+32 Da). A mass increase of 32 Da would also occur if a DsrC trisulfide had been formed, however the main portion of monomeric DsrC after the reaction with 25 µM sulfite and rDsrABL was still accessible for two MalPEG (Figure 26B). A DsrC trisulfide would not be accessible for MalPEG at all.

When the sulfite concentration was higher (250 µM) another product was observed, DsrC with a mass increase of about 80 Da (Figure 29B+E). Analysis of a control group without rDsrABL showed that this mass increase is unspecific, as it also occurs independent of the

reaction catalyzed by rDsrABL (Figure 30A+C) and presumably is due to a sulfonate group ($R\text{-}SO_3^-$) bound to Cys_A of DsrC (Stockdreher *et al.,* 2012). Sulfite reacts with proteins by reducing inter- or intramolecular disulfide bonds in a reversible reaction ($RS\text{-}SR + SO_3^{2-} \rightleftharpoons RS\text{-}SO_3^- + RS^-$) (Cecil and Wake, 1962). In the shown chemical equilibrium equation, a high sulfite and disulfide concentration promotes the forward reaction, while a high concentration of thiols and sulfonates promotes the reverse reaction. As DsrC was shown to form dimers via a disulfide bond between the Cys_A residues of two DsrC proteins (Cort *et al.,* 2008), the high sulfite concentration of 250 µM accordingly leads to the formation of DsrC Cys_A sulfonates, which are detectable through a mass increase of 80 Da. The reaction with sulfite and rDsrABL seems to support the formation of DsrC dimers (Figure 28), which presumably further contributes to the promotion of the forward reaction.

For a long time a mixture of products (sulfide, thiosulfate and tetrathionate) were detected for sulfite reduction catalyzed by DsrAB in the absence of DsrC, later thiosulfate and tetrathionate were found to be artificial products caused by the reaction of an access of sulfite with S^{II} and S^{I} intermediates in sulfite reduction (Santos *et al.,* 2015). In the results discussed above an access of sulfite leads to the formation of unspecific DsrC products *in vitro.* Taken together this demonstrates that the highly reactive sulfite has a considerable impact on the products of sulfite reduction catalyzed by (r)DsrAB in *in vitro* assays.

The characterization of the DsrC product after sulfite reduction catalyzed by rDsrABL also has an impact on our understanding of the dissimilatory oxidation of sulfane sulfur. As the product is not a DsrC trisulfide but a persulfide at Cys_A, it is probable that the substrate for rDsrABL in the oxidative pathway is also a DsrC persulfide. Accordingly persulfurated DsrC was applied as a potential substrate for rDsrABL in the oxidative direction (Figure 31). However no activity could be measured with the potential physiological electron acceptor NAD^+ nor with artificial electron acceptors with higher redox potentials like MTT, ferricyanide or dichloroindophenol. This could have versatile reasons, which will be discussed in the following.

Persulfurated DsrC could be the wrong substrate for rDsrABL, this is however improbable in light of the finding that a DsrC persulfide is the product of sulfite reduction catalyzed by rDsrABL. As discussed above, the oxidation of DsrC-bound sulfur by rDsrABL could be the endergonic partial reaction of an electron confurcation, which is only enabled by the

oxidation of a further substrate with a substantially lower redox potential. The absence of this unknown low-potential substrate in the assays could have prevented the electron transfer from DsrC-bound sulfur to the physiological electron donor NAD^+. But even if this were the case, a measurable reaction would have been expected with the artificial electron acceptors with higher redox potentials nonetheless.

A further possibility is that the product of the oxidation of DsrC-bound sulfur inhibits the reaction catalyzed by rDsrABL so strongly that a reaction rate cannot be measured. All enzymes are inhibited to some extent by the product or products of their catalyzed reaction (Schmidt *et al.,* 1983). In most cases this does not prevent the reaction from taking place *in vitro* as the required product concentration for an inhibition is not reached in the assays. However for enzymes which catalyze energetically unfavorable reactions, the product inhibition is likely to be very potent (Schmidt *et al.,* 1983). As the oxidation of DsrC-bound sulfur to sulfite is the reverse reaction of the energetically favorable sulfite reduction catalyzed by rDsrABL, it is likely to be strongly inhibited by the reaction product. Most probably this reaction product is a DsrC sulfonate (DsrC-Cys_A-SO_3^-).

Under physiological conditions strong product inhibition can be compensated through the continuous removal of the inhibitory product by another enzyme. Hence the DsrC sulfonate is presumably rapidly metabolized *in vivo* to sulfite and reduced DsrC, which can once more be persulfurated. Sulfite can be released from a protein sulfonate, when the latter reacts with a thiol group to form a disulfide ($RS\text{-}SO_3^- + RS^- \rightleftharpoons RS\text{-}SR + SO_3^{2-}$) (Cecil and Wake, 1962). It has been proposed that the thiol group of Cys_B could react with Cys_A to form an intramolecular disulfide bond and to release sulfite (Stockdreher *et al.,* 2012). This however did not occur in the assays with persulfurated DsrC as substrate for rDsrABL. Another potential candidate for the thiol is Cys_A of another DsrC protein, which is in a reduced state. The concentration of DsrC is likely to be high enough to promote the forward reaction towards the production of disulfide and sulfite, as DsrC is highly expressed under photolithoautotrophic conditions (Grimm *et al.,* 2010; Weissgerber *et al.,* 2013).

Two Models of Sulfane Sulfur Oxidation in *A. vinosum*

On the basis of above-mentioned results and considerations a new hypothetical model of sulfane sulfur oxidation in *A. vinosum* was postulated (Figure 36), which highlights the

central role of DsrC (Figure 36A). In this model the stored sulfur is transported from the periplasm into the cytoplasm by an unknown low molecular weight persulfide and shuttled onto DsrC via a sulfur relay system involving a rhodanese, TusA and DsrEFH (Figure 36B). The DsrC persulfide is then oxidized by the sulfite-generating rDsrABL complex to DsrC sulfonate (DsrC-S-SO_3^-). Thereby six electrons are transferred onto three NAD^+ molecules generating three NADH. The presumably inhibitory product DsrC sulfonate then reacts with reduced DsrC to sulfite and a DsrC dimer.

Thereafter sulfite has to be rapidly further metabolized, as it is a highly reactive and toxic substance and its accumulation would promote the reverse reaction leading to the formation of DsrC sulfonates once more. Sulfite is further oxidized to sulfate either by the APS reductase and ATP sulfurylase via the intermediate APS or it is directly oxidized via the cytoplasmically oriented membrane-bound SoeABC complex (Dahl *et al.,* 2013; Dahl, 2015). The DsrC dimer interconnected by a Cys_A disulfide bond is presumably reduced at the DsrMKJOP complex (Figure 36). This is supported by the fact that an electron flow from the periplasm into the cytoplasm is the strongly suggested mode of action for the DsrMKJOP complex from *A. vinosum* (Grein *et al.,* 2010).

However, this model does not give an explanation for the conservation of Cys_B in DsrC from sulfur oxidizers. It is possible that after the formation of the DsrC dimer via Cys_A to release sulfite and to prevent product inhibition of rDsrABL, an intramolecular disulfide bond between Cys_A and Cys_B is formed, as this is the thermodynamically more stable form (Cort *et al.,* 2008). Possibly a DsrC with an intramolecular disulfide bond is the appropriate substrate for the DsrMKJOP complex and not the DsrC dimer. To elucidate whether an intermolecular or an intramolecular DsrC disulfide is the substrate for the DsrMKJOP complex further experimental data is necessary.

Taken together the new model of sulfane sulfur oxidation via the rDsr pathway (Figure 36) integrates the sulfur relay system resulting in a persulfurated DsrC (Stockdreher *et al.,* 2014), which is the substrate for the rDsrABL complex. It demonstrates how sulfite can be released from the formed DsrC sulfonate and it presents a DsrMKJOP complex transferring electrons into the cytoplasm, which is the strongly suggested direction of electron flow (Grein *et al.,* 2010).

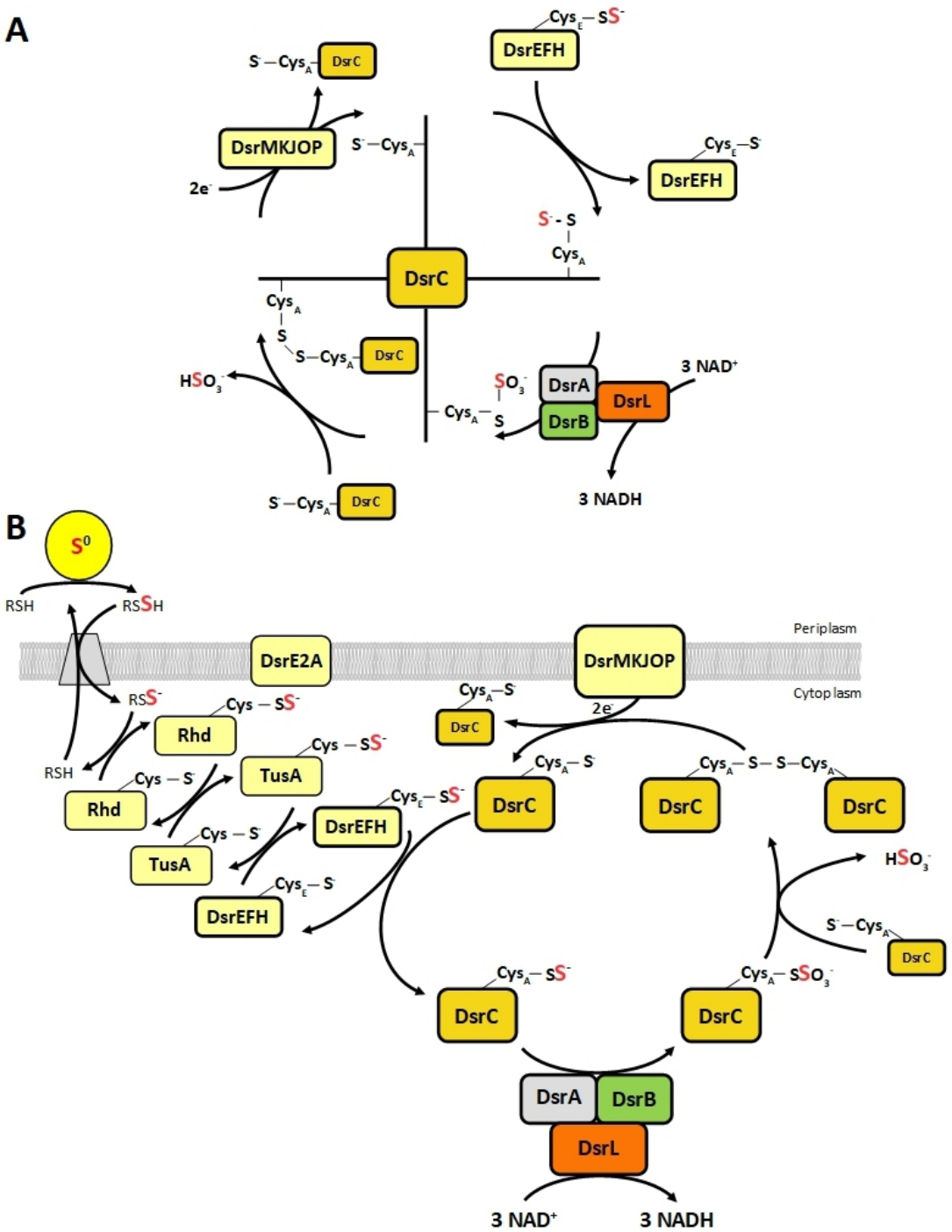

Figure 36: Hypothetical model of sulfane sulfur oxidation in *A. vinosum* via the rDsr pathway with emphasis on the central role of DsrC. (A) This model emphasizes the central position DsrC has in the oxidation of sulfane sulfur via the rDsr pathway and displays DsrCs many interaction partners. (B) Sulfur is transferred from the periplasmic sulfur deposits into the cytoplasm onto a rhodanese (Rhd). A cascade of protein persulfids, including TusA and DsrEFH, shuttles sulfur onto DsrC. The DsrC persulfide is presumably oxidized to a DsrC sulfonate at the rDsrABL complex, which transfers the electrons via DsrL onto NAD^+. Sulfite is released when the DsrC sulfonate reacts with another DsrC protein to a DsrC dimer interconnected via Cys_A. The membrane-bound DsrMKJOP complex reduces the DsrC dimer, so that reduced DsrC can be persulfurated once more.

The exact mechanism, in which DsrC-bound sulfur is oxidized at the active site of rDsrABL is however unclear and on the basis of the proposed reactions of sulfite reduction (Santos *et al.,* 2015), a further alternative mechanism was postulated (Figure 37).

The active site of the sulfite-generating rDsrABL complex contains a siroheme coupled to a [4Fe4S] cluster. The sulfane sulfur of DsrC persulfide is postulated to bind to the central iron of the siroheme and to be oxidized to a Fe-ligated sulfenate (-S-OH) while DsrC leaves the active site. The two electrons of this first oxidation are transferred via the central iron of the siroheme and the [4Fe4S] cluster onto NAD^+ to form NADH. In the following the sulfenate is further oxidized to a Fe-ligated sulfinate ($-S-O_2^-$) intermediate, the electrons of this oxidation are once more transferred to NADH. Finally sulfite is generated through hydrolytic cleavage. This mechanism is inspired by the reaction taking place at the siroheme iron of DsrAB in sulfite reduction (Santos *et al.,* 2015).

Many sulfur oxidizers lacking the rDsr pathway contain a sulfur-oxidizing heterodisulfide reductase-like (sHdr) complex (Quatrini *et al.,* 2009; Venceslau *et al.,* 2014), which is proposed to also couple the oxidation of sulfane sulfur to the generation of NADH (Ernst *et al.,* 2020). For these organisms a similar mechanism, in which a protein persulfide is oxidized to sulfite, was postulated (Ernst *et al.,* 2020).

The main difference between the two presented mechanisms (Figure 36, Figure 37) is that in the first sulfane sulfur is oxidized from a protein-bound persulfide ($DsrC-S-S^-$) to a protein-bound sulfonate ($DsrC-S-SO_3^-$) and sulfite is reductively released by formation of a disulfide bond between two cysteine residues. In the second mechanism the protein-bound persulfide is oxidized to sulfinate ($-S-O_2^-$), which is then released from the active site through hydrolytic cleavage resulting in the formation of sulfite (HSO_3^-).

A drawback of this second model (Figure 37) is that there is no clear role for the membrane-bound DsrMKJOP complex, although it is known to be essential for the oxidation of stored sulfur via the rDsr pathway (Sander *et al.,* 2006).

The results gathered in this study strongly indicate that the substrate for sulfur oxidation catalyzed by rDsrABL is a DsrC persulfide and the here shown models (Figure 36, Figure 37) are further approaches to apprehend the mechanism of sulfane sulfur oxidation. However, additional experimental data is necessary to clarify which intermediate steps lead to the final product sulfite.

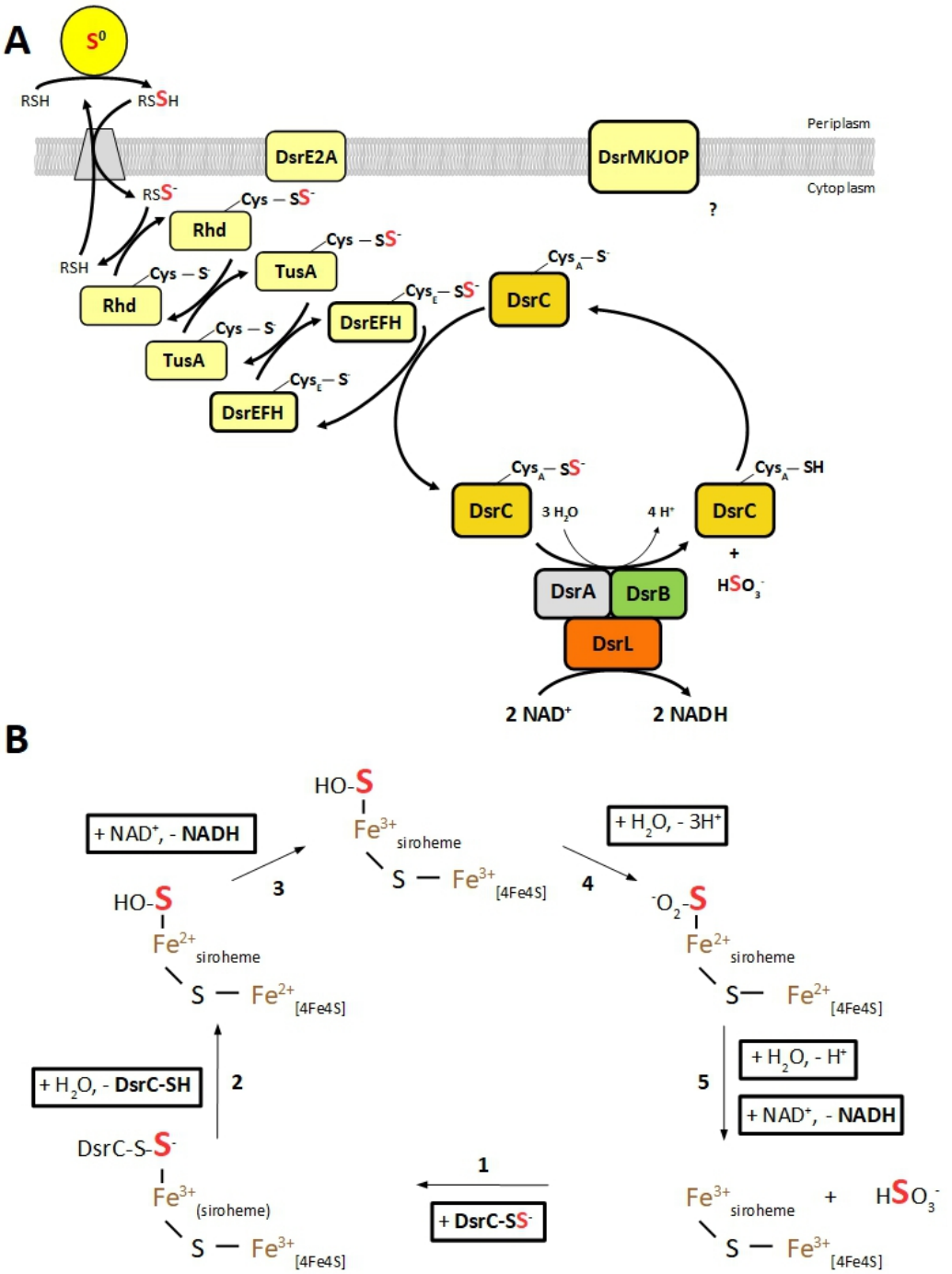

Figure 37: Alternative model of sulfane sulfur oxidation in *A. vinosum* including a mechanistic scheme. (A) Sulfur is transferred from the periplasmic sulfur deposits into the cytoplasm onto a rhodanese (Rhd). A cascade of protein persulfids, including TusA and DsrEFH, shuttles sulfur onto DsrC. Sulfane sulfur is presumably oxidized to sulfite while DsrC is released. Reduced DsrC can once more be persulfurated by DsrEFH. (B) DsrC persulfide binds to the siroheme iron of the rDsrABL active site (1) and sulfane sulfur is oxidized to iron-ligated sulfenate, while DsrC is released and two electrons reduce the siroheme and coupled [4Fe4S] cluster (2). The electrons are then transferred to NADH (3) and the sulfenate is further oxidized to iron-ligated sulfinate, while two electrons once more reduce siroheme + [4Fe4S] (4). The electrons are used to generate another NADH and sulfite is released from the active site by hydrolytic cleavage of iron-ligated sulfinate (5).

6 Summary

Microbial pathways of sulfur dissimilation have strongly contributed to the evolution of the biogeochemical sulfur cycle and still play a major role in it today. Dissimilatory sulfite reductases, which occur in both sulfate reducing and sulfur oxidizing organisms, belong to the key enzymes of this nutrient cycle. The characterization of the reverse-acting dissimilatory sulfite reductase rDsrAB from the sulfur oxidizing model organism *Allochromatium vinosum* has an impact on our understanding of the (r)Dsr pathway in both sulfur oxidizers and sulfate reducers.

The sulfite reductase rDsrAB was shown to interact both structurally and functionally with the iron-sulfur flavoprotein DsrL in an rDsrABL complex ($\alpha_2\beta_2\gamma_2$). Due to its function as NAD(P)H:oxidoreductase and its interaction with rDsrAB, DsrL enables the electron transfer from NAD(P)H via rDsrABL onto sulfite. Accordingly DsrL seems to be the so far unknown physiological electron donor for sulfite reduction in those reducers, which encode for DsrL. In sulfur oxidizers DsrL presumably functions as NAD^+ reductase, transferring electrons stemming from sulfite formation catalyzed by rDsrAB onto NAD^+. As DsrL shows great homologies to NfnB, the bifurcating subunit of the NfnAB complex, it could potentially enable an electron bifurcation in which for instance ferredoxin is reduced driven by sulfite reduction and an electron confurcation in which protein-bound sulfur is oxidized driven by ferredoxin oxidation. The electron transfer between ferredoxin and DsrL was demonstrated in this study, an electron bifurcation could however not be proven so far.

Furthermore the functional interaction of rDsrABL with the small protein DsrC was demonstrated. DsrC with its two highly conserved cysteines Cys_A and Cys_B was shown to increase sulfite reduction rate of rDsrABL and to be consumed in the reaction in a Cys_A-dependent manner just like observed for DsrAB and DsrC from the sulfate reducer *Archaeoglobus fulgidus*. However the product of sulfite reduction in the presence of DsrC was a DsrC Cys_A persulfide and not a DsrC trisulfide as observed for the sulfate reducer. This indicates that a DsrC persulfide is also the substrate for sulfur oxidation catalyzed by rDsrABL, by which sulfite is generated.

7 References

Akhtar, M.K., and Jones, P.R. (2008) Deletion of *iscR* stimulates recombinant clostridial Fe–Fe hydrogenase activity and H2-accumulation in *Escherichia coli* BL21(DE3). *Applied Microbiology and Biotechnology* **78**: 853–862, doi: 10.1007/s00253-008-1377-6.

Aliverti, A., Curti, B., and Vanoni, M.A. (1999) Identifying and quantitating FAD and FMN in simple and in iron-sulfur-containing flavoproteins. *Methods in Molecular Biology* **131**: 9–23, doi: 10.1385/1-59259-266-X:9.

Anantharaman, K., Hausmann, B., Jungbluth, S.P., Kantor, R.S., Lavy, A., Warren, L.A., *et al.* (2018) Expanded diversity of microbial groups that shape the dissimilatory sulfur cycle. *ISME Journal* **12**: 1715–1728, doi: 10.1038/s41396-018-0078-0.

Aravind, L., Anantharaman, V., Balaji, S., Babu, M.M., and Iyer, L.M. (2005) The many faces of the helix-turn-helix domain. Transcription regulation and beyond. *FEMS Microbiology Reviews* **29**: 231–262, doi: 10.1016/j.fmrre.2004.12.008.

Askenasy, I., Pennington, J.M., Tao, Y., Marshall, A.G., Young, N.L., Shang, W., and Stroupe, M.E. (2015) The N-terminal domain of *Escherichia coli* assimilatory NADPH-sulfite reductase hemoprotein is an oligomerization domain that mediates holoenzyme assembly. *The Journal of Biological Chemistry* **290**: 19319–19333. doi: 10.1074/jbc.M115.662379.

Atkinson, J.T., Campbell, I., Bennett, G.N., and Silberg, J.J. (2016) Cellular assays for ferredoxins: a strategy for understanding electron flow through protein carriers that link metabolic pathways. *Biochemistry* **55**: 7047–7064, doi: 10.1021/acs.biochem.6b00831.

Barton, L.L., Fardeau, M-L., and Fauque, G.D. (2014) Hydrogen sulfide: a toxic gas produced by dissimilatory sulfate and sulfur reduction and consumed by microbial oxidation. *Metal Ions in Life Sciences* 14: 237–277, doi: 10.1007/978-94-017-9269-1_10.

Benning, C. (1998) Biosynthesis and function of the sulfolipid sulfoquinovosyl diacylglycerol. *Annual Review of Plant Physiology and Plant Molecular Biology* **49**: 53–75, doi: 10.1146/annurev.arplant.49.1.53.

Bergmeyer, H.U. (1975) Neue Werte für die molaren Extinktions-Koeffizienten von NADH und NADPH zum Gebrauch im Routine-Laboratorium. *Zeitschrift fur Klinische Chemie und Klinische Biochemie* **13**: 507–508.

Buckel, W., and Thauer, R.K. (2013) Energy conservation via electron bifurcating ferredoxin reduction and proton/Na^+ translocating ferredoxin oxidation. *Biochimica et Biophysica Acta* **1827**: 94–113, doi: 10.1016/j.bbabio.2012.07.002.

Buckel, W., and Thauer, R.K. (2018) Flavin-based electron bifurcation, a new mechanism of biological energy coupling. *Chemical Reviews* **118**: 3862–3886, doi: 10.1021/acs.chemrev.7b00707.

Canfield, D.E. (1999) The evolution of the sulfur cycle. *American Journal of Science* **299**: 697–723, doi: 10.2475/ajs.299.7-9.697.

Canfield, D.E., Stewart, F.J., Thamdrup, B., Brabandere, L. de, Dalsgaard, T., Delong, E.F., *et al.* (2010) A cryptic sulfur cycle in oxygen-minimum-zone waters off the Chilean coast. *Science* **330**: 1375–1378, doi: 10.1126/science.1196889.

Cecil, R., and Wake, R.G. (1962) The reactions of inter- and intra-chain disulphide bonds in proteins with sulphite. *The Biochemical Journal* **82**: 401–406, doi: 10.1042/bj0820401.

Chou, C-L. (1990) Geochemistry of sulfur in coal. In *Geochemistry of Sulfur in Fossil Fuels*, Wilson L.O., Curt M.W. (ed) Washington, DC, USA: American Chemical Society (ACS Symposium Series), pp. 30–52.

Colín-García, M., Heredia, A., Cordero, G., Camprubi, A., Negrón-Mendoza, A., Ortega-Gutiérrez, F., *et al.* (2016) Hydrothermal vents and prebiotic chemistry: a review. *Boletín de la Sociedad Geológica Mexicana* **68**: 599–620, doi: 10.18268/BSGM2016v68n3a13.

Cort, J.R., Mariappan, S.V., Kim, C.Y., Park, M.S., Peat, T.S., Waldo, G.S., *et al.* (2001) Solution structure of *Pyrobaculum aerophilum* DsrC, an archaeal homologue of the gamma subunit of dissimilatory sulfite reductase. *European Journal of Biochemistry* **268**: 5842–5850, doi: 10.1046/j.0014-2956.2001.02529.x.

Cort, J.R., Selan, U., Schulte, A., Grimm, F., Kennedy, M.A., and Dahl, C. (2008) *Allochromatium vinosum* DsrC: solution-state NMR structure, redox properties, and interaction with DsrEFH, a protein essential for purple sulfur bacterial sulfur oxidation. *Journal of Molecular Biology* **382**: 692–707, doi: 10.1016/j.jmb.2008.07.022.

Crane, B.R., Siegel, L.M., and Getzoff, E.D. (1995) Sulfite reductase structure at 1.6. Å: evolution and catalysis for reduction of inorganic anions. *Science* **270**: 59–67, doi: 10.1126/science.270.5233.59.

Crane, B.R., Siegel, L.M., and Getzoff, E.D. (1997) Probing the catalytic mechanism of sulfite reductase by X-ray crystallography: structures of the *Escherichia coli* hemoprotein in complex with substrates, inhibitors, intermediates, and products. *Biochemistry* **36**: 12120–12137, doi: 10.1021/bi971066i.

Crane, B.R., and Getzoff, E.D. (1996) The relationship between structure and function for the sulfite reductases. *Current Opinion in Structural Biology* **6**: 744–756, doi: 10.1016/S0959-440X(96)80003-0.

Dagert, M., and Ehrlich, S.D. (1979) Prolonged incubation in calcium chloride improves the competence of *Escherichia coli* cells. *Gene* **6**: 23–28, doi: 10.1016/0378-1119(79)90082-9.

Dahl, C. (2017) Sulfur metabolism in phototrophic bacteria. In *Modern Topics in the Phototrophic Prokaryotes. Metabolism, Bioenergetics, and Omics*, Hallenbeck, P.C. (ed) Cham, Switzerland: Springer International Publishing, pp. 27–66.

Dahl, C., Kredich, N.M., Deutzmann, R., and Trüper, H.G. (1993) Dissimilatory sulphite reductase from *Archaeoglobus fulgidus*: physico-chemical properties of the enzyme and cloning, sequencing and analysis of the reductase genes. *Journal of General Microbiology* **139**: 1817–1828, doi: 10.1099/00221287-139-8-1817.

Dahl, C. (2015) Cytoplasmic sulfur trafficking in sulfur-oxidizing prokaryotes. *IUBMB Life* **67**: 268–274, doi: 10.1002/iub.1371.

Dahl, C., Engels, S., Pott-Sperling, A.S., Schulte, A., Sander, J., Lübbe, Y., *et al.* (2005) Novel genes of the *dsr* gene cluster and evidence for close interaction of Dsr proteins during sulfur oxidation in the phototrophic sulfur bacterium *Allochromatium vinosum*. *Journal of Bacteriology* **187**: 1392–1404, doi: 10.1128/JB.187.4.1392-1404.2005.

Dahl, C., Franz, B., Hensen, D., Kesselheim, A., and Zigann, R. (2013) Sulfite oxidation in the purple sulfur bacterium *Allochromatium vinosum*: identification of SoeABC as a major player and relevance of SoxYZ in the process. *Microbiology* **159**: 2626–2638, doi: 10.1099/mic.0.071019-0.

Demmer, J.K., Huang, H., Wang, S., Demmer, U., Thauer, R.K., and Ermler, U. (2015) Insights into flavin-based electron bifurcation via the NADH-dependent reduced ferredoxin:NADP oxidoreductase structure. In *Journal of Biological Chemistry* **290**: 21985–21995, doi: 10.1074/jbc.M115.656520.

Denkmann, K., Grein, F., Zigann, R., Siemen, A., Bergmann, J., van Helmont, S., *et al.* (2012) Thiosulfate dehydrogenase: a widespread unusual acidophilic *c*-type cytochrome. *Environmental Microbiology* **14**: 2673–2688, doi: 10.1111/j.1462-2920.2012.02820.x.

Dhillon, A., Goswami, S., Riley, M., Teske, A., and Sogin, M. (2005) Domain evolution and functional diversification of sulfite reductases. *Astrobiology* **5**: 18–29, doi: 10.1089/ast.2005.5.18.

Eisenberg, D., Gill, H.S., Pfluegl, G.M.U., and Rotstein, S.H. (2000) Structure–function relationships of glutamine synthetases. *Biochimica et Biophysica Acta* **1477**: 122–145, doi: 10.1016/S0167-4838(99)00270-8.

Ernst, C., Kayastha, K., Koch, T., Venceslau, S.S., Pereira, I.A.C., Demmer, U., *et al.* (2020) Structural and spectroscopic characterization of a HdrA-like subunit from *Hyphomicrobium denitrificans*. *The FEBS Journal*, 2020 [published online ahead of print, 2020 Aug 4] doi: 10.1111/febs.15505.

Fauque, G., Lino, A.R., Czechowski, M., Kang, L., DerVartanian, D.V., Moura, J.J.G., *et al.* (1990) Purification and characterization of bisulfite reductase (desulfofuscidin) from *Desulfovibrio thermophilus* and its complexes with exogenous ligands. *Biochimica et Biophysica Acta* **1040**: 112–118, doi: 10.1016/0167-4838(90)90154-8.

Fike, D.A., Bradley, A.S., and Rose, C.V. (2015) Rethinking the ancient sulfur cycle. *Annual Review of Earth and Planetary Sciences* **43**: 593–622, doi: 10.1146/annurev-earth-060313-054802.

Friedrich, M., and Schink, B. (1993) Hydrogen formation from glycolate driven by reversed electron transport in membrane vesicles of a syntrophic glycolate-oxidizing bacterium. *European Journal of Biochemistry* **217**: 233–240, doi: 10.1111/j.1432-1033.1993.tb18238.x.

Frigaard, N.U., and Dahl, C. (2008) Sulfur metabolism in phototrophic sulfur bacteria. *Advances in Microbial Physiology* 54: 103–200, doi: 10.1016/S0065-2911(08)00002-7

Grein, F., Pereira, I.A.C., and Dahl, C. (2010) Biochemical characterization of individual components of the *Allochromatium vinosum* DsrMKJOP transmembrane complex aids understanding of complex function *in vivo*. *Journal of Bacteriology* **192**: 6369–6377, doi: 10.1128/JB.00849-10.

Grein, F., Ramos, A.R., Venceslau, S.S., and Pereira, I.A.C. (2013) Unifying concepts in anaerobic respiration: insights from dissimilatory sulfur metabolism. *Biochimica et Biophysica Acta* **1827**: 145–160, doi: 10.1016/j.bbabio.2012.09.001.

Grimm, F., Dobler, N., and Dahl, C. (2010) Regulation of *dsr* genes encoding proteins responsible for the oxidation of stored sulfur in *Allochromatium vinosum*. *Microbiology* **156**: 764–773, doi: 10.1099/mic.0.034645-0.

Hanahan, D. (1983) Studies on transformation of *Escherichia coli* with plasmids. *Journal of Molecular Biology* **166**: 557–580, doi: 10.1016/S0022-2836(83)80284-8.

Hase, T., Schürmann, P., and Knaff, D.B. (2006) The interaction of ferredoxin with ferredoxin-dependent enzymes. In *Photosystem I. The Light-Driven Plastocyanin:Ferredoxin Oxidoreductase*, Golbeck, J.H (ed) Dordrecht, The Netherlands: Springer, pp. 477–498.

Heiden, S., Hedderich, R., Setzke, E., and Thauer, R.K. (1994) Purification of a two-subunit cytochrome-*b*-containing heterodisulfide reductase from methanol-grown *Methanosarcina barkeri*. *European Journal of Biochemistry* **221**: 855–861, doi: 10.1111/j.1432-1033.1994.tb18800.x.

Hensen, D., Sperling, D., Trüper, H.G., Brune, D.C., and Dahl, C. (2006) Thiosulphate oxidation in the phototrophic sulphur bacterium *Allochromatium vinosum*. *Molecular Microbiology* **62**: 794–810, doi: 10.1111/j.1365-2958.2006.05408.x.

Herrmann, G., Jayamani, E., Mai, G., and Buckel, W. (2008) Energy conservation via electron-transferring flavoprotein in anaerobic bacteria. *Journal of Bacteriology* **190**: 784–791, doi: 10.1128/JB.01422-07.

Hipp, W.M., Pott, A.S., Thum-Schmitz, N., Faath, I., Dahl, C., and Trüper, H.G. (1997) Towards the phylogeny of APS reductases and sirohaem sulfite reductases in sulfate-reducing and sulfur-oxidizing prokaryotes. *Microbiology* **143**: 2891–2902, doi: 10.1099/00221287-143-9-2891.

Hsieh, Y.-C., Liu, M.-Y., Wang, V.C.-C., Chiang, Y.-L., Liu, E.-H., Wu, W.-g., *et al.* (2010) Structural insights into the enzyme catalysis from comparison of three forms of dissimilatory sulphite reductase from *Desulfovibrio gigas*. *Molecular Microbiology* **78**: 1101–1116, doi: 10.1111/j.1365-2958.2010.07390.x.

Huang, C.J., and Barrett, E.L. (1991) Sequence analysis and expression of the *Salmonella typhimurium asr* operon encoding production of hydrogen sulfide from sulfite. *Journal of Bacteriology* **173**: 1544–1553, doi: 10.1128/jb.173.4.1544-1553.1991.

Ikeuchi, Y., Shigi, N., Kato, J.-I., Nishimura, A., and Suzuki, T. (2006) Mechanistic insights into sulfur relay by multiple sulfur mediators involved in thiouridine biosynthesis at tRNA wobble positions. *Molecular Cell* **21**: 97–108, doi: 10.1016/j.molcel.2005.11.001.

Janick, P.A., and Siegel, L.M. (1982) Electron paramagnetic resonance and optical spectroscopic evidence for interaction between siroheme and Fe_4S_4 prosthetic groups in *Escherichia coli* sulfite reductase hemoprotein subunit. *Biochemistry* **21**: 3538–3547, doi: 10.1021/bi00258a003.

Johnson, D.C., Dean, D.R., Smith, A.D., and Johnson, M.K. (2005) Structure, function, and formation of biological iron-sulfur clusters. *Annual Review of Biochemistry* **74**: 247–281, doi: 10.1146/annurev.biochem.74.082803.133518.

Johnson, E.F., and Mukhopadhyay, B. (2005) A new type of sulfite reductase, a novel coenzyme F_{420}-dependent enzyme, from the methanarchaeon *Methanocaldococcus jannaschii*. *The Journal of Biological Chemistry* **280**: 38776–38786, doi: 10.1074/jbc.M503492200.

Jordan, P.M. (1994) Highlights in haem biosynthesis. *Current Opinion in Structural Biology* **4**: 902–911, doi: 10.1016/0959-440X(94)90273-9.

Kappler, U., and Dahl, C. (2001) Enzymology and molecular biology of prokaryotic sulfite oxidation. *FEMS Microbiology Letters* **203**: 1–9, doi: 10.1111/j.1574-6968.2001.tb10813.x.

Karas, M., and Hillenkamp, F. (1988) Laser desorption ionization of proteins with molecular masses exceeding 10,000 daltons. *Analytical Chemistry* **60**: 2299–2301, doi: 10.1021/ac00171a028.

Kaster, A.-K., Moll, J., Parey, K., and Thauer, R.K. (2011) Coupling of ferredoxin and heterodisulfide reduction via electron bifurcation in hydrogenotrophic methanogenic archaea. *Proceedings of the National Academy of Sciences of the United States of America* **108**: 2981–2986, doi: 10.1073/pnas.1016761108.

Knaff, D.B. (1996) Ferredoxin and ferredoxin-dependent enzymes. In *Oxygenic Photosynthesis: The Light Reactions*, Ort, D.R., Yocum, C.F., and Heichel, I.F. (ed) Dordrecht, The Netherlands: Springer, pp. 333–361.

Krueger, R.J., and Siegel, L.M. (1982) Spinach siroheme enzymes: isolation and characterization of ferredoxin-sulfite reductase and comparison of properties with ferredoxin-nitrite reductase. *Biochemistry* **21**: 2892–2904, doi: 10.1021/bi00541a014.

Kuchenreuther, J.M., Grady-Smith, C.S., Bingham, A.S., George, S.J., Cramer, S.P., Swartz, J.R., and Tyagi, A.K. (2010) High-yield expression of heterologous [FeFe] hydrogenases in *Escherichia coli*. *PloS One* **5**: e15491. doi: 10.1371/journal.pone.0015491.

Li, F., Hinderberger, J., Seedorf, H., Zhang, J., Buckel, W., and Thauer, R.K. (2008) Coupled ferredoxin and crotonyl coenzyme A (CoA) reduction with NADH catalyzed by the butyryl-CoA dehydrogenase/Etf complex from *Clostridium kluyveri*. *Journal of Bacteriology* **190**: 843–850, doi: 10.1128/JB.01417-07.

Löffler, M., Feldhues, J., Venceslau, S.S., Kammler, L., Grein, F., Pereira, I.A.C., and Dahl, C. (2020) DsrL mediates electron transfer between NADH and rDsrAB in *Allochromatium vinosum*. *Environmental Microbiology* **22**: 783–795, doi: 10.1111/1462-2920.14899.

Loy, A., Duller, S., and Wagner, M. (2008) Evolution and ecology of microbes dissimilating sulfur compounds: insights from siroheme sulfite reductases. In *Microbial Sulfur Metabolism*, Dahl, C., and Friedrich, C.G. (ed) Berlin, Germany: Springer, pp. 46–59.

Loy, A., Duller, S., Baranyi, C., Mussmann, M., Ott, J., Sharon, I., *et al.* (2009) Reverse dissimilatory sulfite reductase as phylogenetic marker for a subgroup of sulfur-oxidizing prokaryotes. *Environmental Microbiology* **11**: 289–299, doi: 10.1111/j.1462-2920.2008.01760.x.

Lu, J., and Deutsch, C. (2001) Pegylation. A method for assessing topological accessibilities in Kv1.3. *Biochemistry* **40**: 13288–13301, doi: 10.1021/bi0107647.

Lübbe, Y.J., Youn, H.-S., Timkovich, R., and Dahl, C. (2006) Siro(haem)amide in *Allochromatium vinosum* and relevance of DsrL and DsrN, a homolog of cobyrinic acid a,c-diamide synthase, for sulphur oxidation. *FEMS Microbiology Letters* **261**: 194–202, doi: 10.1111/j.1574-6968.2006.00343.x.

Mander, G.J., Weiss, M.S., Hedderich, R., Kahnt, J., Ermler, U., and Warkentin, E. (2005) X-ray structure of the gamma-subunit of a dissimilatory sulfite reductase: fixed and flexible C-terminal arms. *FEBS Letters* **579**: 4600–4604, doi: 10.1016/j.febslet.2005.07.029.

Matthews, J.C., Timkovich, R., Liu, M.Y., and Le Gall, J. (1995) Siroamide: a prosthetic group isolated from sulfite reductases in the genus *Desulfovibrio*. *Biochemistry* **34**: 5248–5251, doi: 10.1021/bi00015a039.

Middelburg, J.J. (2000) The geochemical sulfur cycle. *In Environmental Technologies to Treat Sulphur Pollution. Principles and Engineering*, Lens, P., and Hulshoff Pol, L. (ed) London, UK: IWA Publishing, pp. 33–46.

Mitchell, P. (1975) The protonmotive Q cycle. A general formulation. *FEBS Letters* **59**: 137–139, doi: 10.1016/0014-5793(75)80359-0.

Mizuno, N., Voordouw, G., Miki, K., Sarai, A., and Higuchi, Y. (2003) Crystal structure of dissimilatory sulfite reductase D (DsrD) protein—possible interaction with B- and Z-DNA by its winged-helix motif. *Structure* **11**: 1133–1140, doi: 10.1016/S0969-2126(03)00156-4.

Mohan, S.B., and Cole, J.A. (2007) The dissimilatory reduction of nitrate to ammonia by anaerobic bacteria. In *Biology of the Nitrogen Cycle*, Bothe, H., Ferguson, S.J., and Newton, W.E. (ed) Amsterdam, The Netherlands: Elsevier, pp. 93–106.

Molitor, M., Dahl, C., Molitor, I., Schäfer, U., Speich, N., Huber, R., *et al.* (1998) A dissimilatory sirohaem-sulfite-reductase-type protein from the hyperthermophilic archaeon *Pyrobaculum islandicum*. *Microbiology* **144**: 529–541, doi: 10.1099/00221287-144-2-529.

Murphy, M.J., and Siegel, L.M. (1973) Siroheme and sirohydrochlorin. The basis for a new type of porphyrin-related prosthetic group common to both assimilatory and dissimilatory sulfite reductases. *The Journal of Biological Chemistry* **248**: 6911–6919.

Murphy, M.J., Siegel, L.M., Kamin, H., and Rosenthal, D. (1973) Reduced nicotinamide adenine dinucleotide phosphate-sulfite reductase of enterobacteria. II. Identification of a new class of heme prosthetic group: an iron-tetrahydroporphyrin (isobacteriochlorin type) with eight carboxylic acid groups. *The Journal of Biological Chemistry* **248**: 2801–2814.

Murphy, M.J., Siegel, L.M., Tove, S.R., and Kamin, H. (1974) Siroheme: a new prosthetic group participating in six-electron reduction reactions catalyzed by both sulfite and nitrite reductases. *Proceedings of the National Academy of Sciences of the United States of America* **71**: 612–616, doi: 10.1073/pnas.71.3.612.

Muyzer, G., and Stams, A.J.M. (2008) The ecology and biotechnology of sulphate-reducing bacteria. *Nature Reviews Microbiology* **6**: 441–454, doi: 10.1038/nrmicro1892.

Nakayama, M., Akashi, T., and Hase, T. (2000) Plant sulfite reductase. Molecular structure, catalytic function and interaction with ferredoxin. *Journal of Inorganic Biochemistry* **82**: 27–32, doi: 10.1016/S0162-0134(00)00138-0.

Nitschke, W., and Russell, M.J. (2012) Redox bifurcations: mechanisms and importance to life now, and at its origin: a widespread means of energy conversion in biology unfolds… *BioEssays* **34**: 106–109, doi: 10.1002/bies.201100134.

Novick, R.P. (1987) Plasmid incompatibility. *Microbiological Reviews* **51**: 381–395.

Oliveira, T.F., Vonrhein, C., Matias, P.M., Venceslau, S.S., Pereira, I.A.C., and Archer, M. (2008) The crystal structure of *Desulfovibrio vulgaris* dissimilatory sulfite reductase bound to DsrC provides novel insights into the mechanism of sulfate respiration. *Journal of Biological Chemistry* **283**: 34141–34149, doi: 10.1074/jbc.M805643200.

Ostrowski, J., and Kredich, N.M. (1989) Molecular characterization of the *cysJIH* promoters of *Salmonella typhimurium* and *Escherichia coli*: regulation by *cysB* protein and *N*-Acetyl-L-Serine. In *Journal of Bacteriology* **171**: 130–140, doi: 10.1128/jb.171.1.130-140.1989.

Ostrowski, J., Wu, J.Y., Rueger, D.C., Miller, B.E., Siegel, L.M., and Kredich, N.M. (1989) Characterization of the *cysJIH* regions of *Salmonella typhimurium* and *Escherichia coli* B. DNA sequences of *cysI* and *cysH* and a model for the siroheme-Fe_4S_4 active center of sulfite reductase hemoprotein based on amino acid homology with spinach nitrite reductase. *The Journal of Bological Chemistry* **264**: 15726–15737.

Ough, C.S., and Were, L. (2005) Sulfur dioxide and sulfites. In *Antimicrobial in Food*, Davidson, P.M., Sofos, J.N., and Branen, A.L. (ed) Boca Raton, USA: Taylor & Francis (Food Science and Technology), pp. 143-168

Parey, K., Warkentin, E., Kroneck, P.M.H., and Ermler, U. (2010) Reaction cycle of the dissimilatory sulfite reductase from *Archaeoglobus fulgidus*. *Biochemistry* **49**: 8912–8921, doi: 10.1021/bi100781f.

Pattaragulwanit, K., Brune, D.C., Trüper, H.G., and Dahl, C. (1998) Molecular genetic evidence for extracytoplasmic localization of sulfur globules in *Chromatium vinosum*. *Archives of Microbiology* **169**: 434–444, doi: 10.1007/s002030050594.

Peakman, T., Busby, S., and Cole, J. (1990) Transcriptional control of the *cysG* gene of *Escherichia coli* K-12 during aerobic and anaerobic growth. *European Journal of Biochemistry* **191**: 325–331, doi: 10.1111/j.1432-1033.1990.tb19126.x.

Peters, J.W., Miller, A.-F., Jones, A.K., King, P.W., and Adams, M.W.W. (2016) Electron bifurcation. *Current Opinion in Chemical Biology* **31**: 146–152, doi: 10.1016/j.cbpa.2016.03.007.

Pfennig, N. and Trüper, H.G. (1992) The family *Chromatiaceae*. In *The Prokaryotes. A handbook on the biology of bacteria: ecophysiology, isolation, identification, applications*, Balows, A., Trüper, H.G., Dworkin, M., Harder, W., and Schleifer, K-H. (ed). New York, USA: Springer, pp. 3200-3221.

Pierik, A.J., Duyvis, M.G., van Helvoort, J.M., Wolbert, R.B., and Hagen, W.R. (1992) The third subunit of desulfoviridin-type dissimilatory sulfite reductases. *European Journal of Biochemistry* **205**: 111–115, doi: 10.1111/j.1432-1033.1992.tb16757.x.

Pott, A.S., and Dahl, C. (1998) Sirohaem sulfite reductase and other proteins encoded by genes at the *dsr* locus of *Chromatium vinosum* are involved in the oxidation of intracellular sulfur. *Microbiology* **144**: 1881–1894, doi: 10.1099/00221287-144-7-1881.

Quatrini, R., Appia-Ayme, C., Denis, Y., Jedlicki, E., Holmes, D.S., and Bonnefoy, V. (2009) Extending the models for iron and sulfur oxidation in the extreme acidophile *Acidithiobacillus ferrooxidans*. *BMC Genomics* **10** 394, doi: 10.1186/1471-2164-10-394.

Sander, J., Engels-Schwarzlose, S., and Dahl, C. (2006) Importance of the DsrMKJOP complex for sulfur oxidation in *Allochromatium vinosum* and phylogenetic analysis of related complexes in other prokaryotes. *Archives of Microbiology* **186**: 357–366, doi: 10.1007/s00203-006-0156-y.

Santos, A.A., Venceslau, S.S., Grein, F., Leavitt, W.D., Dahl, C., Johnston, D.T., and Pereira, I.A.C. (2015) A protein trisulfide couples dissimilatory sulfate reduction to energy conservation. *Science* **350**: 1541–1545, doi: 10.1126/science.aad3558.

Schedel, M., Vanselow, M., and Trüper, H.G. (1979) Siroheme sulfite reductase isolated from *Chromatium vinosum*. Purification and investigation of some of its molecular and catalytic properties. *Archives of Microbiology* **121**: 29–36, doi: 10.1007/BF00409202.

Schiffer, A., Parey, K., Warkentin, E., Diederichs, K., Huber, H., Stetter, K.O., *et al.* (2008) Structure of the dissimilatory sulfite reductase from the hyperthermophilic archaeon *Archaeoglobus fulgidus*. *Journal of Molecular Biology* **379**: 1063–1074, doi: 10.1016/j.jmb.2008.04.027.

Schmidt, N.D., Peschon, J.J., and Segel, I.H. (1983) Kinetics of enzymes subject to very strong product inhibition. Analysis using simplified integrated rate equations and average velocities. *Journal of Theoretical Biology* **100**: 597–611, doi: 10.1016/0022-5193(83)90325-9.

Schnell, R., Sandalova, T., Hellman, U., Lindqvist, Y., and Schneider, G. (2005) Siroheme- and [Fe_4-S_4]-dependent NirA from *Mycobacterium tuberculosis* is a sulfite reductase with a covalent Cys-Tyr bond in the active site. *The Journal of Biological Chemistry* **280**: 27319–27328, doi: 10.1074/jbc.M502560200.

Schwartz, C.J., Giel, J.L., Patschkowski, T., Luther, C., Ruzicka, F.J., Beinert, H., and Kiley, P.J. (2001) IscR, an Fe-S cluster-containing transcription factor, represses expression of *Escherichia coli* genes encoding Fe-S cluster assembly proteins. *Proceedings of the National Academy of Sciences* **98**: 14895–14900, doi: 10.1073/pnas.251550898.

Scott, A.I. (1993) How nature synthesizes vitamin B12 - A survey of the last four billion years. *Angewandte Chemie, International Edition in English* **32**: 1223–1243, doi: 10.1002/anie.199312233.

Siegel, L.M., and Davis, P.S. (1974) Reduced nicotinamide adenine dinucleotide phosphate-sulfite reductase of enterobacteria. IV. The *Escherichia coli* hemoflavoprotein: subunit structure and dissociation into hemoprotein and flavoprotein components. *The Journal of Biological Chemistry* **249**: 1587–1598.

Siegel, L.M., Davis, P.S., and Kamin, H. (1974) Reduced nicotinamide adenine dinucleotide phosphate-sulfite reductase of enterobacteria. III. The *Escherichia coli* hemoflavoprotein: catalytic parameters and the sequence of electron flow. *The Journal of Biological Chemistry* **249**: 1572–1586.

Siegel, L.M., Rueger, D.C., Barber, M.J., Krueger, R.J., Orme-Johnson, N.R., and Orme-Johnson, W.H. (1982) *Escherichia coli* sulfite reductase hemoprotein subunit. Prosthetic groups, catalytic parameters, and ligand complexes. *The Journal of Biological Chemistry* **257**: 6343–6350.

Spencer, J.B., Stolowich, N.J., Roessner, C.A., and Scott, A.I. (1993) The *Escherichia coli cysG* gene encodes the multifunctional protein, siroheme synthase. *FEBS Letters* **335**: 57–60, doi: 10.1016/0014-5793(93)80438-Z.

Steudel, R., and Chivers, T. (2019) The role of polysulfide dianions and radical anions in the chemical, physical and biological sciences, including sulfur-based batteries. *Chemical Society Reviews* **48**: 3279–3319, doi: 10.1039/C8CS00826D.

Stockdreher, Y., Sturm, M., Josten, M., Sahl, H.-G., Dobler, N., Zigann, R., and Dahl, C. (2014) New proteins involved in sulfur trafficking in the cytoplasm of *Allochromatium vinosum*. *The Journal of Biological Chemistry* **289**: 12390–12403, doi: 10.1074/jbc.M113.536425.

Stockdreher, Y., Venceslau, S.S., Josten, M., Sahl, H.-G., Pereira, I.A.C., and Dahl, C. (2012) Cytoplasmic sulfurtransferases in the purple sulfur bacterium *Allochromatium vinosum*: evidence for sulfur transfer from DsrEFH to DsrC. *PloS One* **7**: e40785, doi: 10.1371/journal.pone.0040785.

Stroupe, M.E., Leech, H.K., Daniels, D.S., Warren, M.J., and Getzoff, E.D. (2003) CysG structure reveals tetrapyrrole-binding features and novel regulation of siroheme biosynthesis. *Nature Structural Biology* **10**: 1064–1073, doi: 10.1038/nsb1007.

Swamy, U., Wang, M., Tripathy, J.N., Kim, S.-K., Hirasawa, M., Knaff, D.B., and Allen, J.P. (2005) Structure of spinach nitrite reductase: implications for multi-electron reactions by the iron-sulfur:siroheme cofactor. *Biochemistry* **44**: 16054–16063, doi: 10.1021/bi050981y.

Tanabe, T.S., Leimkühler, S., and Dahl, C. (2019) The functional diversity of the prokaryotic sulfur carrier protein TusA. *Advances in Microbial Physiology* **75**: 233–277, doi: 10.1016/bs.ampbs.2019.07.004.

Thauer, R.K., Jungermann, K., and Decker, K. (1977) Energy conservation in chemotrophic anaerobic bacteria. *Bacteriological Reviews* **41**: 100–180.

Tripathy, J.N., Hirasawa, M., Kim, S.-K., Setterdahl, A.T., Allen, J.P., and Knaff, D.B. (2007) The role of tryptophan in the ferredoxin-dependent nitrite reductase of spinach. *Photosynthesis Research* **94**: 1–12, doi: 10.1007/s11120-007-9198-5.

Urban, P.J. (1961) Colorimetry of sulphur anions. *Fresenius' Zeitschrift für Analytische Chemie* **179**: 415–422, doi: 10.1007/BF00465088.

Vanoni, M.A., and Curti, B. (1999) Glutamate synthase: a complex iron-sulfur flavoprotein. *Cellular and Molecular Life Sciences* **55**: 617–638, doi: 10.1007/s000180050319.

Venceslau, S.S., Stockdreher, Y., Dahl, C., and Pereira, I.A.C. (2014) The "bacterial heterodisulfide" DsrC is a key protein in dissimilatory sulfur metabolism. *Biochimica et Biophysica Acta* **1837**: 1148–1164, doi: 10.1016/j.bbabio.2014.03.007.

Venceslau, S.S., Cort, J.R., Baker, E.S., Chu, R.K., Robinson, E.W., Dahl, C., *et al.* (2013) Redox states of *Desulfovibrio vulgaris* DsrC, a key protein in dissimilatory sulfite reduction. *Biochemical and Biophysical Research Communications* **441**: 732–736, doi: 10.1016/j.bbrc.2013.10.116.

Wagner, M., Roger, A.J., Flax, J.L., Brusseau, G.A., and Stahl, D.A. (1998) Phylogeny of dissimilatory sulfite reductases supports an early origin of sulfate respiration. *Journal of Bacteriology* **180**: 2975–2982, doi: 10.1128/JB.180.11.2975-2982.1998.

Wallerang, K., Löffler, M., and Dahl, C. (2020) Function and phylogeny of DsrL, a NAD(P)H oxidoreductase in dissimilatory sulfur metabolism. *6th Joint Conference of DGHM & VAAM*. Leipzig, Germany.

Warren, M.J., Bolt, E.L., Roessner, C.A., Scott, A.I., Spencer, J.B., and Woodcock, S.C. (1994) Gene dissection demonstrates that the *Escherichia coli cysG* gene encodes a multifunctional protein. *The Biochemical Journal* **302**: 837–844, doi: 10.1042/bj3020837.

Warren, M.J., Stolowich, N.J., Santander, P.J., Roessner, C.A., Sowa, B.A., and Scott, A.I. (1990) Enzymatic synthesis of dihydrosirohydrochlorin (precorrin-2) and of a novel pyrrocorphin by uroporphyrinogen III methylase. *FEBS Letters* **261**: 76–80, doi: 10.1016/0014-5793(90)80640-5.

Weaver, P.F., Wall, J.D., and Gest, H. (1975) Characterization of *Rhodopseudomonas capsulata*. *Archives of Microbiology* **105**: 207–216, doi: 10.1007/BF00447139.

Weghoff, M.C., Bertsch, J., and Müller, V. (2015) A novel mode of lactate metabolism in strictly anaerobic bacteria. *Environmental Microbiology* **17**: 670–677, doi: 10.1111/1462-2920.12493.

Weissgerber, T., Dobler, N., Polen, T., Latus, J., Stockdreher, Y., and Dahl, C. (2013) Genome-wide transcriptional profiling of the purple sulfur bacterium *Allochromatium vinosum* DSM 180T during growth on different reduced sulfur compounds. *Journal of Bacteriology* **195**: 4231–4245, doi: 10.1128/JB.00154-13.

Wu, J.Y., Siegel, L.M., and Kredich, N.M. (1991) High-level expression of *Escherichia coli* NADPH-sulfite reductase: requirement for a cloned *cysG* plasmid to overcome limiting siroheme cofactor. *Journal of Bacteriology* **173**: 325–333, doi: 10.1128/jb.173.1.325-333.1991.

Zeghouf, M., Fontecave, M., Macherel, D., and Covès, J. (1998) The flavoprotein component of the *Escherichia coli* sulfite reductase: expression, purification, and spectral and catalytic properties of a monomeric form containing both the flavin adenine dinucleotide and the flavin mononucleotide cofactors. *Biochemistry* **37**: 6114–6123, doi: 10.1021/bi9728699.

Ziegenhorn, J., Senn, M., and Bücher, T. (1976) Molar absorptivities of beta-NADH and beta-NADPH. *Clinical Chemistry* **22**: 151–160, doi: 10.1093/clinchem/22.2.151.

Appendix

Table 7: Identification by mass spectrometry of protein present in the 55 kDa band from SDS-PAGE of the rDsrAB purification (Figure 10).

Protein name	NCBI entry[a]	Locus tag	Coverage (%)[b]	Peptides[c]	Mass (kDa)[d]
Glutamine synthetase	ADC63901	Alvin_3000	48	14	51.8

[a] NCBI entry is the NCBI-ProteinID.

[b] Coverage is the protein sequence coverage by the matching peptides.

[c] Peptides indicate the number of different peptides matching the protein sequence.

[d] Mass corresponds to the theoretical molecular mass of the identified protein only from its amino acid sequence.

Table 8: Identification by mass spectrometry of proteins present in the 170 kDa band from Blue Native PAGE (Figure 11).

Protein name	NCBI entry[a]	Locus tag	Gene	Coverage (%)[b]	Peptides[c]	Mass (kDa)[d]
rDsrA	ADC62190	Alvin_1251	*dsrA*	52	16	46.8
rDsrB	ADC62191	Alvin_1252	*dsrB*	37	10	40

[a] NCBI entry is the NCBI-ProteinID.

[b] Coverage is the protein sequence coverage by the matching peptides.

[c] Peptides indicate the number of different peptides matching the protein sequence.

[d] Mass corresponds to the theoretical molecular mass of the identified protein only from its amino acid sequence.

Table 9: Identification by mass spectrometry of proteins present in the 283 kDa band from Blue Native PAGE (Figure 11).

Protein name	NCBI entry[a]	Locus tag	Gene	Coverage (%)[b]	Peptides[c]	Mass (kDa)[d]
rDsrA	ADC62190	Alvin_1251	*dsrA*	38	12	46.8
rDsrB	ADC62191	Alvin_1252	*dsrB*	22	9	40
DsrL	ADC62198	Alvin_1259	*dsrL*	26	11	71.4

[a] NCBI entry is the NCBI-ProteinID.

[b] Coverage is the protein sequence coverage by the matching peptides.

[c] Peptides indicate the number of different peptides matching the protein sequence.

[d] Mass corresponds to the theoretical molecular mass of the identified protein only from its amino acid sequence.

Table 10: Identification by mass spectrometry of protein present in the 554 kDa band from Blue Native PAGE (Figure 11).

Protein name	NCBI entry[a]	Locus tag	Coverage (%)[b]	Peptides[c]	Mass (kDa)[d]
Glutamine synthetase	ADC63901	Alvin_3000	46	15	51.8

[a] NCBI entry is the NCBI-ProteinID.

[b] Coverage is the protein sequence coverage by the matching peptides.

[c] Peptides indicate the number of different peptides matching the protein sequence.

[d] Mass corresponds to the theoretical molecular mass of the identified protein only from its amino acid sequence.

Acknowledgement

Zuerst möchte ich mich bei PD Dr. Christiane Dahl bedanken. Du hast mir die Möglichkeit gegeben, an diesem spannenden Thema in deiner Arbeitsgruppe zu arbeiten, warst immer interessiert am Fortschritt meiner Arbeit und hattest gute Ideen, wenn es irgendwo hakte. Vielen Dank für deine Unterstützung und deine wissenschaftliche Expertise.

Vielen Dank auch an Prof. Dr. Uwe Deppenmeier für die Übernahme des Zweitgutachtens. Danke, dass Sie mich 2013 zusammen mit Christiane für den Master Mikrobiologie begeistert haben, sodass ich überhaupt diesen Weg bis zur Promotion am Institut für Mikrobiologie und Biotechnologie eingeschlagen habe.

Ein weiteres Dankeschön geht an Prof. Dr. Lukas Schreiber und Prof. Dr. Sigurd Höger für die Teilnahme an meiner Prüfungskommission als fachnahes und fachfremdes Mitglied.

A special thanks goes to Inês Pereira and her lab at ITQB in Portugal where I twice had the opportunity to work together with and learn from her and the members of her lab. Thank you Sofia Venceslau for always having an open ear, for your expertise and the countless things you taught me. Thank you Andre Santos for showing me how to use the ÄKTA to purify the sulfite reductase – the core enzyme of this study. Thank you Delfin for the good time in the lab and for showing me beautiful places in Portugal. Thanks to all other members of the lab, especially Ana who also visited our lab in Bonn and helped me with my project.

Ein großes Dankeschön an Maria – meine Dsr Partnerin :) Du warst immer interessiert an meinen Planungen, Problemen und Ergebnissen und hattest viele gute Ideen für weitere Experimente. Wie schön, dass wir zusammen so eine schöne und produktive Zeit in Portugal verbracht haben.

Ich danke der gesamten AG Dahl für die schöne Zeit und die gute Arbeitsatmosphäre in unterschiedlichen Konstellationen über die Jahre. Danke an Julia, Tobias, Sebastian, Maria, Corvin, Sebastian, Jingjing. Danke an Renate und Elisabeth für euren Überblick im Labor bzw. Institut und eure Hilfe. Danke an alle Studierenden der letzten Jahre, es hat Spaß gemacht, mit euch zu arbeiten.

Des Weiteren danke ich der AG Deppenmeier für gute Zusammenarbeit in Lehre und Forschung und danke für lustige und (manchmal zu) laute Pausen ;-)

Dem ganzen IfMB danke ich für die tolle Atmosphäre im Institut und für viele lustige Promotions- und Weihnachtsfeiern.

Danke an Toni Kühl vom Pharmazeutischen Institut, Universität Bonn (Abteilung Pharmazeutische Biochemie und Bioanalytik) für die massenspektrometrische Analyse und umfassende Auswertung meiner Daten.

Sebastian Tanabe und Julia Deisinger, danke für die präzisen Korrekturen dieser Arbeit. Ihr wart mir eine große Hilfe. Danke auch an Thomas Franke, der immer eine Antwort auf meine ganzen Fragen bzgl. der Formalien rund um die Dissertation und das Promotionsverfahren hatte.

Anne und Sofie, ich bin so dankbar für unsere wertvolle Freundschaft. Danke, dass ich meine Sorgen, meine Freude und viel Ausgelassenheit nicht nur in den letzten Jahren der Promotion mit euch teilen konnte.

Danke an meine Familie für viel Rückhalt und Verständnis, entspannte Auszeiten und leckeres Essen :)

Sven, danke für deine Unterstützung und für die schöne, entspannte und aufregende Zeit mit dir. Wie schön, dass es dich in meinem Leben gibt.